DESIGN, SYNTHESIS, AND UTILITY OF FUNCTIONALIZED NANOSCALE

AMPHIPHILIC MACROMOLECULES FOR BIOMEDICAL APPLICATIONS

by

SARAH MARIE SPARKS

A Dissertation submitted to the

Graduate School-New Brunswick

Rutgers, The State University of New Jersey

In partial fulfillment of the requirements

For the degree of

Doctor of Philosophy

Graduate Program in Chemistry

Written under the direction of

Professor Kathryn E. Uhrich

And approved by

_____

_____

_____

_____

New Brunswick, New Jersey

JANUARY 2011

ABSTRACT OF THE DISSERTATION

Design, Synthesis, and Utility of Fuctionalized Nanoscale Amphiphilic Macromolecules

for Biomedical Applications

By SARAH MARIE SPARKS

Dissertation Director:

Kathryn E. Uhrich

Polymeric micelles are spherical assemblies of amphiphilic polymers widely studied for many biomedical applications. Nanoscale amphiphilic macromolecules (AMs) are novel amphiphilic polymers composed of an alkylated sugar backbone covalently linked to poly(ethylene glycol) (PEG). In aqueous solution, AMs self-assemble to form 10-20 nm micelles with critical micelle concentrations as low as 100 nM, making them more stable than other common micelles. In addition, the basic structure of AMs has multiple points of modification such that the polymer can be modified and evaluated for virtually any application. This work highlights the promise of functionalized AMs as a novel, versatile biomaterial.

Carboxy-terminated AMs were previously shown to inhibit highly oxidized low-density lipoprotein (hoxLDL) uptake in macrophage cells. To gain a mechanistic understanding of this inhibition, a series of AMs were designed and synthesized by

modifying the basic polymer structure to evaluate several characteristics including: amphiphilicity, PEG chain length, anionic charge location, type of anionic charge, number of anionic charges, rotational motion of the anionic group, and PEG architecture. The optimal AM for inhibiting hoxLDL uptake was determined to be one with a rigid, rotationally-restricted carboxylic acid within the hydrophobic portion of the polymer.

Building upon previous work that showed AMs deliver cargo intracellulary, a series of cationic polymers were designed and synthesized for nucleic acid delivery. The cationic moiety was added within the hydrophobic component of the AMs such that when the cationic portion complexed with anionic nucleic acids, the nucleic acids would be localized in the micellar interior. Three cationic AMs were evaluated with varying surface charges. The polymer with the highest surface charge was the most effective at complexing with and delivering small interfering RNA to U87 glioma cells.

Finally, without modification, AMs are capable of water-solubilizing hydrophobic drugs. This property can be applied to hydrophobic fluorescent nanocrystals, which are useful for biological imaging. In the last chapter, AMs were utilized to water-solubilize white light-emitting nanocrystals without altering the emission properties of the nanocrystals. By modifying the polymer structure to incorporate functionalities that can coordinate to the surface of the nanocrystals, smaller, water-soluble assemblies that maintain white light-emission were obtained.

PREFACE

"From the ashes of disaster grow the roses of success!"

From Chitty-Chitty Bang-Bang

DEDICATION

To my family (especially my parents Dave and Laurie, my sisters Wendy, Melissa, Rachael, and Kelly, my brother David Jr., Grandma & Grandpa Schermerhorn and Grandma & Grandpa Sparks), my fiancé, Evan, and his family (especially Arthur, Billie, Stephen, and William) for always believing in me, giving me inspiration, constant support and unwavering love.

ACKNOWLEDGEMENTS

TABLE OF CONTENTS

LIST OF TABLES

ABBREVIATIONS, SYMBOLS AND UNITS

δ	Chemical shift
λ	Wavelength
λ_{max}	Wavelength of maximum absorbance
°	Degree
°C	Degree Celsius
ACAT	Cholesterol acyl-transferase
AMs	Amphiphilic macromolecules
b	Broad
BODIPY	Boron-dipyrromethene
C	Carbon; control
CBZ-Cl	Benzyl chloroformate
CH_2Cl_2	Methylene chloride, dichloromethane
CdSe	Cadmium selenide
CdS	Cadmium sulfide
cells/cm^2	Cells per centimeter squared
cm	Centimeter
CMC	Critical micelle concentration
CO_2	Carbon dioxide
$CuSO_4$	Copper sulfate
d	Doublet
Da	Dalton
DCU	Dicyclohexyl urea
DLS	Dynamic light scattering
DMF	Dimethyl formamide
DMSO	Dimethylsulfoxide
DSC	Differential scanning calorimetry
EDTA	Ethylenediaminetetraacetic acid
EPR	Enhanced permeation and retention
FBS	Fetal Bovine Serum
FRET	Förster resonance energy transfer
FITC	Fluorescein
g	Gram
GFP	Green fluorescent protein

GPC	Gel permeation chromatography
H	Hydrogen
^{1}H	Proton
^{1}H NMR	Proton nuclear magnetic resonance
H_2O	Water
HCl	Hydrochloric acid
hoxLDL	Highly oxidized low-density lipoprotein
HPLC	High performance/pressure liquid chromatography
hrs	Hours
HUVEC	Human umbilical endothelial cells
kDa	Kilodalton
L	Liter
LC	Liquid Chromatography
LDL	Low-density lipoprotein
LED	Light-emitting diode
L-PEI	Linear poly(ethylene imine)
m	Multiplet
M	Molar
mg	Milligram
mg/mL	Milligram per milliliter
$MgSO_4$	Magnesium sulfate
MHz	Megahertz
min	Minute
mL	Milliliter
mM	Millimolar
mmol	Millimol
mV	Millivolts
M_w	Weight-average molecular weight
N	Nitrogen
NaOH	Sodium hydroxide
NDHF	Normal dermal human fibroblasts
NEt_3	Triethylamine
NHS	N-hydroxysuccinimide
NIR	Near infrared

nm	Nanometer	Scr	Scrambled
nM	Nano molar	SCM	Succinimidyl carboxymethyl
NMR	Nuclear magnetic resonance	SEBS	Poly (styrene-b-ethylene butylene-b-styrene)
N/P	Nitrogen to phosphate ratio	siRNA	Small interfering RNA
O	Oxygen	$SOCl_2$	Thionyl chloride
ODNs	Oligonucleotides	SRA	Scavenger receptor-A
oxLDL	Oxidized low-density lipoprotein	SRB	Scavenger receptor-B
		t	Triplet
PAMAM	Poly(amido amine)	THF	Tetrahydrofuran
PBS	phosphate buffer solution	THP-1 cells	Human acute monocytic leukemia cells
PbSe	Lead selenide		
PDI	Polydispersity index	T_m	Melting temperature
PECM	Polyelectrolyte complex micelles	TOPO	Tri-octyl phosphine oxide
		U87 cells	Human glioblastoma cell line
PEG	Poly(ethylene glycol)		
PEO	Poly(ethylene oxide)	μg	Microgram
PEI	Polyethyleneimine	μL	Microliter
PLGA	Poly(lactide-*co*-glycolide)	μm	Micrometer
PLL	Poly(L-lysine)	μM	Micromolar
ppm	Parts per million	USAM	Umbilical arterial smooth muscle cells
PPO	Poly(propylene oxide)		
PVA	Poly(vinyl alcohol)	UV	Ultraviolet, ultraviolet spectroscopy
PVP	Poly(*N*-vinyl-2-pyrrolidone)		
		UV/Vis	Ultraviolet/visible
QDs	Quantum dots	V	Volt
RNAi	RNA interference	WLNCs	White light-emitting nanocrystals
RT	Room temperature		
s	Singlet	w/v	Weight per volume ratio

1. INTRODUCTION

A polymer is a macromolecule composed of simple, small organic or inorganic molecules covalently linked in a repeating fashion with hundreds to thousands of repeats. Their high molecular weights give polymers unique properties compared to small molecules including higher viscosities, decreased solubility, and increased mechanical strengths, which can be fine-tuned based upon size (or number of repeat units) and chemical composition. These properties make polymers useful for a multitude of applications including clothing, rubber, and plastics, as well as many biomedical applications including the delivery of drugs and diagnostics.[1, 2]

1.1. Polymers for Drug Delivery: Polymer Therapeutics

The therapeutic efficacy of pharmaceutical compounds to treat diseases (i.e. drugs) is often limited by the ability of the drug to 1) accumulate at the active site of the therapeutic and 2) maintain a therapeutic level.[3, 4] Without adequate accumulation at the active site, the drug could be ineffective in one of two ways; if the concentration is too high toxic levels are likely to be obtained, while if the concentration is too low, no therapeutic effect will be achieved.[4, 5] Drug delivery is the formulation of a therapeutic compound by "whatever means possible" (generally within a carrier system) administered to the active site at an adequate and sustainable dosage.[4]

One class of widely used drug carrier systems are biocompatible polymers. Generally, polymers are attractive for drug delivery because their inherent properties discussed above allow for multiple options of formulation, such as microspheres, films, fibers, and hydrogels, which is chosen based upon the specific application.[1] Within the

general class of polymers, biocompatible polymers are used for drug delivery applications to avoid vehicle toxicity to biological systems while enhancing drug efficacy and reducing overall drug toxicity.[5] Biocompatible polymers have also been shown to increase the circulation time, cellular uptake, and tolerability of therapeutics.[4, 6]

Biocompatible polymers for drug delivery can be categorized into two classes: biodegradable and non-degradable.[4, 5, 7] Biodegradable polymers are macromolecules consisting of covalent bonds that can be broken down by biological means, such as hydrolysis and/or enzymes. Biodegradable polymers are advantageous for bioactive delivery because, following or during therapeutic delivery, the polymers degrade into materials that can be readily excreted from biological systems. In contrast, non-degradable polymers need to be retrieved or manipulated further following drug delivery.[5, 7] However, this degradation has to happen such that the bioactive is released in a controlled manor before the polymer completely degrades; otherwise the bioactives are released all at once, i.e. dose-dumping, which can lead to issues including toxicity and the need for frequent dosing.[4, 5, 8] Additionally, the bioactive needs to be released in such quantities to achieve a therapeutic level.[4, 5]

The combination of a polymer and a bioactive/therapeutic may be considered a polymer therapeutic. Multiple types of polymer therapeutics are known, encompassing physical and chemical means of drug incorporation (examples of which are shown in **Figure 1.1**): polymeric drugs or sequestrants, polymer-protein conjugates, complexes of polymers with nucleic acids (polyplexes), polymer-drug conjugates, formulation of the drug into a polymer, physical incorporation of the drug into a polymer matrix (hydrogels

or microspheres), and physical and/or chemical incorporation of the drug into a polymeric micelle.[9, 10]
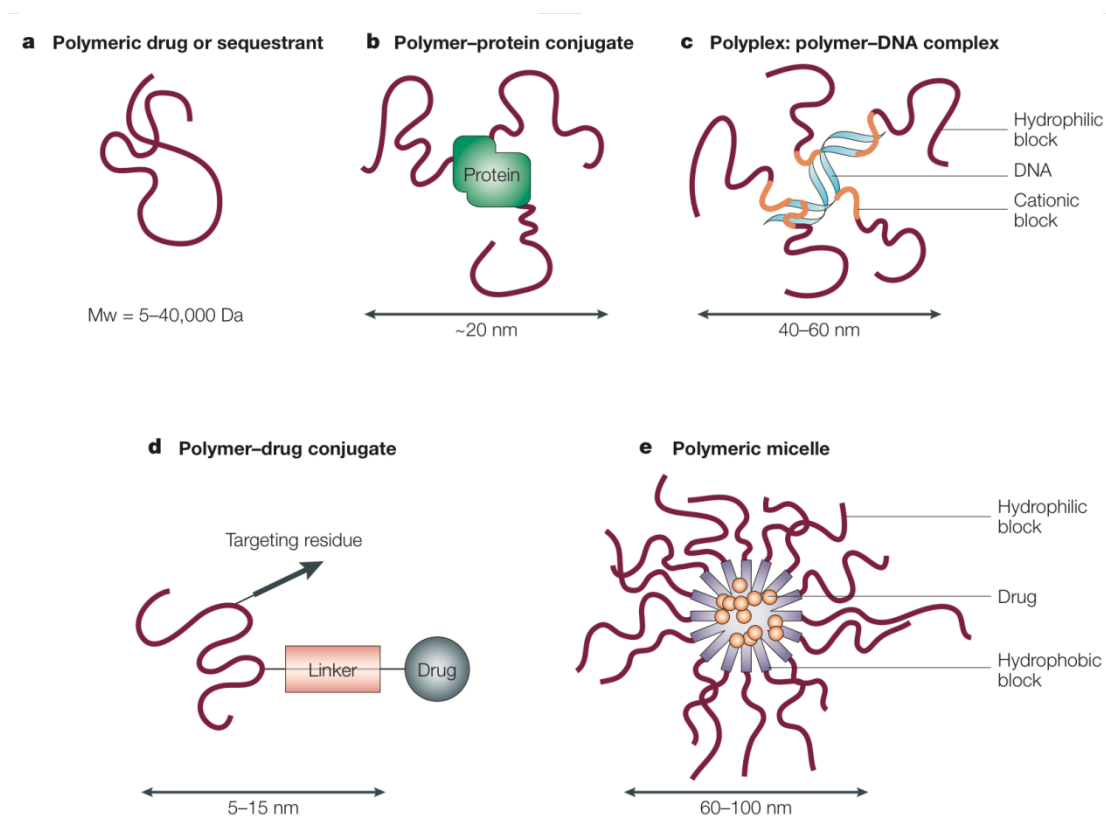
Figure 1.1. Schematic representation of the types of polymer therapeutics.[9, 10]

For the purpose of the work done herein, physical incorporation of the drug into a polymeric micelle, complexes of polymers with nucleic acids, and the polymers as drugs will be described in detail.

1.1.1. Physical Incorporation of a Drug Into a Polymer Micelle

1.1.1.1. Polymer Micelles

Polymer micelles, which are dynamic assemblies of amphiphilic polymers, are one type of polymer therapeutic. They have many attractive features including the ability to achieve a nanoscale size and their inherent amphiphilicity. In general, materials on the

nanoscale are attractive for biomedical applications as this size mimics that of many biological entities. This feature enhances the circulation time of the material as the nanomaterials are not immediately recognized as being foreign to biological systems.[3] In addition to nanoscale size mimicing biological entities, the amphiphilicity of polymer micelles mimics the amphiphilicity of cell membranes, which enhances the permeability of the micelles.[11] Polymer micelles can be composed of a variety of structural components but all polymer micelles are composed of unimers that have a hydrophobic block covalently bound to a hydrophilic block. To be classified as a polymer micelle, one or both of these blocks must be a polymer. Some common hydrophobic polymers include subunits such as poly(propylene oxide) (PPO), poly(D,L-lactide-co-glycolide) (PLGA), and polycaprolactone while common hydrophilic polymers are poly(ethylene glycol) (PEG), poly(*N*-vinyl-2-pyrrolidone) (PVP), and poly(vinyl alcohol) (PVA).[6] One of the most commonly used hydrophilic polymers is PEG because not only is it inexpensive, but PEG also has extremely low toxicity and is capable of efficient water solubilization while further increasing circulation time of the polymer micelle by being a "stealth carrier"; it is not recognized by biological systems as a foreign material and therefore no immune response is elicited.[6, 12, 13] It also increases stability of micelles, both for storage and within the serum of the body,[6, 12, 13] and aids in shielding cargo (such as drugs and nucleic acids) in the core from enzymatic degradation.[6, 12-14]

Three main types of amphiphilic unimers are known self-assemble into polymer micelles as shown in **Figure 1.2**.[6] When both components of a unimer are polymers, the resulting polymers are termed diblock or triblock copolymers. Poly(ε-caprolactone)-PEG and Pluronic® are examples of commercially available diblock and triblock copolymers,

respectively, that self-assemble to form polymer micelles, shown in **Figure 1.2A** and **B**. The triblock copolymer Pluronic® is composed of poly(ethylene oxide) (PEO)-poly(propylene oxide), (PPO)-PEO. Alternatively, the hydrophobic component of polymer micelles can be composed of a lipophilic small molecule linked to a hydrophilic polymer. One example of this type of polymeric unimer is PEGylated cholesterol (**Figure 1.2C**).
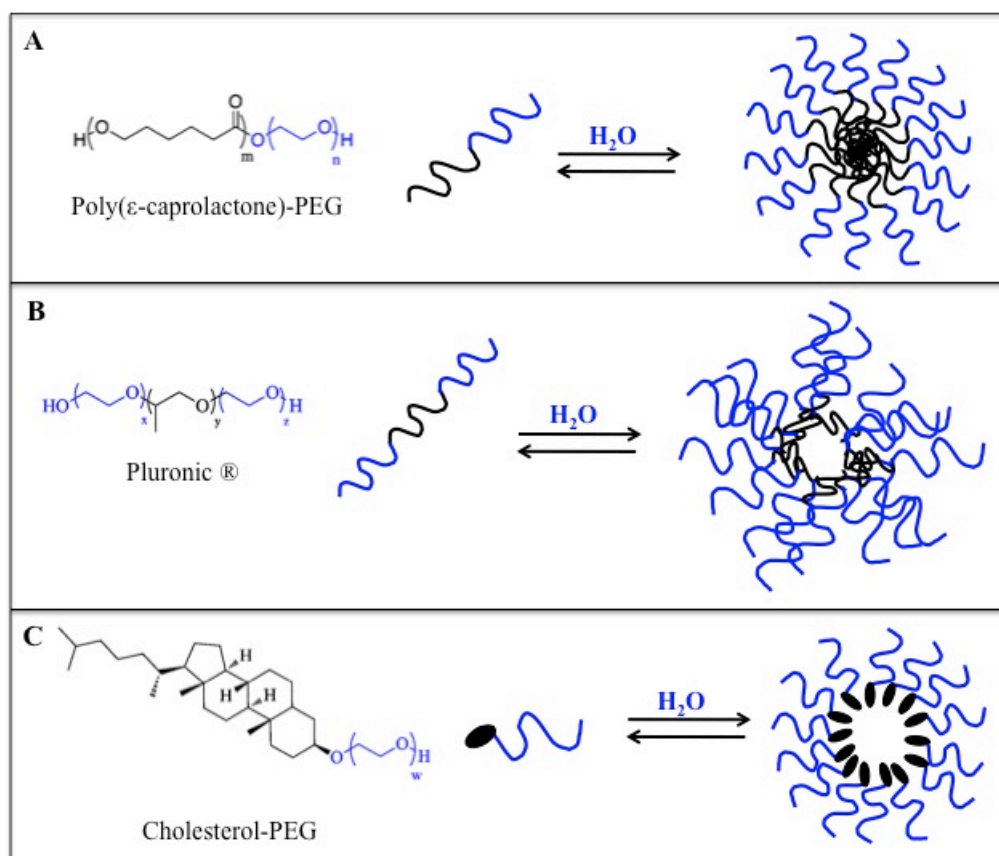
Figure 1.2. The three types of unimers that self-assemble in aqueous media to form polymer micelles: A) diblock copolymers, B) triblock copolymers, and C) a lipophilic component conjugated to a hydrophilic polymer, where blue represents the water-soluble component(s) and black represents the hydrophobic component.

1.1.1.2. Polymer Micelles as Polymer Therapeutics

Polymer micelles self-assemble in aqueous media such that the hydrophobic components of the unimers form a hydrophobic core that is 'protected' from the hydrophilic media and solubilized by the hydrophilic components that form a hydrophilic corona, **Figure 1.3**. The hydrophobic core of the polymer micelle can then be used to water-solubilize hydrophobic materials, such as drugs, based upon interactions with the hydrophobic domain of the polymer. The examples of the different unimer types that self-assemble into polymer micelles shown in **Figure 1.2** are biocompatible polymers widely investigated for drug delivery.
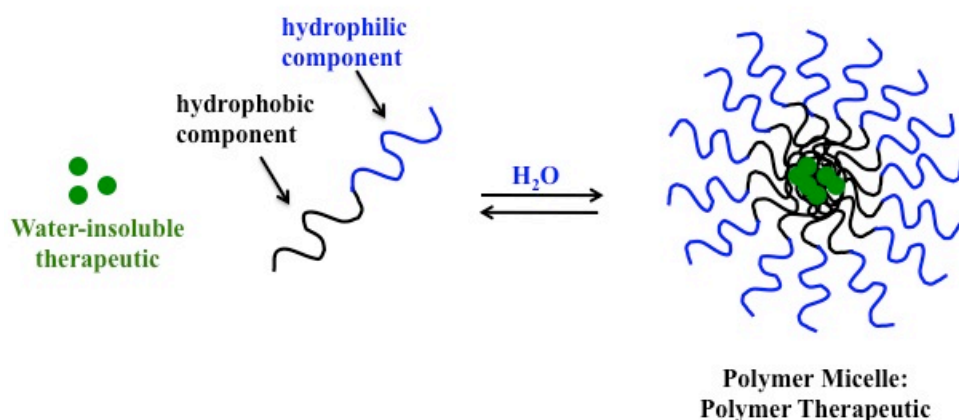
Figure 1.3. Polymer micelles as polymer therapeutics: self-assembly of a diblock copolymer and water-insoluble therapeutics in aqueous solution to form a polymer therapeutic.

The combination of many features make polymer micelles particularly attractive as polymer therapeutics: their amphiphilicity allows them to permeate well through cell membranes[11], their nanoscale size increases circulation time, they generally have good shelf and *in vivo* stability, and depending on the structure the loading of hydrophobic

drugs can be highly efficient.[3, 6] However, the use of polymeric micelles is often limited due to micellar instability, as the micelle is in constant equilibrium with the unimers. The assembly of polymeric micelles is controlled by the critical micelle concentration (CMC), or the lowest concentration at which micelles form. Micelles with lower CMCs (such as 100 nM as compared with 100 μM) are more stable as micelle systems at higher concentrations (i.e. there are less free unimers in solution) and, therefore, drug loading is more efficient.[6]

1.1.2. Complexes of Polymers with Nucleic Acids

In addition to conventional small molecule drugs, nucleic acids are often used as therapeutics. Commonly referred to as gene delivery, the delivery of nucleic acids for the treatment of disease has the potential to offer a treatment option for diseases that are currently untreatable. Such diseases are the result of mutations to genes and/or missing genes. However, unlike many small molecule therapeutics, nucleic acids must be protected from enzymatic degradation by nucleases in biological systems. Cationic polymers that can electrostatically complex with and condense the nucleic acid are a viable, and widely studied option, for nucleic acid delivery.[9, 15]

1.1.2.1. Strategies for Nucleic Acid Therapy

Strategies for treatment using gene therapy include introduction of a therapeutic gene as well as the silencing of abnormal gene expression within diseased tissue. The technology includes traditional antisense delivery as well as the more recent RNA interference (RNAi) as a mechanism to control gene expression.[15] Traditional antisense oligonucleotides (ODNs), synthetic single-stranded DNA, selectively inhibit gene expression by base-pairing to selected regions on mRNA. However, this therapeutic

approach is only a short-term silencing technique.[16] On the other hand, antisense RNA can result in longer-term gene silencing with inducible and reversible gene inhibition, which can be tuned to fit different circumstances. The new-found approach of RNAi has shown potential as a potent antisense approach in which small interfering RNAs (siRNAs) assemble with a multiprotein nuclease complex, which eventually unwinds double-stranded RNA causing degradation of target mRNAs that are sequentially homologous to the siRNA.[16] Currently, vectors for gene therapy remain in the research and trial phase.

1.1.2.1.1. Viral Vectors

Currently, the most effective delivery devices for genes are viral vectors, those carrier systems derived from viruses such as retroviruses and adenoviruses.[17] These viral vectors are biocompatible, 100 nm self-assemblies of lipids, proteins, and nucleic acids that include the desired gene. In the case of retroviruses, the lipids form a bilayer to protect the gene. In contrast, the adenovirus has proteins which form a tightly packed coat-like protective structure. The stages involved in the delivery of DNA to the nucleus by these viral vectors are condensation of DNA into nanoparticles, protection of DNA from degradation, adsorption of the nanoparticles to cells, delivery into the cytoplasm and nucleus, and final release of the "package", as depicted in **Figure 1.4**.[15] Viruses are successful at all stages of delivery. However, while these viral vectors have extremely high transfection efficiencies, they also provoke an immune response which can lead to inflammation and possible oncogenesis, or the development of a malignant tumor.[15] In addition, these vectors are difficult to scale-up.[18] As the disadvantages due to safety far outweigh advantageous transfection, non-viral synthetic vectors are necessary.
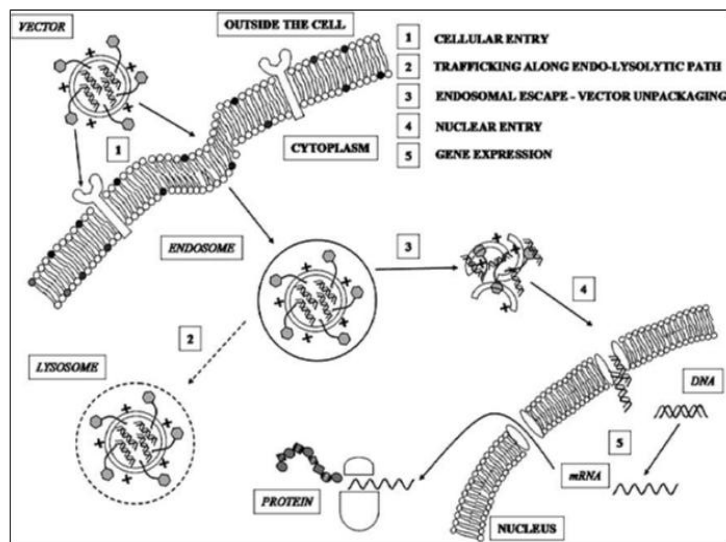
Figure 1.4. Schematic depicting the processes necessary to effectively achieve nucleic acid delivery.[15]

1.1.2.1.2. Non-viral Vectors

Conceptually, non-viral gene vectors could be designed and synthesized to improve upon safety issues associated with viral vectors while retaining efficient transfection. As non-viral vectors are indeed synthetic, they can be tailored to meet the delivery needs of the particular nucleic acid. However, synthesizing macromolecules to carry nucleic acids for use in humans yields generates several new problems including insufficient stability of the carrier molecules, non-specific uptake by the reticulo-endothelial system (RES), and the most significant problem, cytotoxicity.[17] Efficiency of gene delivery requires the daunting task of efficient gene complexation, reaction with extracellular macromolecules, cellular uptake, endosomal escape, nuclear entry, and DNA release from the complexes. Severe failure at any of these stages results in an ineffective gene delivery device.[18] Thus, viral vectors provide cues for synthetic

systems; their nano-size is mimicked by synthesizing nanomaterials for ease of circulation and successful cellular uptake by. Other factors may be modified by structurally altering synthetic vectors to incorporate moieties that complex with DNA efficiently and have high buffering capabilities to enhance endosomal release.

Numerous synthetic approaches are known to effectively deliver nucleic acids into cells. Early approaches involved the formation of electrolyte complexes of genes with cationic lipids or polymers (such as polyethyleneimine (PEI)), known as lipoplexes and polyplexes that are less than 200 nm in size.[19] Undesirable *in vivo* effects, including rapid clearance in the blood stream, non-specificity[13], and embolism due to the formation of aggregates greater than 400 nm following intravenous injection that cause precipitation of the complexes and entrapment within the capillaries of the lung,[17] exclude these vectors from use without further modification.

Liposomes are another, more promising, approach to nucleic acid delivery. Cationic liposomes possess a positively charged, polar head group and a hydrophobic tail, which self-assemble to form liposomes. The liposomes can solubilize and intracellulary transport the nucleic acids. [15, 18] However, while liposomes are promising, problems include toxicity as well as inefficient delivery of the gene into the cell due to pinocytosis or endocytosis by leucocytes during circulation.[14]

1.1.2.1.3. Polymeric Micelles as Non-viral Vectors

As discussed in **Section 1.1.1**, polymeric micelles have been widely studied as hydrophobic drug delivery systems. However, more research has been directed towards the use of micelles to protect genes during transport by association inside the hydrophobic core as well as for their increased complex stability and circulation.

While many polymers are used in biomedical applications, the most common polymers for nucleic acid delivery are PEI and poly(L-lysine) (PLL), as cationic polymers that complex with DNA. PEI is often taken as the "gold standard" for comparison with new synthetic delivery devices due to its outstanding ability to condense DNA, permeate into the cell, and escape from the endosome.[20] With its extremely large concentration of amines capable of protonation at physiological pH, PEI readily achieves endosomal escape *via* the proton sponge effect.[15] However, it is this same amine concentration that is PEIs greatest fault, as the polymer is cytotoxic as a result of the large overall positive charge. In addition, once inside the cytoplasm, the DNA is generally not released due to tight interactions of PEI and DNA. To decrease cytotoxicity and increase release capabilities, PEI is often modified by PEGylation, acetylation, or an environmentally labile group (such as a ketal) to reduce the charge.[20-22] In addition, other cationic polymers, such as PLL and poly(amido amine) (PAMAM) dendrimers, are studied as alternatives.[15, 23]

Generally, two types of micelles are used in nucleic acid delivery, those composed of unimers that self-assemble spontaneously in aqueous media and those micelles where self-assembly must be chemically induced. The chemically induced assembly of micelles is commonly found in gene delivery, as self-assembly is not possible with too much cationic charge in the hydrophobic core. Polyelectrolyte complex micelles (PECM) are such examples, in which the gene is conjugated to the hydrophilic portion of the micelle and a cationic core-forming agent is used to induce micelle formation. In two studies by Kim et. al., siRNA and an ODN modified with a primary amine are covalently linked to PEG *via* enzymatically and hydrolytically degradable

bonds, respectively. A cationic core forming agent, PEI, PLL, or Lipofectamine, is then added to the unimer to induce assembly of the 70-90 nm micelles which were potent suppressors of the desired genes.[12, 13]

Similarly, two or more polymers can be covalently linked to form block copolymers. In the case of gene delivery, the copolymer is typically composed of a hydrophilic polymer conjugated to an amine-containing polymer, PLL or PEI, which can then be complexed with DNA to induce self-assembly in which the DNA is compacted within the core.[24, 25] Copolymers such as PEI or PLL grafted with PEG are often studied for their increased stability, blood circulation, and transfection efficiencies while also resulting in decreased cytotoxicity.[21, 26, 27] Lipoplexes can also be PEGylated to prevent aggregation and excretion by the RES and increased stability over long periods of time.[27]

Amphiphilic polymers represent the second general type of micelles in which the unimers have a hydrophobic and hydrophilic portion, and are designed to self-assemble into micelles. These types of micelles are not widely studied for gene delivery due to the difficult nature of loading negatively charged genes into the hydrophobic core. However, one example reported by Wang et. al. is a unimer in which the hydrophobic portion is cholestryl chloroformate while the hydrophilic shell is formed from a synthetically designed cationic polymer of a poly (N-methyldiethyleneamine sebacate), whose cationic properties result from a tertiary amine. These cationic micelles were shown to induce higher gene expression than PEI in various cell lines and therefore show promise as non-viral vectors for gene delivery.

1.1.3. Polymers as Drugs

An alternate approach for polymers in therapeutics is when the polymer itself displays bioactivity. These polymers can be either natural polymers extracted from plants or animals or synthetic polymers that exhibit bioactivity. Natural polyanions and polysulphates have long been known to possess antitumor and antiviral activity.[10] Synthetic polymers with bioactivity have been use for numerous applications including the sequestration of molecules to treat diseases such as hyperkalemia and iron disorders and to sequestor toxins such as anthrax.[9] Further, polymers have been designed as anticancer agents, to treat HIV, and hepatitis C, to provide just a few examples.[9, 10]

As with non-polymeric drugs, biocompatibility, patient tolerability, and specificity are factors that need to be considered. In contrast to small molecule therapeutics, the advantage of bioactive polymers is the variety of formulation options available to polymers, as discussed in **Section 1.1**, without the need for additional components that could alter therapeutic efficacy.

1.2. Polymers for Biological Imaging Applications

In addition to their utility in drug delivery, polymers have also found use in biological imaging applications, using both conjugated fluorescent polymers and polymers to biostabilize imaging agents. For the purpose of the work done herein, the use of polymers to biostabilize fluorescence imaging agents will be described in more detail in the subsequent sections.

1.2.1. Nanoparticle Imaging Agents

The vast majority of nanoparticle imaging agents currently evaluated for biological imaging are formed of heavy metals, such as iron, titanium, and cadmium. The formulation of these heavy metals into nanoparticles yields particles with magnetic and fluorescent properties useful for imaging.[3, 28-31]

Fluorescent nanoparticles, or semiconductor quantum dots (QDs), have several advantages over typical fluorophores including size-dependent optical properties that can be easily tuned and have enhanced photostability relative to organic fluorophores. However, these nanoparticles are often water-insoluble and cytotoxic in nature.[28, 30, 32, 33] Thus, the biocompatible, water-soluble polymers previously described for drug delivery have found widespread use in the biocompatibilization of nanoparticles.

1.2.2. Water-solubilization of Nanoparticle Imaging Agents Using Polymers

As synthesized, the metal surfaces of many fluorescent nanoparticles are hydrophobic alkanes such as tri-octyl phosphine oxide (TOPO), hexadecylamine, or octadecylamine that render the nanocrystals hydrophobic.[34, 35] Additionally, due to their heavy metal composition, fluorescent nanocrystals are not biocompatible.[36] Thus, for use in biological applications, they must be modified to render them both hydrophilic and biocompatible.[36]

Multiple methods to induce hydrophilicity and biocompatibility to QDs can be envisioned. Two commonly employed methods are encapsulation and ligand exchange[30, 31, 34] (shown in **Figure 1.5**). These methods will be discussed in greater detail in **Chapter 4**.
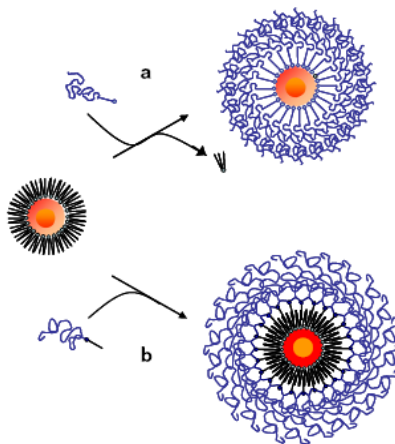
Figure 1.5. Schematic image of a) ligand exchange coating of semiconductor nanocrystals and b) ligand capping, or encapsulation, of semiconductor nanocrystals.[34]

1.2.3. Biological Imaging Using Water-soluble Nanoparticle Imaging Agents

Nanoparticle imaging agents have been used for applications from cellular imaging and material tracking to disease diagnosis and treatment.[3, 28, 30-33]

1.2.3.1. Imaging & Tracking

Generally, it is well known and accepted that cells regulate and control biological processes; but the mechanisms are poorly understood. A greater understanding of cells, the mechanisms by which cells function "normally", and the deficiencies leading to disease states will provide a platform towards the "smart" design of therapeutics to correct cellular difficiencies to treat disease.[3] One way to gain more insight into these mechanisms is cellular imaging of fixed and live cells using polymer-solubilized nanoparticles.[3, 28, 37-40]

In addition to gaining a better understanding of cellular mechanisms, imaging techniques have been used to track nanomaterials within biological systems to determine where they accumulate as well as learn more about the relationship between

nanomaterials and organisms.[28, 41, 42] As discussed in **Section 1.1**, one of the purposes of using a delivery vehicle to "carry" a therapeutic is to more effectively administer the therapeutic to the active site. Fluorescence imaging techniques can be used to instantaneously and terminally follow drug delivery in two ways: 1) organic fluorophores that do not affect the mechanism of the drug can be added to the vehicle or 2) nanoparticles (fluorescent or magnetic) can be formulated within the delivery vehicle and their release rates followed to model therapeutic release. In instance 1, the fate of the vehicle is followed, while in instance 2, the fate of a model therapeutic is profiled.

1.2.3.2. Diagnostics

Fluorescence imaging techniques have also found widespread use in the diagnosis of disease, termed biosensing. A biosensor is built on two components; a biorecognition element and a signaling element. In the case of fluorescence-based biosensors, the signaling element, i.e. fluorescence, is often based upon Förster resonance energy transfer (FRET) in which energy is transferred from a donor chromophore to an acceptor chromophore resulting in a change in the fluorescence signal (enhancement or depletion).[30, 31] An example of a fluorescent biosensor is one in which the biorecognition element is an antibody that, upon binding with the protein or receptor it is specific to, produces a stronger fluorescent signal.[43] The optimal biosensors are those that are selective to the desired target, fast, sensitive, produce accurate and reproducible results, and reusable.[30]

1.2.3.3. Theragnostics

Theragnostics are relatively new treatment techniques that combine disease diagnosis with a treatment modality. Theragnostics span a range of topics including

predictive medicine, integrated medicine, and pharmocodiagnostics. The development and use of theragnostics has the potential to revolutionize disease therapy – shifting care towards "personalized medicine".[44] Polymer micelles are attractive candidates for development as theragnostics as they can carry multiple types of cargo.

1.3. Nanoscale Amphiphilic Macromolecules

Nanoscale amphiphilic macromolecules (AMs) are novel, polymeric micelles. In aqueous media, the unimers self-assemble to form biocompatible[45], nano-sized micelles at concentrations as low at 100 nM (the CMC),[46] making them more stable than other polymeric micellar systems that have CMCs only as low as 2 μM.[6]

1.3.1. Synthesis of AMs

The basic unimer structure is a branched hydrophobic component formed by the tetra-alkylation of a biocompatible sugar, which is further derivatized with linear, hydrophilic PEG – all of which are linked *via* biodegradable bonds.[46] The synthesis of the parent compound, **1cM**, from the biocompatible sugar, mucic acid, is shown in **Figure 1.6**.
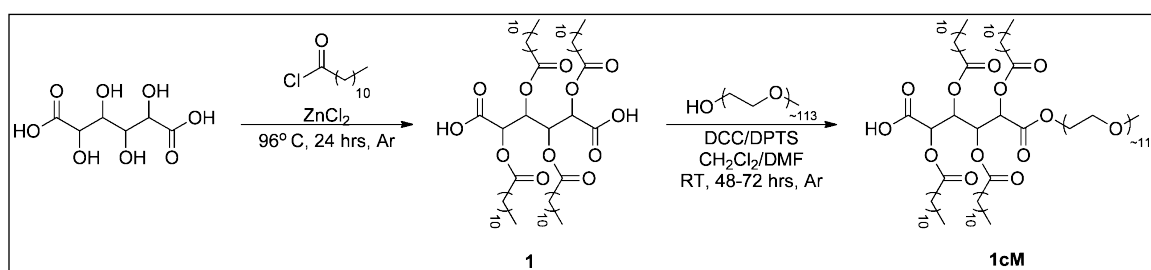
Figure 1.6. Synthesis of the parent polymer, **1cM**, by derivatizing mucic acid with lauroyl chloride and poly (ethylene glycol).

Many facets of the AM structure can be readily tuned depending upon the desired application: 1) hydrophobicity can be enhanced by the increasing the number of sugar

hydroxyl groups (i.e., alkyl group modification points) as well as the increasing the alkyl group chain length used to derivatize the sugar, 2) hydrophilicity can be enhanced by lengthening the PEG length (or increasing molecular weight), and 3) sugar stereochemistry can be modified.

Sugar stereochemistry has been shown extremely important in numerous biomedical applications. In work by Liu et. al. utilizing similar sugars incorporated into cationic polymers, the sugar stereochemistry had a significant affect on the complexation and delivery of siRNA.[47] In addition, preliminary work in collaboration with Professor Prabhas Moghe's group (Rutgers, Biomedical engineering) has determined the sugar stereochemistry has a significant effect on AM binding to scavenger receptors.[48-50] In this work, the sugar stereochemistry was held constant by utilizing a mucic acid backbone with the stereochemistry shown in **Figure 1.7**.
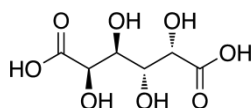
Figure 1.7. Structure of mucic acid showing hydroxyl stereochemistry.

1.3.2. Applications of AMs

Previous research has employed AMs as polymer therapeutics for applications as drug delivery vehicles[51-53], to deliver cargo intra- and subcellularly, and as polymer drugs for the management of cardiovascular disease[54-58]. However, AMs are attractive for multiple other applications due to their low CMC values, lending micellar stability, solution stability (lack of aggregation) for up to three weeks[46, 51], and biocompatibility[45]. As mentioned in **Section 1.3.1**, numerous facile, applications-driven modifications can be made to tune AM hydrophobicity and hydrophilicity. Further, AM

functional groups can also be modified on both the hydrophilic and hydrophobic portions of the unimer. The modification of the hydrophobic portion with functional groups for specific biomedical applications is the major feature explored in this work.

1.3.3. Research Projects

Previous research in our laboratory investigated **1cM** as a biocompatible, micellar polymer therapeutic for the delivery of cancer therapeutics.[51-53] In addition, preliminary work with collaborators showed **1cM** was capable of acting as a drug itself, inhibiting highly oxidized low-density lipoprotein (hoxLDL) uptake in macrophage cells.[54-57]

Stemming from this early work, several research projects were designed to explore the use of AMs in different applications. By utilizing the free carboxylic acid within the hydrophobic moiety as a point of functionalization, the AMs can be modified in numerous ways to be used in a variety of biomedical applications. In Chapter 2, the ability of the AMs as bioactive ligands for the treatment of cardiovascular disease was further explored. Through the design, synthesis, and evaluation of anionic AMs with numerous structural modifications, the interaction between the bioactive AMs with the scavenger receptors on macrophage cells was better understood to enable the "smart" design of future AMs. In Chapter 3, the carboxylic acid of the AMs was functionalized with cationic moieties, specifically ethyleneimines, to complex with and deliver nucleic acids for gene therapy. Finally, in Chapter 4, the ability of AMs to biostabilize white light-emitting nanocrystals was explored utilizing encapsulation and ligand exchange to design a novel imaging, biosensing, and/or theragnostic system.

1.3.3.1. Carboxy-terminated AMs for Managing Cardiovascular Disease

Our early research collaborations with Prof. Prabhas Moghe, Biomedical Engineering Department at Rutgers University, demonstrated that carboxy-terminated AMs inhibited the uptake of oxidized low-density lipoprotein (oxLDL), the harmful form of cholesterol, by competitive binding to scavenger receptors on macrophage cells.[54-58] The unihibited uptake of oxLDL by scavenger receptors on macrophage cells is known to be a critical step in the progression of atherosclerosis[59-68] – a major cause of cardiovascular disease.[69-71] However, our understanding of how the amphiphilic polymers outlined in **Section 1.3.1** inhibit oxLDL uptake was limited. Thus, anionic polymers with varying structures were designed, synthesized, and evaluated for their ability to inhibit oxLDL uptake in macrophage cells. A rigid, sterically hindered carboxylic acid was observed to be the most efficient structure at inhibiting oxLDL uptake. We hypothesized that the carboxylic acid rigidity enables the appropriate confirmation for binding to the cationic scavenger receptor on macrophage cells. This hypothesis has since been confirmed by molecular modeling studies.[58]

1.3.3.2. Cationic AMs for Nucleic Acid Delivery

The biocompatibility and solution stability of AMs makes them a highly attractive candidate for biomedical applications. To utilize the polymers as nonviral vectors for nucleic acid delivery, cationic moieties were incorporated into the hydrophobic component of the unimer backbone to render the systems positively charged. These positively charged moieties allow the negatively charged nucleic acid to complex with the polymer. Additionally, as these positive charges are localized within the hydrophobic component of the unimer, the nucleic acids will reside within the hydrophobic core of the

polymer and be protected from degradation by nucleases. The cationic moieties incorporated were small, linear ethyleneimines of varying lengths chosen with the goal of achieving the efficiency of PEI without the cytotoxicity observed using PEI. The resuling cationic AMs formed electrostatic complexes with nucleic acids, specifically small interfering RNA (siRNA). The complexes successfully the delivered the siRNA intracellularly and produced gene silencing in U87 glioblastoma cells equivalent to complexes of siRNA with a linear PEI (L-PEI) control.

1.3.3.3. AMs to Biostabilize White Light-emitting Nanocrystals

New safe and efficient fluorescence systems for imaging, biosensing, and other applications as discussed in **Section 1.2** are highly desirable for the design of better treatment options. Previous research performed in our laboratory utilized the AMs to water-solubilize and deliver hydrophobic drugs.[51-53] Similarly, fluorescent nanocrystals are hydrophobic and often cytotoxic due to their heavy metal composition. To utilize fluorescent nanocrystals for the biomedical imaging applications discussed in **Section 1.2**, the nanocrystals must be water-soluble. In this work, white light-emitting nanocrystals (WLNCs) were biostabilized by encapsulation within AMs and additional ligand exchange, whereby a functionalized AM coordinated to the metal surface of the nanocrystals. The WLNCs were successfully water-solubilized using both an unmodified (**1cM** for encapsulation) and phosphonic acid-modified AM (for ligand exchange) without significantly hindering the nanocrystal fluorescence. The highest fluorescence was achieved with AM-encapsulated WLNCs while the smallest sized systems were achieved using ligand exchange-solubulized WLNC. Preliminary *in vitro* uptake in human THP-1 macrophage cells qualitatively showed no significant decrease in cell

numbers or morphology change, indicating excellent cytocompatibility and more efficient uptake of the ligand exchange-solubilized WLNC.

1.4. Summary

The many favorable attributes of AMs warrant exploration for biomedical applications beyond the typical use for drug delivery. By utilizing the carboxylic acid within the hydrophobic portion of the unimer, many new polymers were designed and synthesized for multiple applications. By modifying the architecture of the polymers, new information about the efficient binding of AMs to scavenger recptors on macrophages was obtained, allowing the better design of future polymer systems. The incorporation of cationic moieties to the AMs resulted in cytocompatible polymers with the ability to deliver nucleic acids *in vitro* for gene therapy. Additionally, early studies indicate that AMs are promising for the biostabilization of fluorescent nanocrystals for imaging, diagnostics, and/or biosensing applications.

1.5. References

[1]   C. E. Carraher, Jr, *Introduction to Polymer Chemistry*, Second ed., CRC Press, Boca Raton, London, New York, **2010**.
[2]   Y. Gnanou, M. Fontanille, *Organic and Physical Chemistry of Polymers*, John Wiley & Sons, Inc, Hoboken, **2008**.
[3]   V. K. Varadan, L. Chen, J. Xie, *Nanomedicine: Design and Applications of Magnetic Nanomaterials, Nanosensors, and Nanosystems*, John Wiley & Sons, Ltd, West Sussex, UK, **2008**.
[4]   V. T. Ranade, M. A. Hollinger, *Drug Delivery Systems*, Second ed., CRC Press, Boca Raton, London, New York, Washington, D.C., **2004**.
[5]   K. E. Uhrich, S. M. Cannizzaro, R. S. Langer, K. M. Shakesheff, *Chemical Reviews* **1999**, *99*, 3181.
[6]   V. P. Torchilin, *Pharmaceutical Research* **2007**, *24*, 1.

[7]   M. Chasin, R. Langer, *Biodegradable Polymers as Drug Delivery Systems, Vol. 45*, Marcel Dekker, Inc., New York, Basel, Hong Kong, **1990**.

[8]   G. S. Kwon, T. Okano, *Advanced Drug Delivery Reviews* **1996**, *21*, 107.

[9]   R. Duncan, R. Satchi-Fainaro, *Polymer Therapeutics I*, Springer, Germany, **2006**.

[10]   R. Duncan, *Nature Reviews Drug Discovery* **2003**, *2*, 347.

[11]   D. F. Evans, B. W. Ninham, *Journal of Physical Chemistry* **1986**, *90*, 226.

[12]   S. Kim, J. Jeong, S. Lee, S. Kim, T. Park, *Journal of Controlled Release* **2006**, *116*, 123.

[13]   S. Kim, J. Jeong, H. Mok, S. Lee, S. Kim, T. Park, *Biotechnology Progress* **2007**, *23*, 232.

[14]   K. Greish, J. Fang, T. Inutsuka, A. Nagamitsu, H. Maeda, *Clinical Pharmacokinetics* **2003**, *42*, 1089.

[15]   C. Roth, S. Sundaram, *Annual Review of Biomedical Engineering* **2004**, *6*, 397.

[16]   K. L. Lee, C. M. Roth, *Current Opinion in Biotechnology* **2003**, *14*, 505.

[17]   K. Osada, K. Kataoka, *Advances in Polymer Science* **2006**, *202*, 113.

[18]   Z. Hyvonen, A. Plotniece, I. Reine, B. Chekavichus, G. Duburs, A. Urtti, *Biochimica et Biophysica Acta* **2000**, *1509*, 451.

[19]   N. Nishiyama, K. Kataoka, *Pharmacology & Therapeutics* **2006**, *112*, 630.

[20]   M. S. Shim, Y. J. Kwon, *Biomacromolecules* **2008**, *9*, 444.

[21]   P. Banerjee, R. Weissleder, A. J. Bogdanov, *Bioconjugate Chemistry* **2006**, *17*, 125.

[22]   N. Gabrielson, D. Pack, *Biomacromolecules* **2006**, *7*, 2427.

[23]   C. Waite, S. Sparks, K. Uhrich, C. Roth, *BMC Biotechnology* **2009**, *9*.

[24]   C. Deng, X. Chen, H. Yu, J. Sun, T. Lu, X. Jing, *Polymer* **2007**, *48*, 139.

[25]   A. Agarwal, R. Unfer, S. Mallapragada, *Journal of Biomedical Materials Research Part A* **2007**, *81A*, 24.

[26]   M. Walsh, M. Tangney, M. O'Neill, J. Larkin, D. Soden, S. McKenna, R. Darcy, G. O'Sullivan, C. O'Driscoll, *Molecular Pharmaceutics* **2006**, *3*, 644.

[27]   K. Remaut, B. Lucas, K. Raemdonck, K. Braeckmans, J. Demeester, S. DeSmedt, *Biomacromolecules* **2007**, *8*, 1333.

[28]   K. T. Thurn, E. M. B. Brown, A. Wu, S. Vogt, B. Lai, J. Maser, T. Paunesku, G. E. Woloschak, *Nanoscale Research Letters* **2007**, *2*, 430.

[29]   K. L. Hultman, A. J. Raffo, A. L. Grzenda, P. E. Harris, T. R. Brown, S. O'Brien, *ACS Nano* **2008**, *2*, 477.

[30]   A. Merkoci, *Biosensing Using Nanomaterials*, John Wiley & Sons, Inc, Hoboken, NJ, **2009**.

[31]   C. S. S. R. Kumar, *Nanomaterials for Biosensors, Vol. 8*, Wiley-VCH, Germany, **2007**.

[32]   X. Michalet, F. F. Pinaud, L. A. Bentolila, J. M. Tsay, S. Doose, J. J. Li, G. Sundaresan, A. M. Wu, S. S. Gambhir, S. Weiss, *Science* **2005**, *307*, 538.

[33]   P. A. Alivisatos, W. Gu, C. Larabell, *Annual Review of Biomedical Engineering* **2005**, *7*, 55.

[34]   A. F. E. Hezinger, J. Tebmar, A. Gopferich, *European Journal of Pharmaceutics and Biopharmaceutics* **2008**, *68*, 138.

[35]   N. I. Hammer, T. Emrick, M. D. Barnes, *2* **2007**.

[36]   R. J. Martin-Palma, M. Manso, V. Torres-Costa, *Sensors* **2009**, *9*, 5149.

[37]   H. Duan, N. Shuming, *Journal of the American Chemical Society* **2007**, *129*, 3333.

[38]   C. Wu, B. Bull, C. Szymanski, K. Christensen, J. McNeill, *ACS Nano* **2008**, *2*, 2415.

[39]   K. Susumu, H. T. Uyeda, I. L. Medintz, T. Pons, J. B. Delehanty, H. Mattoussi, *Journal of the American Chemical Society* **2007**, *129*, 13987.

[40]   G. Ruan, A. Agrawal, A. I. Marcus, N. Shuming, *Journal of the American Chemical Society* **2007**, *129*, 14759.

[41]   J.-H. Park, G. von Maltzahn, E. Ruoslahti, S. N. Bhatia, M. J. Sailor, *Angewandte Chemie International Edition* **2008**, *47*, 7284.

[42]   B. Dubertret, P. Skourides, D. J. Norris, V. Noireaux, A. H. Brivanlou, A. Libchaber, *Science* **2002**, *298*, 1759.

[43]   S. D. Duhachek, J. R. Kenseth, G. P. Casale, G. J. Small, M. D. Porter, R. Jankowiak, *Analytical Chemistry* **2000**, *72*, 3709.

[44]   F. Pene, E. Courtine, A. Cariou, J.-P. Mira, *Critical Care Medicine* **2009**, *37*, S50.

[45]   A. Harmon, K. Uhrich, *Journal of Bioactive and Compatible Polymers* **2009**, *24*, 185.

[46]   L. Tian, L. Yam, N. Zhou, H. Tat, K. Uhrich, *Macromolecules* **2004**, *37*, 538.

[47]   Y. Liu, T. M. Reineke, *Journal of the American Chemical Society* **2005**, *127*, 3004.

[48]   N. M. Plourde, *Thesis (Ph.D.) -- Rutgers University* **2011**.

[49]   N. M. Plourde, S. Hehir, K. E. Uhrich, W. Welsh, P. V. Moghe, *in preparation*.

[50]   S. Hehir, L. Gu, K. E. Uhrich, *in preparation*.

[51]   L. Tao, K. Uhrich, *Journal of Colloid and Interface Science* **2006**, *298*, 102.

[52]   J. Djordjevic, M. Barch, K. Uhrich, *Pharmaceutical Research* **2005**, *22*, 24.

[53]   J. Djordjevic, L. Del Rosario, J. Wang, K. Uhrich, *Journal of Bioactive and Compatible Polymers* **2008**, *23*, 532.

[54]   E. Chnari, H. Lari, L. Tian, K. Uhrich, P. Moghe, *Biomaterials* **2005**, *26*, 3749.

[55]   E. Chnari, J. Nikitczuk, K. Uhrich, P. Moghe, *Biomacromolecules* **2006**, *7*, 597.

[56]   E. Chnari, J. Nikitczuk, J. Wang, K. Uhrich, P. Moghe, *Biomacromolecules* **2006**, *7*, 1796.

[57]   J. Wang, N. Plourde, N. Iverson, P. Moghe, K. Uhrich, *International Journal of Nanomedicine* **2007**, *2*, 697.

[58]   N. Plourde, S. Kortagere, W. Welsh, P. Moghe, *Biomacromolecules* **2009**, *10*, 1381.

[59]   M. Lougheed, C. Lum, W. Ling, H. Suzuki, K. Tatsuhiko, U. Steinbrecher, *Journal of Biological Chemistry* **1997**, *272*, 12938.

[60]   J. Berliner, J. Heinecke, *Free Radical Biology & Medicine* **1996**, *20*, 707.

[61]   M. Ramprasad, T. Valeska, N. Kondratenko, O. Quehenberger, D. Steinberg, *Proceedings of the National Academy of Sciences of the United States of America* **1996**, *93*, 14833.

[62]   D. Steinberg, *Journal of Biological Chemistry* **1997**, *272*, 20963.

[63]   T. Hiltunen, S. Yla-Herttuala, *Atherosclerosis* **1998**, *137 (Suppl)*, s81.

[64]   M. De Winther, K. Van Dijk, L. Havekes, M. Hofker, *Arteriosclerosis, Thrombosis, and Vascular Biology* **2000**, *20*, 290.

[65]   E. Podrez, M. Febbraio, N. Sheibani, D. Schmitt, R. Silverstein, D. Hajjar, P. Cohen, W. Frazier, H. Hoff, S. Hazen, *Journal of Clinical Investigation* **2000**, *105*, 1095.

[66]   A. Zaman, G. Helft, S. Worthley, J. Badimon, *Atherosclerosis* **2000**, *149*, 251.

[67]   A. Nicholson, J. Han, M. Febbraio, R. Silverstein, D. Hajjar, *Annals of the New York Academy of Sciences* **2001**, *947*, 224.

[68]   T. Yoshimoto, Y. Takahashi, T. Kinoshita, T. Sakashita, H. Inoue, T. Tanabe, *Advances in Experimental Medicine and Biology* **2002**, *507*, 403.

[69]   S. Yusuf, S. Reddy, S. Ounpuu, e. al, *Circulation* **2001**, *104*, 2746.

[70]   A. C. Li, C. Glass, *Nature Medicine* **2002**, *8*, 1235.

[71]   D. Lloyd-Jones, R. Adams, M. Carnethon, e. al., *Circulation* **2009**, *119*, 480.

2. STRUCTURE-PROPERTY RELATIONSHIPS OF NANOSCALE AMPHIPHILIC MACROMOLECULES FOR CONTROLLED INHIBITION OF CHOLESTEROL UPTAKE

2.1. Introduction

Atherosclerosis, triggered by interactions of macrophage, smooth muscle and endothelial cells with low-density lipoproteins (LDL) within the vascular wall, continues to be the major cause of cardiovascular disease and leading cause of adult mortality.[1-3] Macrophages play a central role in escalating this athero-inflammatory cycle as macrophages endocytose oxidized LDL (oxLDL) through unregulated scavenger receptors and form foam cells, the early hallmark of atherosclerotic plaques. The localized build-up of cholesterol within the vascular intima and the consequent athero-inflammatory cascade present a major challenge to current therapeutic strategies.[4-7]

2.2. Background

2.2.1. Atherosclerosis

Elevated levels of cellular and plasma cholesterol have serious consequences on the progression of cardiovascular disease, the leading cause of death in America.[5, 8, 9] The major carriers of cholesterol in blood plasma are LDLs, which enter the arterial walls through injured or leaky endothelial lining on the intima.[4, 5] Once LDL enters the intima, it can be oxidized, causing compositional alterations and compromising the ability of native LDL receptors on macrophage cells to recognize the oxidized LDL (oxLDL).[7] Rapid uptake of highly oxLDL (hoxLDL) occurs through scavenger receptors on the

macrophage cellular membrane, including scavenger receptor A (SRA), scavenger receptor B (SRB), CD36 and CD68. Scavenger receptors lack a feedback mechanism to control internalization, leading to excess cholesterol accumulation within the cytoplasm and triggering the development of foam cells and fatty streaks, a key characteristic of early atherogenisis.[10-19]

2.2.2. Current Therapeutic Stategies

Many treatment options have been developed to lower systemic levels of cholesterol, however, they are known to cause adverse side effects - from gastrointestinal complaints to liver enzyme elevation and myopathy.[20, 21] Alternate approaches to directly limit macrophage recruitment and atherogenesis have also been investigated, including scavenger receptor knockdown[22, 23] as well as cholesterol acyl- transferase (ACAT)-1 and ACAT-2 suppression.[24] Deletion of scavenger receptors SR-A and CD36 caused a marked decrease in the progression of advanced necrotic lesions in ApoE-/- mice[25], indicating that scavenger receptors play a key role in disease progression. A parallel approach has been the inhibition of monocyte recruitment and macrophage differentiation;[26] for example, the recent administration of dehydroepiandrosterone inhibited macrophage infiltration, independent of systemic cholesterol levels.[27]

2.2.3. Carboxy-terminated AMs as Bioactive Polymer Ligands

Our laboratory, in collaboration with Professor Prabhas Moghe's laboratory in the Department of Biomedical Engineering at Rutgers University, previously explored AMs for inhibiting hoxLDL uptake through competitive inhibition of scavenger receptors on murine macrophages.[28-32] Preliminary results were performed with three polymers, **1cM**, **1cP**, and **0cM**. These polymers were studied for their variations in location, or existence,

of a carboxylic acid terminal group; **1cM** has a carboxylic acid on the end of the hydrophobic component while **1cP** has its carboxylic acid on the chain end of the hydrophilic PEG and **0cM** has no carboxylic acid (shown in **Figure 2.1**). As shown in **Figure 2.1**, **1cM** inhibited oxLDL with the greatest efficacy compared with the other polymers tested, **1cP** and **0cM**, under serum-free conditions.
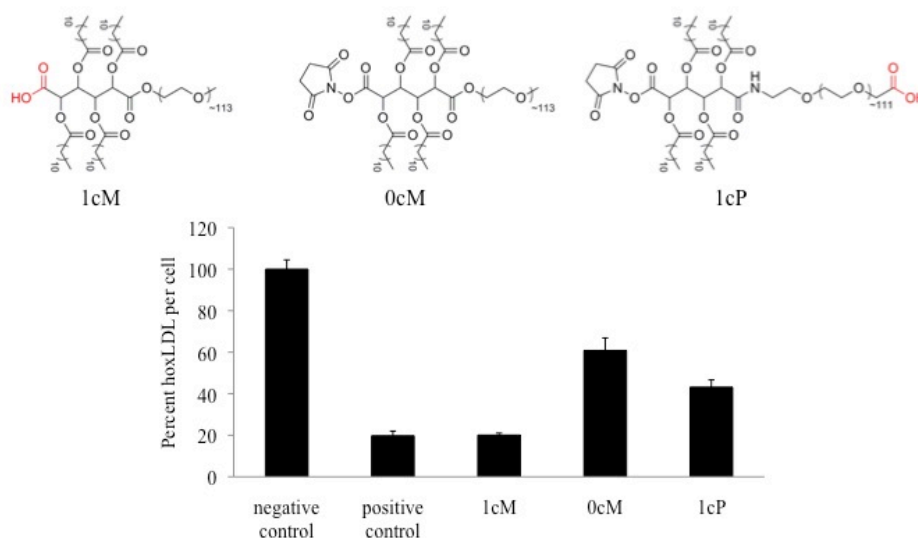
Figure 2.1. Results of preliminary studies to determine the effect of the location of the carboxylic acid on AMs on the ability of the polymers to inhibit hoxLDL uptake under serum-free conditions. The negative control is the uptake of fluorescently labeled hoxLDL in THP-1 macrophages with no polymer and the positive control is the uptake of the hoxLDL in the presence of a SR-A antibody.

Despite the early promise of the AMs, the relationship between polymer structure and activity for controlled inhibition of cholesterol uptake is not clear, particularly under physiological conditions.

In this work, AMs with systematic structural variations were synthesized to identify the critical elements that contribute to the AM's ability to inhibit hoxLDL uptake by human THP-1 macrophage cells cultured *in vitro*, under both serum-lacking and serum-containing conditions. Six key parameters were varied and the resulting degree of hoxLDL uptake was quantitatively compared: length of the PEG chain, anionic charge location, type of anionic charge, number of anionic charges, rotational motion of the anionic group, and PEG architecture. We hypothesized that the most efficient polymer for hoxLDL inhibition would: i) be amphiphilic; ii) have the greatest amount of anionic charge possible within the hydrophobic portion, which would result in increased charge density to promote honing and subsequent binding to the positively charged scavenger receptor; and iii) have two, short-chain linear PEG chains conjugated to the hydrophobic backbone *via* a branch-point, to better shield the anionic charge and stabilize the nanoassemblies from disruption by serum proteins.

2.2 Results and Discussion

2.3.1. Synthesis of Structurally and Architecturally Modified AMs

A range of AMs were designed (see **Table 2.1**) based upon results from previous work[28-32] and synthesized to determine the most effective inhibitor of hoxLDL uptake. Several AMs were previously synthesized for a variety of applications.[28-39] New AMs were synthesized from these previously published compounds as summarized in **Scheme 2.1**.

Polymer Name	Final Structure	Schematic	PEG Length	Charge Location	Charge Number	Type of Charge	PEG Architecture
1cM			Long	Hydrophobic	1	Carboxylic Acid	1 Linear
1cM- 2000			Short	Hydrophobic	1	Carboxylic Acid	1 Linear
0cM			Long	None	0	None	1 Linear
1cP			Long	Hydrophilic	1	Carboxylic Acid	1 Linear
1sM			Long	Hydrophobic	1	Sulfate	1 Linear
2cM			Long	Hydrophobic	2	Carboxylic Acid	1 Linear
2cbM			Long	Hydrophobic	2	Carboxylic Acid	1 Linear
1cM-2000x2			Short x2	Hydrophobic	1	Carboxylic Acid	2 Linear from a branch point
0cM-2000x2			Short x2	None	0	None	2 Linear from a branch point

TABLE 2.1: Chemical structures, schematics representing the placement of anionic charge, and information regarding PEG length (where 2 kDa is indicated by "short" and 5 kDa by "long"), charge location, number of charges, type of anionic charge, and PEG architecture for all AMs.
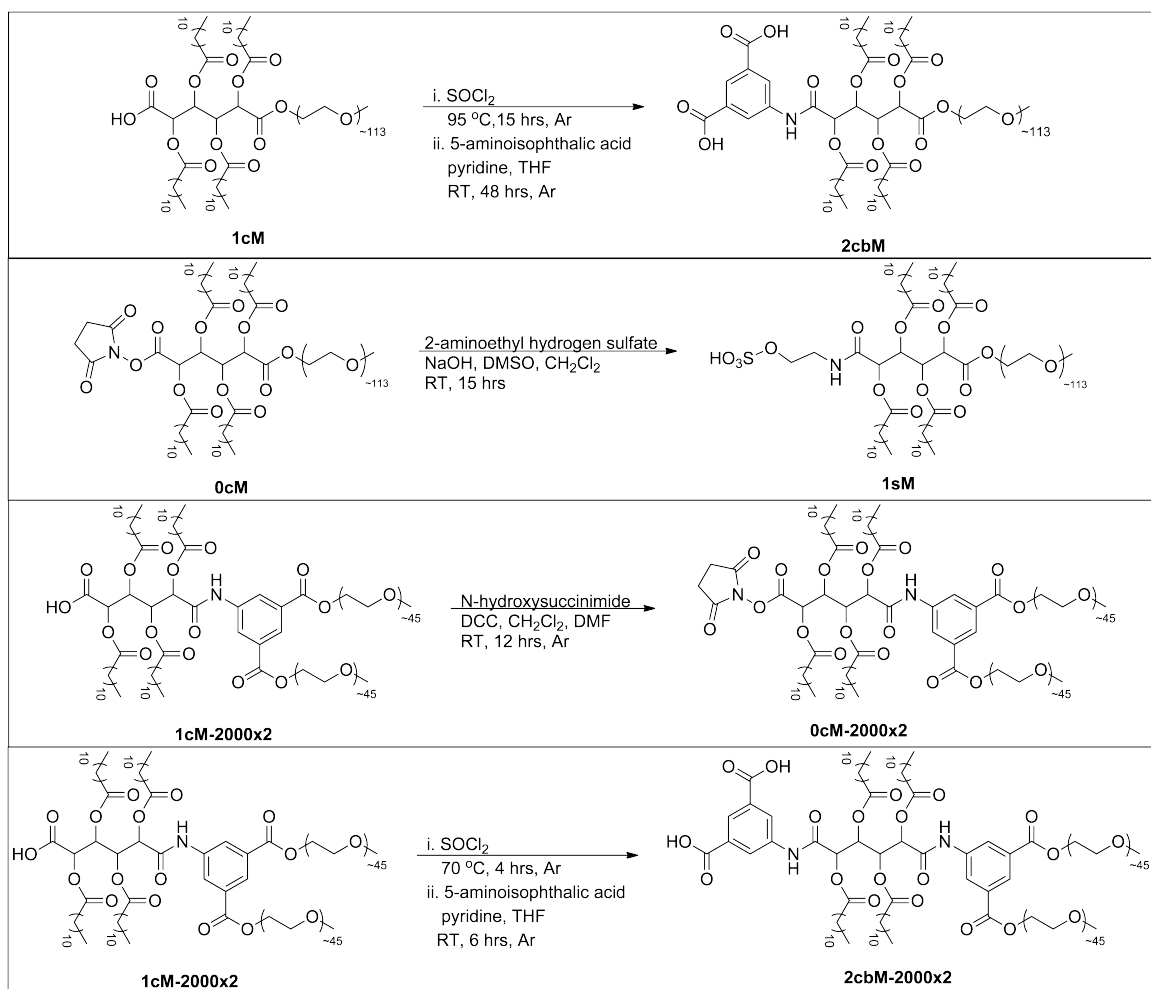
Scheme 2.1: Synthesis of newly synthesized AMs (**2cbM, 1sM, 0cM-2000x2, and 2cbM-2000x2)** for screening as inhibitors of hoxLDL uptake.

The parent compounds, **1cM** and **1cM-2000x2**, served as building blocks for subsequent modifications. Specifically, the carboxylic acid on the mucic acid backbone of **1cM** and **1cM-2000x2** was activated with N-hydroxysuccinimide or thionyl chloride to functionalize the polymers with a small linker molecule containing the desired functionality, such as a sulfate to yield **1sM** or dicarboxylic acid to yield **2cbM** and **2cbM-2000x2**. Polymer structures were verified by proton nuclear magnetic resonance (^{1}H NMR) spectroscopy and molecular weight determined by gel permeation

chromatography (GPC) relative to PEG standards. Due to the abundance of PEG in the polymers (~83 % of protons), the presence of new protons in the ^{1}H NMR spectra were often difficult to detect, particularly from 0.8 to 2.4 ppm where the methylene protons of the hydrophobic chains comprise the majority of that region. Thus, spectra were monitored for the disappearance of the protons of the activating group (N-hydroxysuccinimide) at 2.8 ppm, or the appearance of aromatic protons (**2cbM** and **2cbM-2000x2**) at ~ 8.4 ppm.

In total, ten AMs were tested for their ability to inhibit hoxLDL uptake, both with and without serum. The polymer characteristics tested were amphiphilicity, branching of the hydrophobic region, length of the PEG chain, anionic charge location, type of anionic charge, number of anionic groups, rotational motion of the charged group, and PEG architecture. Structures of all polymers, schematics representing the placement of anionic charge, and information regarding specific variable parameters are shown in **Table 2.1**. As the precise mechanism for uptake was unknown, screening this polymer array was expected to identify the key structural parameters for inhibiting hoxLDL uptake.

2.3.2. Inhibition of hoxLDL Uptake

The in vitro hoxLDL uptake studies were performed by Nicole Iverson, a Ph.D. candidate in Biomedical Engineering (Rutgers University, Piscataway, NJ) supervised by Professor Prabhas V. Moghe. However, the results were mutually and collaboratively discussed and outlined below.

The combined results for hoxLDL uptake were normalized to respective cell number across all polymer configurations synthesized and shown in **Figure 2.2.** Additionally, fluorescent images of boron-dipyrromethene (BODIPY)-labeled hoxLDL

uptake for the two most efficient AMs (**1cM** and **2cbM-2000x2**) compared with hoxLDL uptake alone are shown in **Figure 2.3**. The highly efficient AMs perform comparably to positive control (SRA antibody blockage), with hoxLDL uptake inhibited by about 20% after 24 hours in serum-free conditions. The early serum-free data correlates well with the 48 hour data in serum-containing conditions. These trends suggest that it takes longer (more than 24 hours) to reverse the serum protein-mediated competitive blockage of polymer-receptor binding via serum proteins. Thus, behaviors of polymer binding to macrophages at early times in serum-free conditions, which may be primarily scavenger receptor mediated, are similar to longer times in serum-containing conditions.
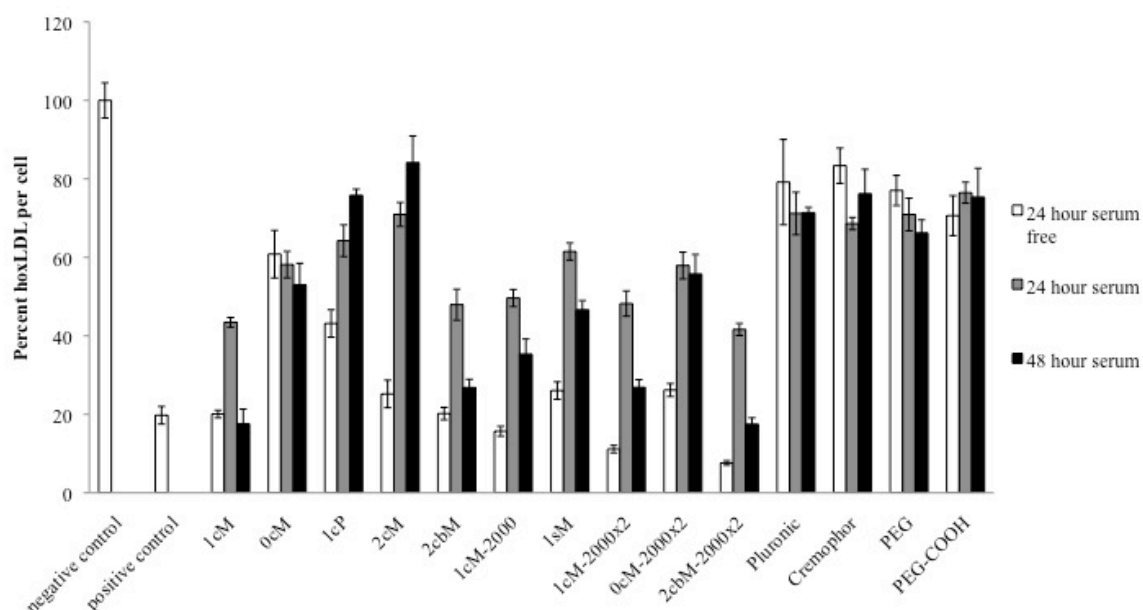
Figure 2.2: Internalization of hoxLDL by THP-1 macrophage cells after incubation with 10^{-6} M AMs for 24 or 48 hours with and without 5 % FBS. Levels of hoxLDL were measured and quantified in comparison to corresponding hoxLDL treated cells that were not treated with any polymers.
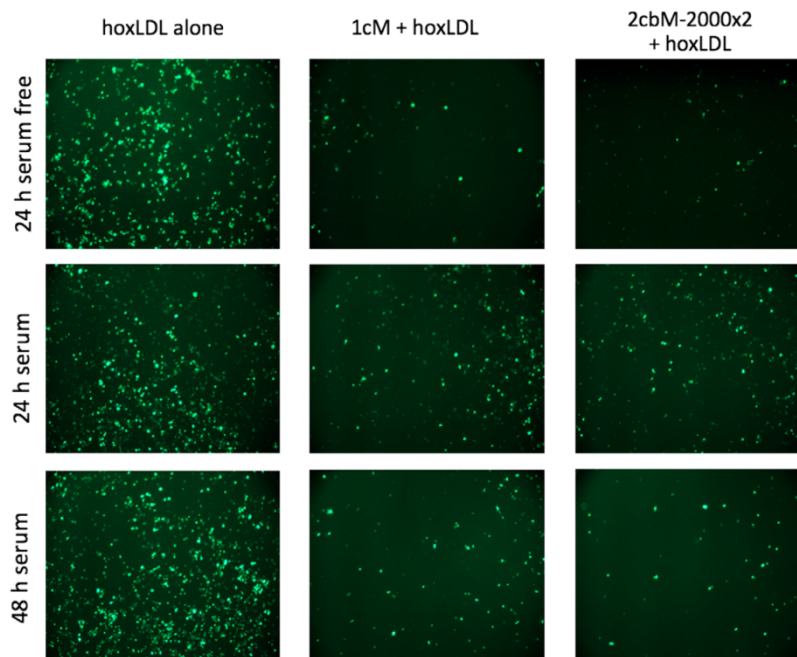
Figure 2.3: Fluorescent images of BODIPY-labeled hoxLDL uptake for hoxLDL alone (negative control), hoxLDL with **1cM**, and hoxLDL with **2cbM-2000x2** (the two most efficient polymers at inhibiting hoxLDL uptake).

The inhibitory results, discussed in depth below, were not due to polymer cytotoxicity as judged by cell morphology and cell counts for each polymer. It has been previously reported using IC21 murine macrophage cultures that these polymers are highly biocompatible *in vitro*, even at two orders-of-magnitude higher concentrations.[28] In addition, the parent polymer, **1cM**, was also reported as non-cytotoxic in human umbilical endothelial cells (HUVEC), umbilical arterial smooth muscle cells (UASM), and normal dermal human fibroblasts (NDHF).[35]

2.3.2.1. Role of Amphiphilicity

To examine the role of the amphiphilicity, the efficiency of control polymers, **PEG** and **PEG-COOH**, to inhibit hoxLDL internalization was tested. **PEG** is a common

hydrophilic polymer chosen for its biocompatibility and ability to evade excretion from the bloodstream by the reticuloendothelial system (RES).[40-42] The PEGs tested here were chosen because they have the same average molecular weight as the PEG of **1cM. PEG-COOH** was chosen due to the presence of the anionic charge, which has been found to be a key parameter for AM inhibition of hoxLDL uptake.[28-32] Additionally, in modeling studies, Plourde et. al. observed that the binding energy of a **PEG-COOH** was half that of **1cM** when docked with an SR-A collagen-like domain homology model.[31] Based on these modeling results, **PEG-COOH** was anticipated to inhibit hoxLDL better than **0cM,** but to a lower extent than **1cM**, while **PEG** was anticipated to behave like **0cM** or have no effect at all.

As shown in **Figure 2.4**, the amphiphilic polymers, **0cM** and **1cM**, consistently inhibited hoxLDL internalization to a greater extent than both anionically terminated or unfunctionalized hydrophilic **PEGs** under all conditions. Notably, **1cM** was the only polymer that showed significant inhibition of uptake at all conditions, whereas **0cM** showed modest levels of effect, suggesting that the combination of amphiphilicity and anionic charge presentation is operative in early competitive studies. Additionally, as **PEG-COOH** had little effect with or without serum, this result suggests that the anionic group on the hydrophobic portion of the polymer may be more effective, which is discussed later (**Section 2.3.2.4**).
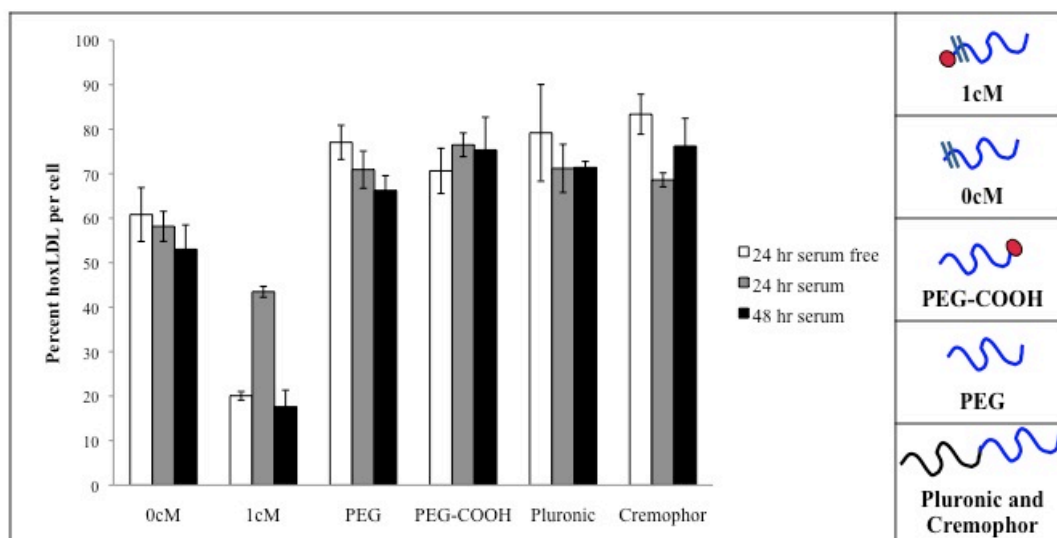
Figure 2.4: The uptake of hoxLDL in THP-1 macrophages as a function of polymer amphiphilicity and branching of the hydrophobic region.

2.3.2.2. Role of Branching of the Hydrophobic Region

To examine the effect of the branched hydrophobic region of AMs, the well-known amphiphiles Pluronic P85 and Cremophor EL were tested for their ability to effect hoxLDL internalization. Pluronic P85 and Cremophor EL were chosen based on their structural similarity to AMs with respect to their hydrophilic PEG regions. Additionally, they are similarly amphiphilic, biocompatible and widely studied for pharmaceutical applications.[43-46]

As shown in **Figure 2.4**, compared with Pluronic P85 and Cremophor EL, the AMs, specifically **1cM** and **0cM** shown here, competed far more effectively with hoxLDL uptake whereas Pluronic P85 and Cremophor EL had little effect on hoxLDL uptake. These results highlight the importance of the branched architecture of the hydrophobic component of the AMs, which allows them to significantly reduce hoxLDL uptake.

2.3.2.3. Role of PEG Chain Length

The ability of PEG to evade excretion by the RES system is generally attributed to PEG's ability to shield the system from disruption by serum proteins.[40-42] Based upon the literature, a longer PEG chain length was anticipated to yield increased stability in serum caused by additional PEG density resulting in more chain entanglements, providing enhanced micelle stability and protection of the critical anionic charge.[40-42] This expectation was confirmed in testing AMs with hydrophilic PEG molecular weights of 2 kDa (**1cM-2000**) and 5 kDa (**1cM**). As shown in **Figure 2.5**, at the 24 hour time point with and without serum, **1cM** and **1cM-2000** have comparable levels of hoxLDL inhibition. However, after 48 hours in the presence of serum, the longer PEG chain length was most effective at hoxLDL inhibition. This result confirms the hypothesis that increased PEG length results in increased chain entanglements, better micellar stability and protection of the anionic charge from serum protein disruption.
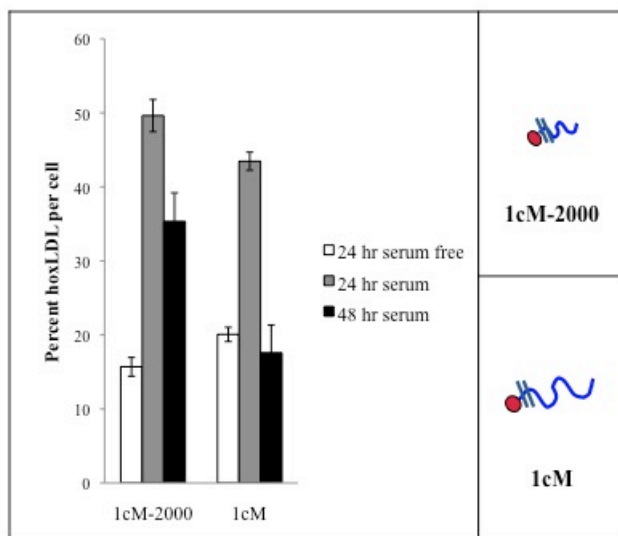
Figure 2.5: The uptake of hoxLDL in THP-1 macrophages as a function of PEG chain length.

2.3.2.4. Role of Carboxylic Acid Location

As previously stated, AM inhibition of hoxLDL uptake by macrophage cells occurs by competitive binding between AMs and hoxLDL for positively charged scavenger receptors.[30, 31] Thus, it is necessary for the anionic group of AMs to be readily available and easily bound in the receptor pocket. Our initial hypothesis was that the anionic group on the hydrophilic, or external, portion of the micelle would be more accessible for binding to scavenger receptors and increased binding would lead to better inhibition of hoxLDL uptake. However, modeling studies and *in vitro* testing in the absence of serum demonstrated that the anionic charge in the <u>hydrophobic region</u> of the polymer was more effective at inhibiting hoxLDL uptake.[30-32] These results were confirmed herein and, expanding on previous work, in the presence of serum both at 24 and 48 hours **1cM** performed significantly better than **1cP**, as shown in **Figure 2.6**. This effect is likely due to the interaction of serum proteins with the carboxylic group, which is not shielded by PEG when it is positioned on the hydrophilic portion of the micelle. For serum- and non-serum-containing conditions, the greater charge density that results from having the anionic charge within the hydrophobic interior when micellization occurs may lead to greater hoxLDL inhibition. In addition, the hydrophobic core is conformationally rigid, such that the carboxylic acid has less rotational freedom and a better ability to lock into the active site on scavenger receptors.[47]
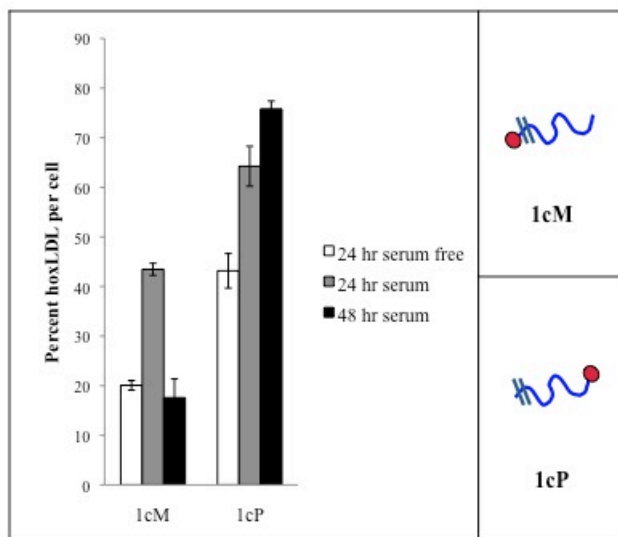
Figure 2.6: The uptake of hoxLDL in THP-1 macrophages as a function of carboxylic acid location.

2.3.2.5. Role of Anionic Charge Type

Like carboxylic acids, sulfates have also been shown to bind to scavenger receptors and thus inhibit hoxLDL uptake.[48] To investigate this nature-mimicking capability, a sulfate moiety (**1sM**) was incorporated into the hydrophobic portion of the polymer. In contrast to **1cM**, whose anionic group would likely have a pKa of 3-4 [49], the pKa of the hydrogen sulfate moiety is likely < -3 [50]. However, independent of their microenvironments, both acids would likely be deprotonated at physiological pH. In the absence of serum, both **1cM** and **1sM** inhibited hoxLDL uptake more than the non-acidic system (**0cM**), but **1cM** did so to a far greater extent than **1sM**, as shown in **Figure 2.7**. However, in serum-containing conditions at 24 and 48 hours, **1sM** inhibited hoxLDL uptake on a similar level to **0cM**, significantly less than **1cM**. This result may be due to the decreased steric hindrance surrounding the sulfate, making it more readily available for interactions such as hydrogen bonding with other residues of the scavenger receptor.

Additionally, the methylene spacer increases the rotational motion available to the **1sM**, which may result in inadequate binding to the active receptor site. The role of decreased steric hindrance surrounding the anionic group and increased rotational motion will be discussed in later sections (**Section 2.3.2.7**).
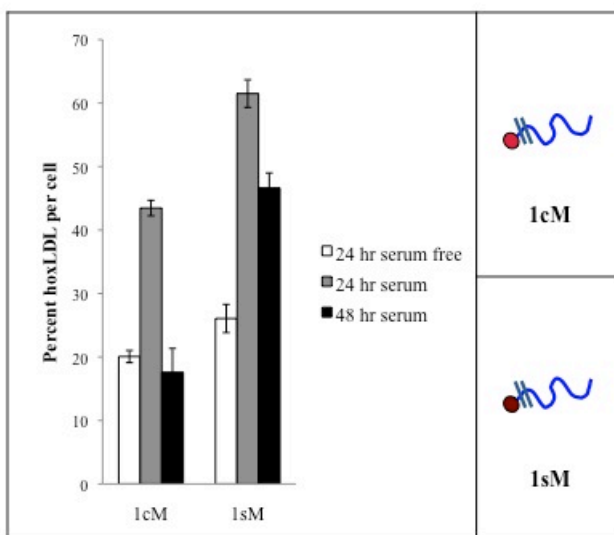
Figure 2.7: Uptake of hoxLDL in THP-1 macrophages as a function of the type of anionic group; carboxylic acid vs. sulfate.

2.3.2.6. Role of Number of Anionic Charges

The number of anionic charges was investigated by comparing **1cM**, **0cM**, and **2cbM**. Increasing the number of charge groups was anticipated to result in greater charge density, which would result in more significant attraction of the AMs to the positively charged binding pocket on scavenger receptors and, therefore, greater hoxLDL uptake inhibition. Additionally, the addition of a spacer molecule was expected to reduce the steric hindrance surrounding the carboxylic acid and allow better access to the binding site, which would decrease hoxLDL uptake. However, as shown in **Figure 2.8**, the additional carboxylic acid with an aromatic spacer, **2cbM**, shows hoxLDL uptake

inhibition comparable to that of **1cM** for all time points.
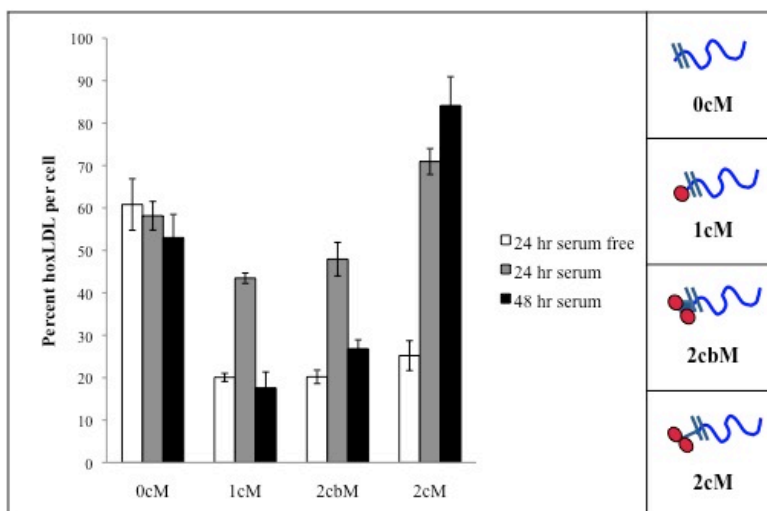
Figure 2.8: The uptake of hoxLDL in THP-1 macrophages as a function of the number of anionic charges and rotational motion of those charges.

We postulate that this result is due to the ability of only one carboxylic acid to bind to scavenger receptors at a time. Thus, the addition of more carboxylic acids does not provide any additional benefit. In fact, modeling studies by Plourde et al. showed that additional carboxylic acids actually <u>lowered</u> the overall AM binding affinity due to hydrogen bonding with residues in the scavenger receptor binding pocket that inhibited binding of the AM to the active site.[31] This result suggests that the carboxylic acids may be too readily accessible for the first interaction they encounter, which is hydrogen bonding rather than binding within the active site. Further, this data indicates that despite the steric hindrance surrounding the carboxylic acid of **1cM**, the carboxylic acid is available for binding and that adding a spacer molecule to increase availability may potentially hinder binding.

2.3.2.7. Role of Anionic Group Rotational Motion

To analyze the impact of rotational motion, the aromatic dicarboxylic acid-containing **2cbM** was compared with the aliphatic dicarboxylic acid-containing **2cM**, which allows the carboxylic acids more freedom for rotation and movement. In addition to the difference in flexibility, the spacers also result in differing carboxylic acid pKa's; independent of their microenvironments, the pKa of the **2cM** carboxylic acids would be approximately 2 and 4 [51] while those of the **2cbM** isophthalic group would be approximately 3.5 and 4.5 [52]. However, at the pH utilized in this work, physiological pH, both carboxylic acids for **2cM** and **2cbM** would likely be deprotonated.

It was anticipated that changing the rotational motion would have a significant impact on scavenger receptor ability to bind the carboxylic acid. As **2cM** has aliphatic carboxylic acids, the rotational motion is less restricted than the aromatic carboxylic acids of **2cbM**. As shown in **Figure 2.8**, the aromatic carboxylic acids on **2bcM** result in significantly greater hoxLDL uptake inhibition than **2cM** for all time points, both with and without serum. Also, **2cM** behaves like **1cP** with respect to the extended time point in serum, both of which did not result in lower percent hoxLDL per cell than 24 hours in serum. Although the carboxylic acids are in different regions of the polymer, in both **1cP** and **2cM** the carboxylic acids have significantly more rotational motion as aliphatic components. These results indicate that restricted rotational motion of the anionic group is essential for the carboxylic acid to effectively bind to the scavenger receptor active site. Additionally, this result suggests that the steric hindrance surrounding the carboxylic acid of **1cM** restricts the rotational motion of the carboxylic acid such that the carboxylic acid is capable of enhanced binding.

2.3.2.8. Role of PEG Architecture

Finally, a structural branching point to which two, short-chained PEGs were attached was anticipated to provide increased stabilization against serum proteins.[34, 53] To maintain overall PEG content, each PEG arm was 2 kDa in molecular weight, compared to the linear AMs with PEG 5 kDa. AMs with zero, one, and two carboxylic acids in the hydrophobic core were synthesized with this architectural branching point and tested for hoxLDL uptake inhibition. As shown in **Figure 2.9**, all AMs with the PEG branching point inhibited hoxLDL more significantly than their linear counterparts without serum. In the absence of serum, **2cbM-2000x2** results in the lowest percent of hoxLDL per cell overall, edging out **1cM**, which typically outperforms all other polymers. In serum-containing conditions for both 24 and 48 hours, the AMs with a PEG branching point inhibited hoxLDL at similar levels to their linear counterparts except for the **2cbM-2000x2** and **2cbM** polymers. At 48 hours, the **2cbM-2000x2** significantly inhibited hoxLDL internalization over **2cbM**. However, while **2cbM-2000x2** out performs its linear counterpart, inhibition of hoxLDL uptake is statistically the same as **1cM**.
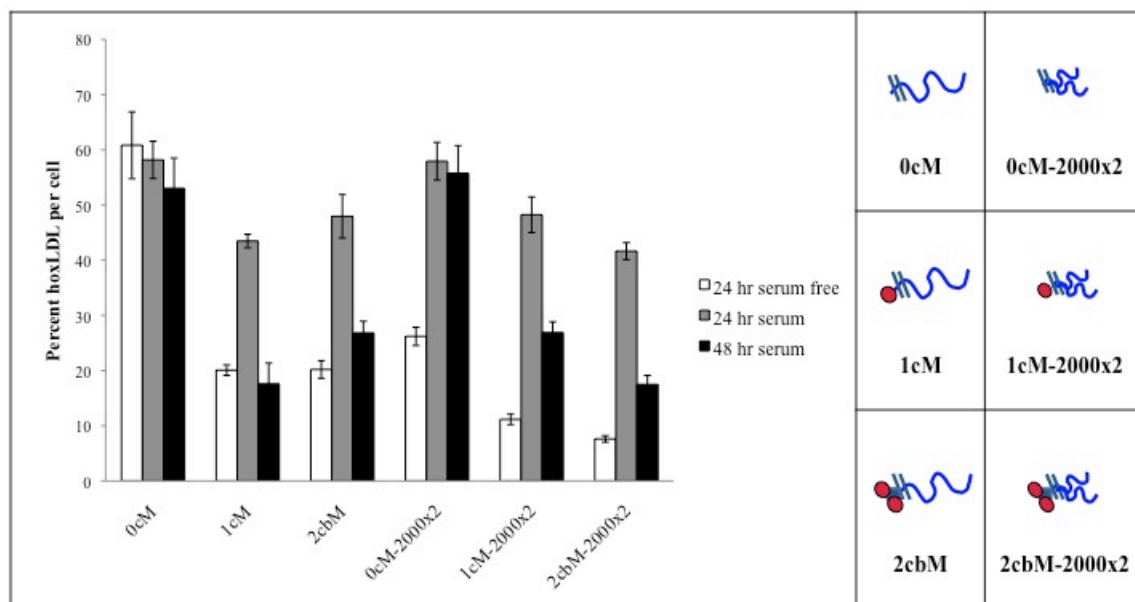
Figure 2.9: The uptake of hoxLDL in THP-1 macrophages as a function of PEG architecture.

Generally, utilizing two, short-chain PEGs emanating from a branch-point resulted in more efficient hoxLDL inhibition compared to their linear counterparts under serum-free conditions. However, providing a PEG branching point did not significantly alter the polymer's hoxLDL inhibitory capacity compared with the linear polymers in serum-containing conditions. While a PEG branching point likely increases shielding of the micellar hydrophobic core, the linear PEG (5 kDa molecular weight) results in significant chain entanglements, as seen with the **1cM-2000** and **1cM** polymers, such that utilizing a branching point with lower molecular weight PEGs did not significantly passivate against serum proteins, and consequently did not alter the hoxLDL inhibition.

2.4. Summary

Overall, AMs exhibit rich structure-function relationship behaviors regarding the hoxLDL uptake inhibition in macrophages. Within the AM compositions, longer PEG chains were more efficient at protecting AMs in serum-containing conditions. One rotationally-restricted carboxylic acid within the hydrophobic core was sufficient for producing the most effective hoxLDL inhibiting AM. By increasing charge and changing the PEG architecture to two, short-chain, linear PEGs emanating from a branch point, significant improvements were not observed for decreasing hoxLDL uptake. These findings have implications for designing polymers for improved competitive inhibition of intimal cholesterol uptake under physiological as well as pathologic conditions.[20, 54]

In summary, the tunability of the parent AMs enables structure optimization. The ultimate goal of this study was to provide insights regarding rational biomaterial design criteria to inhibit hoxLDL uptake. These insights are ultimately relevant for evaluating biomaterial performance *in vivo* for localized treatment of atherosclerotic lesions. To optimize the AM properties, several structural characteristics were analyzed: length of the PEG chain, carboxylic acid location, type of anionic charge, number of anionic charges, rotational motion of the anionic group, and PEG architecture. Each AM was tested without serum and in the presence of serum for 24 and 48 hours to determine its ability to inhibit hoxLDL uptake in THP-1 human macrophage cells. The parent AM **1cM**, with its rigid, hydrophobic carboxylic acid and linear PEG chain of 5 kDa was the most efficient at inhibiting hoxLDL internalization by THP-1 human macrophage cells in serum. While altering the PEG architecture, **1cM-2000x2** and **2cbM-2000x2**, produced AMs equally efficient in their hoxLDL uptake inhbition, **1cM** is far superior when considering

polymer cost and production time. Future efforts will delve deeper into understanding the receptor-mediated processes that effect hoxLDL inhibition. Translational research is also ongoing to test the selected AMs within animal models of atherogenesis and inflammation.

2.5. Experimental

2.5.1. Synthetic Materials

Unless otherwise stated, solvents and reagents were purchased from Fisher Scientific (Pittsburgh, PA) and Sigma-Aldrich (St. Louis, MO) and used as received. PEG 5 kDa was purchased from Polysciences, Inc. (Warrington, PA) and dried by azeotropic distillation from toluene before use. Specialty, functionalized PEGs were purchased from Laysan Bio, Inc (Arab, AL) and used as received. Several polymers were prepared as previously described: **1cM**[33], **1cM-2000**[33], **0cM**[36], **2cM**[32], **1cP**[29], **1cM-2000x2**[34], **0cM-2000x2**[55], **2cbM-2000x2**[55].

2.5.2. Characterization Methods

2.5.2.1. Proton Nuclear Magnetic Resonance (^{1}H NMR) Spectroscopy

Proton nuclear magnetic resonance (^{1}H-NMR) spectra of the products were obtained using a Varian 400 MHz or 500 MHz spectrophotometer. Samples were dissolved in chloroform-d, with a few drops of dimethyl sulfoxide-d_6 if necessary, with tetramethylsilane as an internal reference.

2.5.2.2. Gel Permeation Chromatography (GPC)

Molecular weights (M_w) and polydispersity indices (PDI) were determined using gel permeation chromatography (GPC) with respect to PEG standards (Sigma-Aldrich)

on a Waters Stryagel® HR 3 THF column (7.8 x 300 mm). The Waters LC system (Milford, MA) was equipped with a 2414 refractive index detector, a 1515 isocratic HPLC pump, and 717plus autosampler. An IBM ThinkCentre computer with Waters Breeze Version 3.30 software installed was used for collection and processing of data. Samples were prepared at a concentration of 10 mg/mL in tetrahydrofuran, filtered using 0.45 μm pore size nylon or polytetrafluoroethylene syringe filters (Fisher Scientific) and placed in sample vials to be injected into the system.

2.5.2.3. Differential Scanning Calorimetry (DSC)

Melting points were determined by DSC on a TA DSC Q200. TA Universal Analysis 2000 software was used for data collection on a Dell Dimension 3000 computer. Samples (3-5 mg) were heated under dry nitrogen gas. Data were collected at heating and cooling rates of 10 °C /min with a two-cycle minimum.

2.5.3. Polymer Synthesis

2.5.3.1. 2cbM

The carboxylic acid of **1cM** (0.56 g, 0.094 mmol) was activated with $SOCl_2$ (50 mL) at 90 °C overnight under argon gas. Excess $SOCl_2$ was removed *via* rotary evaporation and the yellow oil subsequently dissolved in anhydrous THF (15 mL) and anhydrous pyridine (1 mL). 5-Aminoisophthalic acid (0.14 g, 0.75 mmol) in anhydrous THF (16 mL) and anhydrous pyridine (2 mL) was then added to the reaction flask and allowed to react for 48 hours at room temperature under argon. THF and pyridine were removed *via* rotary evaporation and the resulting oil dissolved in CH_2Cl_2, washed with 1N HCl and brine, dried over $MgSO_4$, and concentrated. The desired product was then precipitated from CH_2Cl_2 by addition of 10-fold diethyl ether and the solid collected by

centrifugation. Solvent was removed by decanting and the resulting yellow solid was dried under ambient atmosphere (12 hrs) and under high vacuum (12 hrs). Yield: 0.52 g, 91 %. ^{1}H- NMR (CDCl$_3$): δ 8.61 (m, 1H, ArH), 8.17 (m, 2H, ArH), 5.70 (m, 2H, CH), 5.20 (m, 2H, CH), 4.24 (m, 2H, CH$_2$), 3.60 (m, ~0.45 kH, CH$_2$O), 3.38 (s, 3H, CH$_3$), 2.44 (m, 4H, CH$_2$), 2.29 (m,4H, CH$_2$), 1.60 (m, 8H, CH$_2$), 1.26 (m, 64H, CH$_2$), 0.88 (t, 12H, CH$_3$). T_m = 56 °C GPC: M_w: 6.3 kDa; PDI: 1.09.

2.5.3.2. 1sM

2-Aminoethyl hydrogen sulfate (7.0 mg, 0.050 mmol) was dissolved in DMSO (2 mL) by warming over medium heat on a stir plate for 15-30 min. After cooling to room temperature, 0.5 M NaOH (101 μL) was added and the solution stirred for 30 min. In a separate flask, **0cM** (0.20 g, 0.033 mmol) was dissolved in CH$_2$Cl$_2$ (6.0 mL) and subsequently added to the solution of 2-aminoethyl hydrogen sulfate dropwise and the reaction stirred overnight (12 hrs). The CH$_2$Cl$_2$ was then removed *via* rotary evaporation then the DMSO removed *via* lyophilization. The resulting solid was dissolved in CH$_2$Cl$_2$ and the solution filtered to remove excess 2-aminoethyl hydrogen sulfate and the N-hydroxysuccinimide by-product. The desired product was precipitated from CH$_2$Cl$_2$ by addition of 10-fold diethyl ether and the solid collected by centrifugation. Solvent was removed by decanting and the resulting yellow solid was dried under ambient atmosphere (12 hrs) and under high vacuum (12 hrs). Yield: 0.16 g, 78 %. ^{1}H-NMR (CDCl$_3$): δ 5.83 (m, 2H, CH), 5.48 (m, 2H, CH), 3.67 (m, ~0.45 kH, CH$_2$O), 3.38 (s, 3H, CH$_3$), 2.32 (m, 8H, CH$_2$), 1.60 (m, 8H, CH$_2$), 1.22 (m, 64H, CH$_2$), 0.88 (t, 12H, CH$_3$).

T_m = 55 °C. GPC: M_w: 6.4 kDa; PDI: 1.08.

2.5.4. *In Vitro* Inhibition of oxLDL

[Cell studies were performed by Nicole Iverson, Department of Biomedical Engineering, Rutgers University, Piscataway, NJ, under the supervision of Professor Prabhas V. Moghe]

2.5.4.1. Cell Culture

Human THP-1 monocytes (ATCC), were grown in suspension, at a concentration of 100,000 cells/cm$_2$ with Roswell Park Memorial Institute (RPMI) medium containing 0.4 mM Ca^{2+} and Mg^{2+} (ATCC) and supplemented with 10 % fetal bovine serum (FBS), in an incubator with 5 % CO$_2$ at 37 °C and split every four days through centrifugation. The cells were seeded at a concentration of 100,000 cells/cm^2 and differentiated from monocytes into adherent macrophage cells by the addition of 16 nM phorbol myristate acetate. [31] Once differentiated, the macrophage cells were not propagated and were used within one week of differentiation.

2.5.4.2. LDL Oxidation to hoxLDL

Highly oxidized LDL (hoxLDL) was prepared by oxidation of LDL within five days of each experiment. BODIPY-labeled human plasma derived LDL (Molecular Probes, OR) was oxidized by incubation with 10 μM CuSO$_4$ (Sigma) for 18 hrs at 37 °C with 5 % CO$_2$ before oxidation was stopped with the addition of 0.01 % w/v EDTA (Sigma).

2.5.4.3. hoxLDL Internalization

Internalization of hoxLDL by macrophage cells was assayed, either with or without 5% FBS, by incubating fluorescently labeled hoxLDL (10 μg/mL) and the various polymer conditions, at 10^{-6} M, with cells for 24 or 48 hours at 37 °C and 5 %

CO_2. Test conditions also included two controls: RMPI medium and polymers alone to ensure that no cell or polymer auto-fluorescence was observed. The cells were then washed twice with PBS and imaged for cell-associated fluorescence. Images were analyzed using Image Pro Plus 5.1 software (Media Cybernetics, San Diego, CA) and fluorescence was normalized to cell number before being compared to the sample with only hoxLDL,

2.5.4.4. Statistical Analysis

Error bars on graphs indicate standard error of the mean based upon biological triplicate samples in each experiment and three separate experiments for each condition. Single factor ANOVA with Tukey's post-hoc analysis, performed on SPSS software, was used for statistical analysis. Significance is claimed for differences of $p < 0.05$

2.6. References

[1]   S. Yusuf, S. Reddy, S. Ounpuu, e. al, *Circulation* **2001**, *104*, 2746.
[2]   A. C. Li, C. Glass, *Nature Medicine* **2002**, *8*, 1235.
[3]   D. Lloyd-Jones, R. Adams, M. Carnethon, e. al., *Circulation* **2009**, *119*, 480.
[4]   M. Gimbrone, Jr, *Thrombosis and Haemostasis* **1999**, *82*, 722.
[5]   A. Lusis, *Nature (London)* **2000**, *407*, 233.
[6]   M. Brown, J. Goldstein, *Annual Review of Biochemistry* **1983**, *52*, 223.
[7]   J. Goldstein, Y. Ho, S. Basu, M. Brown, *Proceedings of the National Academy of Sciences of the United States of America* **1979**, *76*, 333.
[8]   C. Glass, J. Witztum, *Cell* **2001**, *104*, 503.
[9]   M. Bradley, C. Hong, M. Chen, S. Joseph, D. Wilpitz, X. Wang, A. Lusis, A. Collins, W. Hseuh, J. Collins, R. Tangirala, P. Tontonoz, *The Journal of Clinical Investigation* **2007**, *117*, 2337.
[10]   M. Lougheed, C. Lum, W. Ling, H. Suzuki, K. Tatsuhiko, U. Steinbrecher, *Journal of Biological Chemistry* **1997**, *272*, 12938.
[11]   J. Berliner, J. Heinecke, *Free Radical Biology & Medicine* **1996**, *20*, 707.
[12]   M. Ramprasad, T. Valeska, N. Kondratenko, O. Quehenberger, D. Steinberg, *Proceedings of the National Academy of Sciences of the United States of America* **1996**, *93*, 14833.
[13]   D. Steinberg, *Journal of Biological Chemistry* **1997**, *272*, 20963.
[14]   T. Hiltunen, S. Yla-Herttuala, *Atherosclerosis* **1998**, *137 (Suppl)*, s81.

[15]   M. De Winther, K. Van Dijk, L. Havekes, M. Hofker, *Arteriosclerosis, Thrombosis, and Vascular Biology* **2000**, *20*, 290.

[16]   E. Podrez, M. Febbraio, N. Sheibani, D. Schmitt, R. Silverstein, D. Hajjar, P. Cohen, W. Frazier, H. Hoff, S. Hazen, *Journal of Clinical Investigation* **2000**, *105*, 1095.

[17]   A. Zaman, G. Helft, S. Worthley, J. Badimon, *Atherosclerosis* **2000**, *149*, 251.

[18]   A. Nicholson, J. Han, M. Febbraio, R. Silverstein, D. Hajjar, *Annals of the New York Academy of Sciences* **2001**, *947*, 224.

[19]   T. Yoshimoto, Y. Takahashi, T. Kinoshita, T. Sakashita, H. Inoue, T. Tanabe, *Advances in Experimental Medicine and Biology* **2002**, *507*, 403.

[20]   J. McKenney, *The American Journal of Managed Care* **2001**, *7*, S299.

[21]   A. Gotto, *Circulation* **2002**, *105*, 1514.

[22]   V. Babaev, L. Gleaves, K. Carter, H. Suzuki, T. Kodama, S. Fazio, M. Linton, *Arteriosclerosis, Thrombosis, and Vascular Biology* **2000**, *20*, 2593.

[23]   M. Febbraio, N. Sheibani, D. Schmitt, R. Silverstein, D. Hajjar, P. Cohen, W. Frazier, H. Hoff, S. Hazen, *Journal of Clinical Investigation* **2000**, *105*, 1095.

[24]   Y. Fujiwara, N. Kiyota, M. Hori, S. Matsushita, Y. Iijima, K. Aoki, D. Shibata, M. Takeya, T. Ikeda, T. Nohara, R. Nagai, *Arteriosclerosis, Thrombosis, and Vascular Biology* **2007**, *27*, 2400.

[25]   J. Manning-Tobin, K. Moore, T. Seimon, S. Bell, M. Sharuk, J. Alvarez-Leite, M. Winther, I. Tabas, M. Freeman, *Arteriosclerosis, Thrombosis, and Vascular Biology* **2009**, *29*, 19.

[26]   R. Ross, *Annual Review of Physiology* **1995**, *57*, 791.

[27]   T. Yamakawa, K. Ogihara, M. Nakamura, H. Utsunomiya, K. Kadonosono, S. Kishikawa, Y. Terauchi, *Journal of Atherosclerosis and Thrombosis* **2009**, *16*, 501.

[28]   E. Chnari, H. Lari, L. Tian, K. Uhrich, P. Moghe, *Biomaterials* **2005**, *26*, 3749.

[29]   E. Chnari, J. Nikitczuk, K. Uhrich, P. Moghe, *Biomacromolecules* **2006**, *7*, 597.

[30]   E. Chnari, J. Nikitczuk, J. Wang, K. Uhrich, P. Moghe, *Biomacromolecules* **2006**, *7*, 1796.

[31]   N. Plourde, S. Kortagere, W. Welsh, P. Moghe, *Biomacromolecules* **2009**, *10*, 1381.

[32]   J. Wang, N. Plourde, N. Iverson, P. Moghe, K. Uhrich, *International Journal of Nanomedicine* **2007**, *2*, 697.

[33]   L. Tian, L. Yam, N. Zhou, H. Tat, K. Uhrich, *Macromolecules* **2004**, *37*, 538.

[34]   J. Wang, L. del Rosario, B. Demirdirek, A. Bai, K. Uhrich, *Acta Biomaterialia* **2009**, *5*, 883.

[35]   A. Harmon, K. Uhrich, *Journal of Bioactive and Compatible Polymers* **2009**, *24*, 185.

[36]   J. Djordjevic, L. del Rosario, J. Wang, K. Uhrich, *Journal of Bioactive and Compatible Polymers* **2008**, *23*, 532.

[37]   J. Djordjevic, M. Barch, K. Uhrich, *Pharmaceutical research* **2005**, *22*, 24.

[38]   L. Tao, K. Uhrich, *Journal of Colloid and Interface Science* **2006**, *298*, 102.

[39]   K. Steege, J. Wang, K. Uhrich, E. Castner, Jr, *Macromolecules* **2007**, *40*, 3739.

[40]   G. Fontana, M. Licciardi, S. Mansueto, D. Schillaci, G. Giammona, *Biomaterials* **2001**, *22*, 2857.

[41]   A. Zahr, C. Davis, M. Pishko, *Langmuir* **2006**, *22*, 8178.

[42]   M. Ogris, S. Brunner, S. Schuller, R. Kircheirs, E. Wagner, *Gene Therapy* **1999**, *6*, 595.

[43]   H. Gelderblom, J. Verweij, K. Nooter, A. Sparreboom, *European Journal of Cancer* **2001**, *37*, 1590.

[44]   Z. Yang, G. Sahay, S. Sriadibhatla, A. Kabanov, *Bioconjugate Chem.* **2008**, *19*, 1987.

[45]   Y. Tian, L. Bromberg, S. Lin, T. Alan Hatton, K. Tam, *Journal of Controlled Release* **2007**, *121*, 137.

[46]   S. Patel, A. Datta, *Chemical Physics Letters* **2005**, *413*, 31.

[47]   B. Alberts, A. Johnson, J. Lewis, M. Raff, K. Roberts, P. Walter, *Molecular Biology of The Cell*, Fourth ed., Garland Science, New York, **2002**.

[48]   K. Yoshiizumi, F. Nakajima, R. Dobashi, N. Nishimura, S. Ikeda, *Bioorganic & Medicinal Chemistry* **2002**, *10*, 2445.

[49]   J. F. J. Dippy, S. R. C. Hughes, A. Rozanski, *Journal of the Chemical Society* **1959**, 2492.

[50]   I. M. Kolthoff, *Treatise on Analytical Chemistry*, Interscience Encyclopedia, Inc., New York, **1959**.

[51]   D. Voet, J. G. Voet, C. W. Pratt, *Fundamentals of Biochemistry*, Wiley & Sons, Inc., USA, **2002**.

[52]   H. K. Hall, Jr, *Journal of the American Chemical Society* **1957**, *79*, 5441.

[53]   C. Fee, *Biotechnology and Bioengineering* **2007**, *98*, 725.

[54]   D. DeNoon, in *WebMD Health News*, **2002**.

[55]   B. Demirdirek, *Thesis (M.S.) -- Rutgers University* **2009**.

3. CATIONIC NANOSCALE AMPHIPHILIC MACROMOLECULES AS SYNTHETIC POLYMERS FOR NUCLEIC ACID DELIVERY

3.1. Introduction

Gene therapy is the modification of genetic information to treat a disease. As discussed in **Chapter 1**, nucleic acid delivery is a therapeutic option for currently untreatable diseases. However, many technical challenges must be overcome for gene therapy to be realized as a viable therapy. One of these challenges, which is the focus of this work, is the development of more <u>safe</u>, <u>efficient</u>, and <u>versatile</u> (i.e., the ability to use the same carrier for the treatment of numerous diseases) synthetic carriers for the nucleic acids.[1]

3.2. Background

3.2.1. Gene Silencing

The use of short interfering RNA (siRNA) molecules for gene silencing has enormous clinical potential for treating human disease, particularly for anticancer applications.[2, 3] Recent advances in siRNA delivery technology have led to several human clinical trials using therapeutic siRNA.[4, 5] However, further development of safe, efficient siRNA delivery systems is required to advance siRNA therapeutics for routine clinical use and address diverse disease states. The delivery of siRNA and other nucleic acid molecules to malignant cells has been attempted, for example, with varying degrees of success with numerous non-viral molecules including proteins, peptides, and synthetic polymers.[6]

3.2.2. Synthetic Polymers for Nucleic Acid Delivery

Self-assembled polymeric micelles have shown particular promise as drug and gene delivery vehicles due to their unique properties including steric stability, size suitable for passive tumor targeting, low cytotoxicity, high water solubility, and high drug encapsulation efficiency.[7-9] Polymeric micelle systems are currently being investigated as drug delivery vehicles in several Phase I and II clinical trials.[10-12] More recently, several polymeric micelle systems have been evaluated for siRNA delivery, [11-14] or for the co-delivery of siRNA and hydrophobic anticancer drugs.[15, 16] However, further development is needed for a delivery system that possesses increased stability, lowered toxicity, biodegradability, as well as the versatility for treating multiple disease states and ease of modification (e.g., targeting moieties) to increase specificity. Specifically, for polymeric micelles, improvements on existing systems are necessary to improve their drug loading capacity, stability in the blood stream, and ability to penetrate the cell membrane to make these systems viable for widespread clinical use.[17]

3.2.2.1. Nanoscale Amphiphilic Macromolecules as Synthetic Polymers

In this work, the hydrophobic functionality of AMs was exploited to create non-viral vectors for siRNA delivery. Specifically, linear, cationic ethyleneimine groups were conjugated to the AM's hydrophobic backbone (see **Figure 3.1** and **Scheme 3.1**) to facilitate electrostatic encapsulation of siRNA and delivery to malignant glioma cells. Ethyleneimines were chosen due to their similarity to the highly efficient, non-viral vector, PEI. However, PEI suffers from high cytotoxicity, limiting its use for systemic *in vivo* applications where high polymer concentrations are required.[18, 19] The minimum number of amine groups to efficiently deliver siRNA and elicit a gene-silencing response

in malignant glioma cells, while maintaining the favorable structural properties and low cytotoxicity of the AM materials, was identified in this work. This proof-of-concept study outlines the rational design approach to siRNA delivery systems and identifies a promising new siRNA delivery system.

Figure 3.1. Schematic representation of the modification of AMs, specifically **1cM**, to obtain cationic AMs.

3.3. Results and Discussion

3.3.1. Synthesis of Cationic AMs

The goal was to create novel synthetic vectors that exploit the structural properties of PEI that are beneficial for siRNA delivery while reducing the inherent cytotoxicity associated with PEI. AMs were modified with two different lengths of ethyleneimine chains to yield three novel polymer systems: ethylenediamine to yield **1N**, or pentaethylenehexamine to yield **5N** and **9N** polymers. The polymers were synthesized as shown in **Scheme 3.1** from the amine-specific N-hydroxysuccinimide (NHS)-activated starting materials.
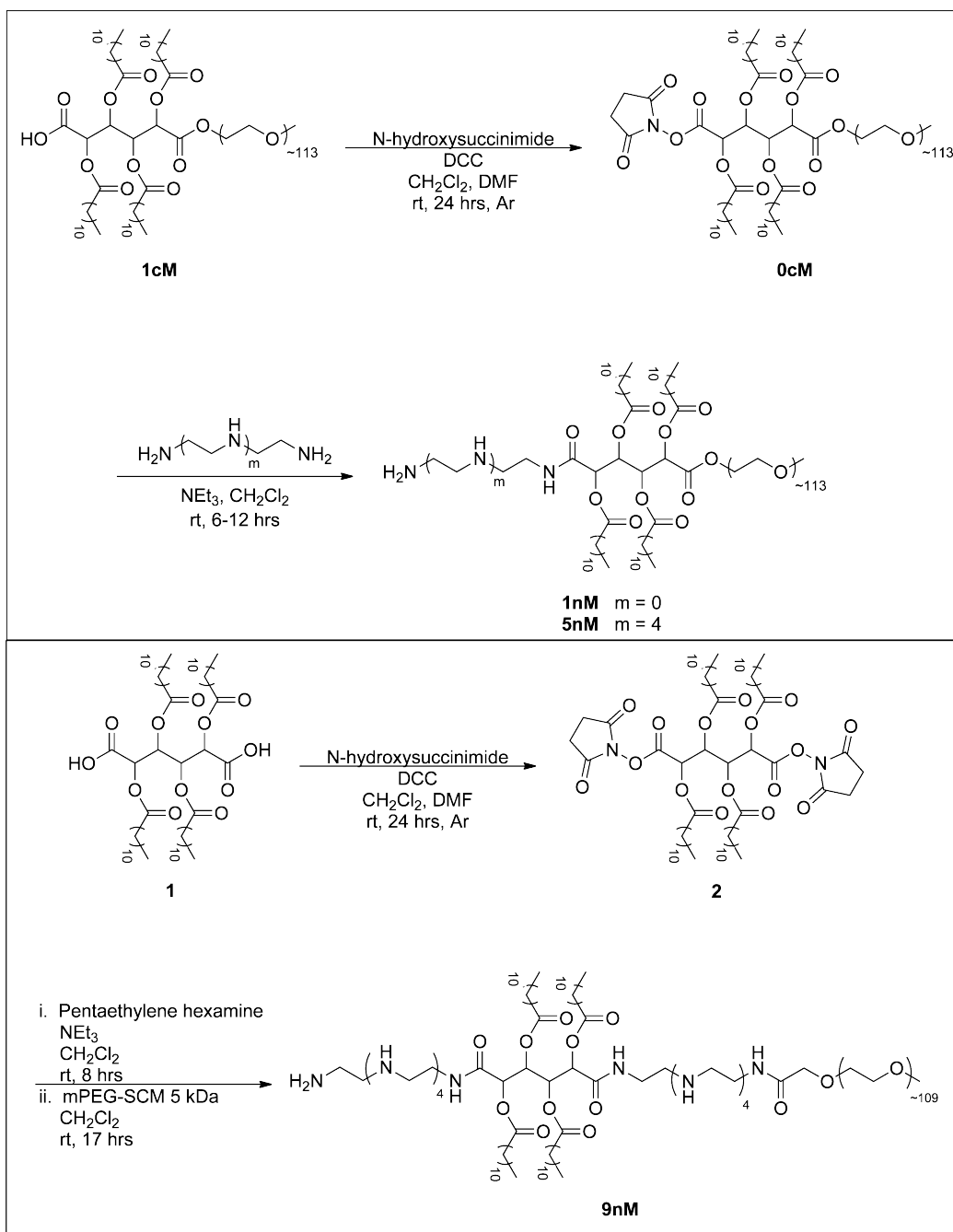
Scheme 3.1. Synthesis of cationic-AMs; (top) synthesis of monomer and dimer mixtures of **1nM** and **5nM** from NHS-activation of **1cM** (**0cM**) [20], (bottom) synthesis of **9nM** *via* di-activation of **1** with NHS (**2**).

The parent polymer, **1cM**, served as the basic building block for the polymer modifications. Specifically, the carboxylic acid was activated with N-hydroxysuccinimide to functionalize the polymers with linear ethyleneimines, systematically increasing the total number of amines from one, **1nM**, up to nine, **9nM**. Isolation of cationic AMs with amines conjugated to, rather than associated with, the polymer was insured by precipitation from diethyl ether; this process precipitates the AM products but not the ethyleneimine starting materials, ethylenediamine and pentaethylenehexamine. Amine conjugation was further verified by ^{1}H NMR spectroscopy and molecular weights determined by GPC relative to PEG standards. In addition to monitoring ^{1}H NMR spectra for the disappearance of protons associated with the NHS activating group (~ 2.8 ppm), new peaks assigned to the ethyleneimine groups were observed resonating at 1.3 and 1.8 ppm for **1nM** and from 2.5-3.0 ppm for **5nM** and **9nM**.

3.3.2. Hydrodynamic Diameter and Zeta Potentials of Cationic Polymers

The AMs modified with their respective ethyleneimines were characterized by dynamic light scattering (DLS) and zeta potentials to ensure that: 1) nanoscale size was retained and 2) resulting assemblies were cationic, a necessary property for complexing with the siRNA. Hydrodynamic diameters and zeta potentials of the polymers are summarized in **Figure 3.2**.
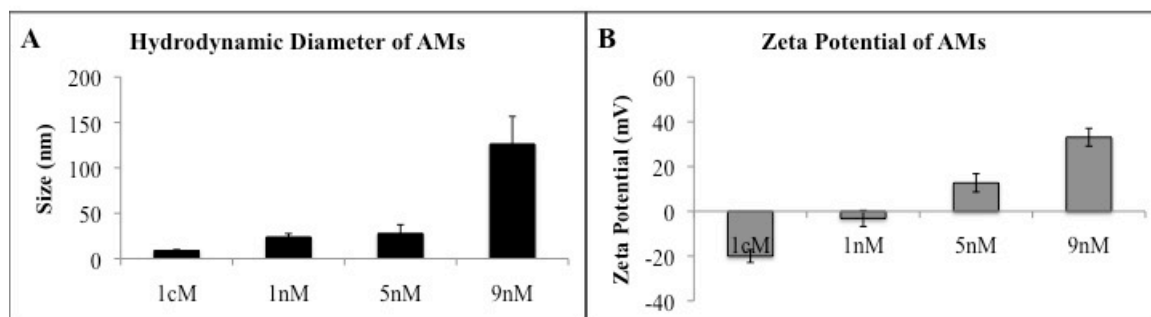
Figure 3.2. Hydrodynamic diameters (A) and zeta potentials (B) of ethyleneimine-modified polymers as compared to **1cM** control.

All cationic AMs formed micelles in the nanoscale size range as determined by dynamic light scattering (**Figure 3.2A**). **1nM** and **5nM** formed micelles of approximately the same size as **1cM**, while micelles formed from **9nM** were significantly larger (~125 nm) presumably due to charge repulsion of the highly cationic ethyleneimine units.

Successful conjugation of the amines was shown by the disappearance of N-hydroxysuccinimide in the ^{1}H NMR spectra as well as by the zeta potential increase from negative (**1cM**), to less negative (**1nM**), and positive (**5nM** and **9nM**), as shown in **Figure 3.2B**. The zeta potential increased with increasing ethyleneimine length, further indicating the successful incorporation of amine groups.

3.3.3. Cytotoxicity of Cationic-AMs

The in vitro cytotoxicity studies were performed by Alexander M. Harmon, a Ph.D. candidate in Chemistry and Chemical Biology (Rutgers University, Piscataway, NJ) supervised by Professor Kathryn E. Uhrich.

To assess the safety of the cationic-AMs, their cytotoxicity was compared to that of linear PEI 25 kDa (L-PEI) in U87 glioma cells. A dose response curve was generated

for all samples by counting viable cells remaining after a 72-hour exposure to the polymers (**Figure 3.3**). A significant decrease in cytotoxicity (p<0.05) was observed for all AMs compared to L-PEI at the highest concentrations tested (10^{-5} and 10^{-4} M). Interestingly, when comparing the AMs, the **9nM** material exhibited the lowest cytotoxicity. One explanation is that the surface charge density of the **9nM** micelles is actually lower as their hydrodynamic diameter (shown in **Figure 3.2A**) has increased by a factor of approximately five and, therefore, the surface area is increased by a factor of 25 compared to the **1nM** and **5nM** micelles.
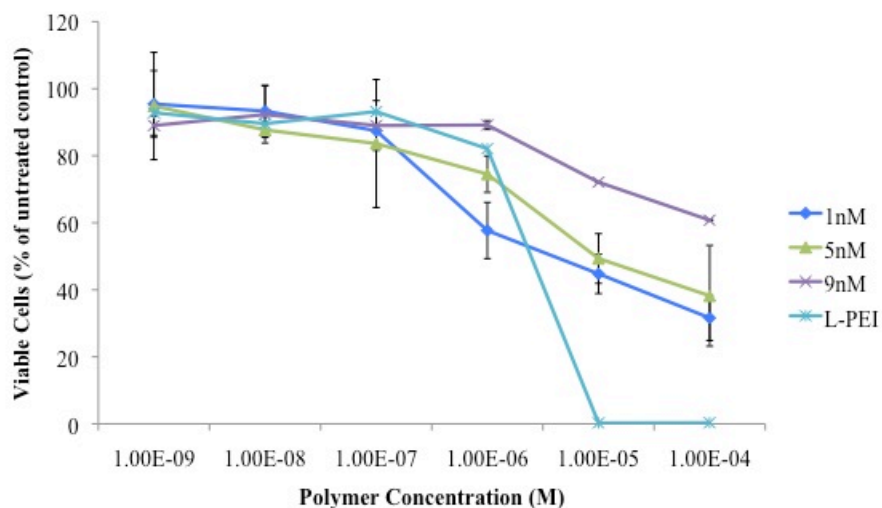
Figure 3.3. Cytotoxicity of cationic-AMs and L-PEI to U87 glioma cells after a 72-hour exposure. Data represent mean $\pm$ standard deviation (*n*=4). Astericks represent concentrations at which cationic-AMs elicited a significantly lower cytotoxicity than L-PEI (*p* < 0.05).

3.3.4. Characterization of siRNA/AM Complexes

3.3.4.1. Gel Electrophoresis

The gel electrophoresis complexation studies were performed by Carolyn Waite, a Ph.D. candidate in Chemical and Biochemical Engineering (Rutgers University, Piscataway, NJ) supervised by Professor Charles M. Roth.

The ability of cationic AMs to complex anionic siRNA was evaluated using gel electrophoresis. Complexes were formed at several nitrogen:phosphate (N/P) ratios and run on an electrophoresis gels to separate un-complexed siRNA from the AM/siRNA complexes. N/P ratios refer to the ratio of polymeric nitrogens-to-nucleic acid phosphates. Generally, lower N/P ratios are desirable to minimize negative vehicle effects (i.e., cytotoxicity).

Efficient complexation by gel electrophoresis is determined by the decreased fluorescence intensity of un-complexed siRNA; when complexed with the carrier molecule, the siRNA no longer fluoresces. Polymers containing zero or one cationic amine group (i.e., **1cM** and **1nM**) displayed no complexation of siRNA at charge ratios up to N/P=80 (**Figure 3.4**). By increasing the number of amine groups to five (**5nM**), a modest extent of siRNA complexation (approximately 20%) was observed at N/P ratios of 60 and higher. Significantly improved siRNA complexation efficiency was observed with the AM containing nine amine groups, **9nM**, where most of the siRNA was encapsulated by N/P=50. Hence, for subsequent physical and biological characterization studies, AM/siRNA complexes were formed at N/P≥50. In comparison with other synthetic vectors, the ratio of polymer to nucleic acid necessary for the cationic AMs to efficiently complex with siRNA is significantly higher; other synthetic vectors have been

shown effective at N/P 10 and under.[21, 22] However, as long as the polymers are non-cytotoxic at the concentrations being used, this ratio is not important. For the cationic AMs used in this work, they are non-cytotoxic (as shown in **Figure 3.3**) at the concentrations utilized ($\leq 10^{-6}$ M).
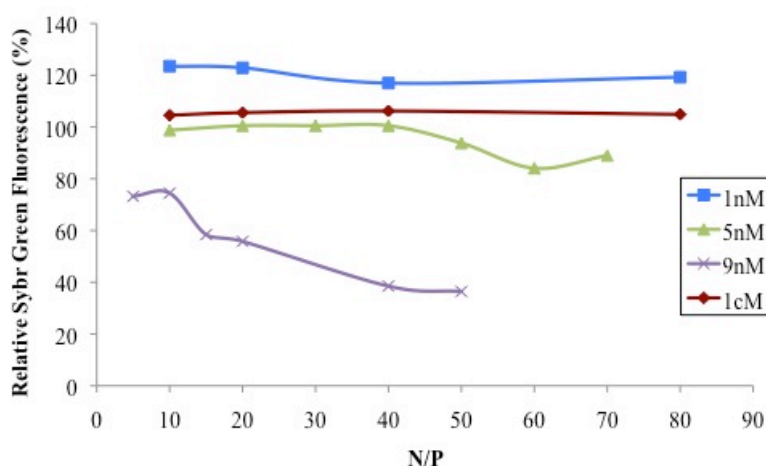
Figure 3.4. Graphical representation of the fluorescence data derived from gel electrophoresis of cationic AM/siRNA complexes as compared to **1cM**/siRNA where decreased Sybr Green Fluorescence indicates successful complexation with siRNA.

The inefficient complexation of **5nM** in comparison to **9nM** is likely due to both the decrease in the number of amines that can be protonated in **5nM** and the location of the amines. With respect to the number of protonated amines, work by Geall et. al. showed that when diamines were linked to cholestorol, the pKa's of the amines varied widely. Specifically, for pentaethylenehexamine the pKa's varied from 2.5 to 10.2, with only 2 amines having pKa's above physiological pH.[23] As cholesterol is similar in hydrophobicity to the alkylated mucic acid component, the pentaethylenehexamine moiety conjugated to the polymer in **5nM** is likely to have similar pKa's to those reported by Geall et. al. – meaning only two of these amines would likely be protonated

at physiological pH. In addition, these amines are likely located deep within the hydrophobic core of the resulting micellar assembly making them: 1) unable to be protonated and 2) if they are protonated, unavailable for siRNA complexation. If the amines are protonated in **5nM**, more incubation time with the siRNA and vigorous agitation may expose the protonated amines for more efficient siRNA complexation. In contrast, while **9nM** has a similar aminated component within the polymer's hydrophobic domain, an additional amine component remains that links the hydrophobic and hydrophilic domains. Due to their proximity to the hydrophilic PEG, these amines likely interact more with the aqueous solution to be more readily protonated. Additionally, these protonated amines are more accessible for siRNA complexation as they are not be buried within the micellar hydrophobic core. Future work to titrate the cationic AMs could provide further insight into the pKa differences that affect siRNA complexation.

3.3.4.2. Hydrodynamic Diameter and Zeta Potential

Once complexed with siRNA (**Figure 3.5A**, N/P=50 and 100), all cationic AMs maintained the nanoscale size of the AMs alone. Nanoscale sizes of less than ~100 nm is desirable for improved circulation time, passive tumor targeting by the enhanced permeation and retention (EPR) effect, and optimal cellular uptake for siRNA/polymer complexes.[24, 25] For **1cM**, **1nM**, and **5nM**, the addition of siRNA to the AM systems had no statistically significant effect on the hydrodynamic diameters as compared with the size of the AMs alone. However, complexeation of siRNA with **9nM** at N/P 50 resulted in a significant reduction in micellar size as compared with the size of **9nM** alone presumably due to the charge neutralization that occurs when the cationic polymer complexes with the anionic siRNA. Additionally, when more **9nM** is added, to yield N/P

100, the size of the resulting complexes returns to the size of the **9nM** alone. This data indicates the available siRNA has complexed with the polymer and the size of the micellar system is again controlled by electrostatic repulsion of the cationic unimers. This data suggests that only **9nM** has significant complexation and condensation of the siRNA, which is in agreement with the gel electrophoresis data discussed previously.

When siRNA was complexed with the cationic-AMs at nitrogen/phosphate (N/P) ratios of 50 and 100, the zeta potentials (shown in **Figure 3.5B**) significantly changed compared to the native polymers in the absence of siRNA ($p < 0.05$). Specifically, at N/P 50, the zeta potentials for complexes of siRNA and **5nM** decreased from 12.7 mV of the **5nM** alone to 5.3 mV with siRNA. Likewise, the zeta potential of **9nM** decreased from 33.1 mV alone to 7.89 mV with siRNA. The zeta potentials for both AMs then increased at N/P 100 – back to that for the vehicle alone for **5N** but only to 22.2 mV for **9nM**. This data suggests that **9nM** complexed most efficiently with siRNA; the decrease in zeta potential is a result of charge neutralization when the negatively charged siRNA complexes with the cationic AMs. Further, these results are in agreement with the gel electrophoresis and sizing data. Based on the physical characterization of AM/siRNA complexes by gel electrophoresis, dynamic light scattering, and zeta potential, **9nM** was expected to be the most effective siRNA delivery vehicle.
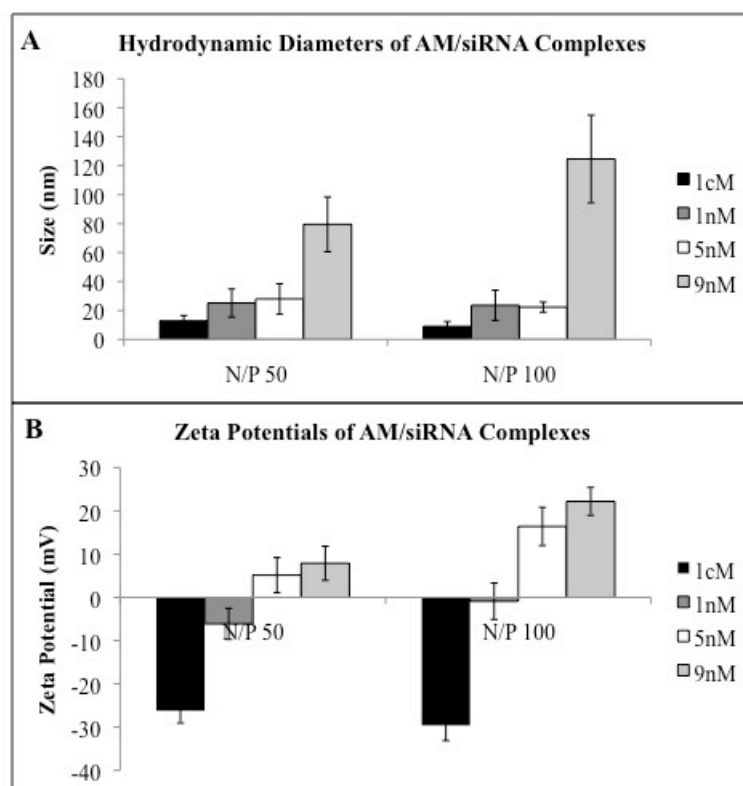
Figure 3.5. Hydrodynamic diameters (A) and zeta potentials (B) of AM/siRNA complexes following incubation of the indicated polymer and siRNA for 60 minutes at room temperature.

3.3.5. Luciferase Silencing of AM/siRNA Complexes

The in vitro silencing studies were performed by Carolyn Waite, a Ph.D. candidate in Chemical and Biochemical Engineering (Rutgers University, Piscataway, NJ) supervised by Professor Charles M. Roth.

The ability of AMs to facilitate cellular delivery of siRNA and elicit silencing of the reporter gene, firefly luciferase, in U87 cells was also evaluated. Polyplexes (i.e., complexes of polymers and siRNA) of anti-luciferase siRNA were formed (siRNA concentration: 100 nM, N/P=50, AM concentration: ~10^{-5} M) and delivered to U87-Luc

cells, which were subsequently assayed for luciferase expression. Significant luciferase silencing ($p <0.05$) was observed using the AMs containing five or nine amines (**5nM** and **9nM**), but not observed for AMs containing just one amine group (**1nM**) (**Figure 3.6A**). A similar luciferase silencing response was observed between the **9nM** and L-PEI, a widely-studied polymeric system for nucleic acid delivery (**Figure 3.6A**). Delivering a scrambled siRNA sequence did not elicit luciferase silencing, demonstrating that the AMs do not induce off-target silencing effects.
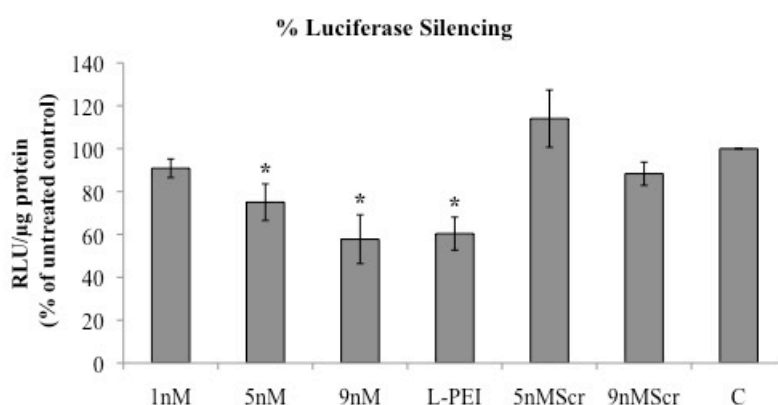
Figure 3.6. Luciferase silencing in U87-Luc cells of the indicated polymers complexed with siRNA 24 hours post-transfection. The samples **5nM**Scr and **9nM**Scr indicate treatments with a scrambled siRNA sequence not specific to firefly luciferase. Data represent mean $\pm$ standard deviation ($n=3$). Asterisks indicate treatments that elicited statistically significant luciferase silencing compared to the untreated control, C, ($p<0.05$).
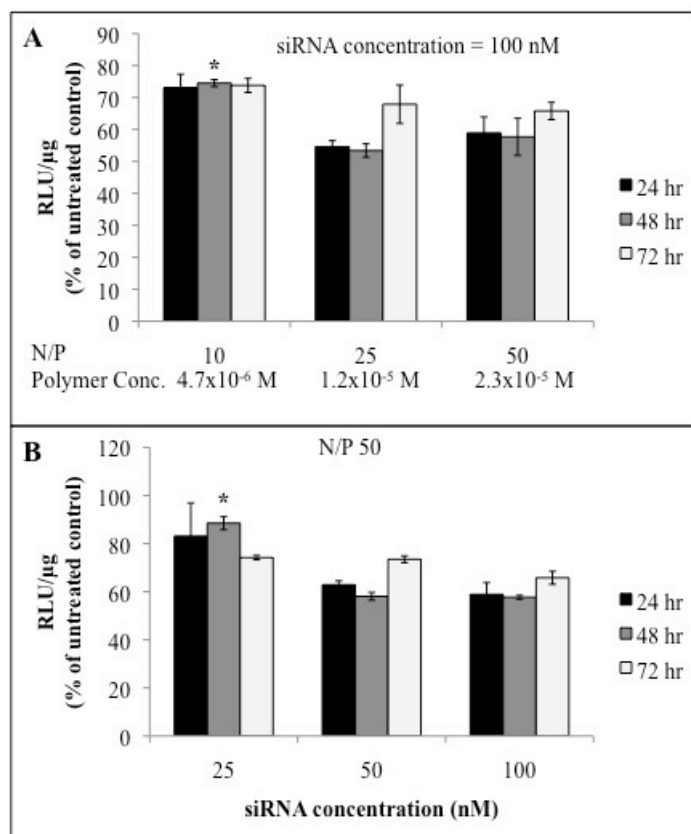
Figure 3.7. Time-course and dose titrations performed with **9nM**/siRNA complexes to U87-Luc cells. siRNA concentration was held constant (100 nM) with varying N/P ratios (A) and the N/P ratio was held constant (N/P= 50) with varying siRNA concentrations (B). Data represent mean $\pm$ standard deviation (n=3). Asterisks indicate treatments that elicited statistically different luciferase silencing compared to the other treatment groups in the experiment (p<0.05).

To study the dynamics and dose-dependence of luciferase silencing by the most promising polymer (**9nM**), siRNA transfection experiments were performed at various time points, polymer concentrations (**Figure 3.7A**) and siRNA concentrations (**Figure 3.7B**). The minimum N/P ratio required for a maximum luciferase silencing response was

N/P=25 (siRNA concentration: 100 nM, AM concentration: 1.2×10^{-5} M), (**Figure 3.7A**), and the minimum siRNA concentration required for optimal silencing response was 50 nM (**Figure 3.7B**).

3.3.6. Uptake of AM/siRNA Complexes

The uptake studies were performed by Carolyn Waite, a Ph.D. candidate in Chemical and Biochemical Engineering (Rutgers University, Piscataway, NJ) supervised by Professor Charles M. Roth.

To qualitatively observe the data collected from the luciferase silencing assay, **5nM**/siRNA and **9nM**/siRNA were incubated with U87 green fluorescent protein (GFP)-labeled cells and their uptake observed using confocal microscopy. GFP cells were utilized to allow simultaneous visualization of the cells and fluorescent siRNA using fluorescent microscopy. Successful cellular association of siRNA delivered by **5nM** and **9nM** was observed and qualitatively comparable to siRNA delivered by L-PEI (**Figure 3.8**). Interestingly, the trends observed in the quantitative luciferase silencing assay differed somewhat from the cellular association of a fluorescently labeled siRNA sequence into U87GFP cells. The **9nM** delivered more siRNA to the cells than L-PEI (as noted in the fluorescent images), however, this trend was not observed in the luciferase silencing assay where both **9nM** and L-PEI elicited similar extents of luciferase silencing. This observation suggests that while **9nM** may be capable of delivering siRNA to cells, other intracellular barriers such as siRNA unpackaging or endosomal escape may be affecting gene silencing activity by **9nM**. This phenomenon will be investigated further in subsequent work.
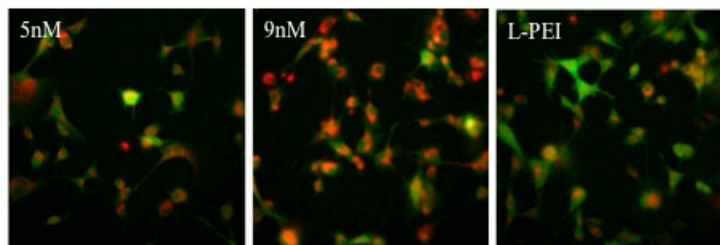
Figure 3.8. Fluorescent microscope images of siRNA distribution (red) in U87-d1EGFP cells (green) when delivered by the indicated polymers.

3.4. Summary

A series of amphiphilic macromolecules were functionalized with linear ethyleneimines to render them positively charged for improved siRNA complexation. By increasing the number of secondary amines from one to five to nine (ie, from **1nM** to **9nM**, respectively), increased zeta potential and stable complexation with siRNA was achieved. All cationic AMs were less cytotoxic to U87 cells than L-PEI at polymer concentrations of 10 µM or greater. The cationic AM with nine amines, **9nM**, successfully delivered siRNA molecules to U87 cells and elicited silencing of the reporter gene, firefly luciferase. This work highlights the promise of AMs for siRNA delivery and specifically identifies a novel AM molecule, **9nM**, that displays low cytotoxicity compared to L-PEI, stable complexes with siRNA while maintaining a nanoscale size, and efficiently delivers siRNA delivery to malignant glioma cells.

3.5. Experimental

3.5.1. Synthetic Materials

Unless otherwise stated, solvents and reagents were purchased from Fisher Scientific (Pittsburgh, PA) and Sigma-Aldrich (St. Louis, MO) and used as received.

PEG 5 kDa was purchased from Polysciences, Inc. (Warrington, PA) and dried by azeotropic distillation from toluene before use. Methoxy-PEG-succinimidyl carboxymethyl (MW 5 kDa) (mPEG-SCM), was purchased from Laysan Bio, Inc (Arab, AL) and used as received. **1**[26], **1cM**[26], and **0cM**[20] were prepared as previously published.

3.5.2. Characterization Methods

3.5.2.1. Proton Nuclear Magnetic Resonance (^{1}H NMR) Spectroscopy

Proton nuclear magnetic resonance (^{1}H-NMR) spectra of the products were obtained using a Varian 400 MHz or 500 MHz spectrophotometer. Samples were dissolved in chloroform-d, with a few drops of dimethyl sulfoxide-d_6 if necessary, with tetramethylsilane as an internal reference.

3.5.2.2. Gel Permeation Chromatography (GPC)

Molecular weights (M_w) and polydispersity indices (PDI) were determined using gel permeation chromatography (GPC) with respect to PEG standards (Sigma-Aldrich) on a Waters Stryagel® HR 3 THF column (7.8 x 300 mm). The Waters LC system (Milford, MA) was equipped with a 2414 refractive index detector, a 1515 isocratic HPLC pump, and 717plus autosampler. An IBM ThinkCentre computer with Waters Breeze Version 3.30 software installed was used for collection and processing of data. Samples were prepared at a concentration of 10 mg/mL in tetrahydrofuran, filtered using 0.45 μm pore size nylon or polytetrafluoroethylene syringe filters (Fisher Scientific) and placed in sample vials to be injected into the system.

3.5.2.3. Differential Scanning Calorimetry (DSC)

Melting points were determined by differential scanning calorimetry (DSC) on a TA DSC Q200. TA Universal Analysis 2000 software was used for data collection on a Dell Dimension 3000 computer. Samples (3-5 mg) were heated under dry nitrogen gas. Data were collected at heating and cooling rates of 10 °C/min with a two-cycle minimum.

3.5.2.4. Hydrodynamic Diameter and Zeta Potential Measurements

Dynamic light scattering (DLS) and zeta potential analyses were performed using a Malvern Instruments Zetasizer Nano ZS-90 instrument (Southboro, MA). DLS measurements were performed at a 90° scattering angle at 25 °C. Size distributions by volume of measurements were collected in triplicate, averaged and reported. Zeta potential measurements were collected in triplicate, averaged and the Z-average charges reported. For all measurements, error bars represent peak widths of the average value. Polymer solutions at a concentration of 1.0 mg/mL were prepared using picopure water and filtered with a 0.45 µM Nylon syringe filter (Fischer Scientific, Pittsburgh, PA).

3.5.3. Polymer Synthesis

3.5.3.1. 1nM

Ethylenediamine (50 μL, 0.75 mmol) was dissolved in HPLC-grade CH_2Cl_2 (3 mL) and triethylamine (0.15 mL, 1.1 mmol). In a separate vessel, **0cM** (0.51 g, 0.085 mmol) was dissolved in HPLC-grade CH_2Cl_2 (9 mL) and subsequently added to the solution of ethylenediamine dropwise *via* syringe pump at a rate of 1.0 mL/hr. The reaction was stirred overnight (~ 18 hrs). The reaction solution was then diluted with CH_2Cl_2 and subsequently washed with 0.1 N HCl/brine (1x) and brine (2x). The combined aqueous portions were extracted with CH_2Cl_2 and the combined organics dried

over $MgSO_4$, and concentrated to a yellow oil. The desired product was precipitated from the oil dissolved in CH_2Cl_2 (5 mL) by addition of 10-fold diethyl ether and cooling over dry ice for 1 hr. The solid was then collected by centrifugation at 3000 rpm for 5 min and the supernatant removed by decanting. The resulting white solid was dried under ambient atmosphere (12 hrs) and under high vacuum (12 hrs). Yield: 0.41 g, 80 %. ^{1}H-NMR ($CDCl_3$): δ 5.67 (m, 2H, CH), 5.14 (m, 2H, CH), 4.24 (m, 3H, CH_2), 3.60 (m, ~0.45 kH, CH_2O), 3.37 (s, 3H, OCH_3), 2.37 (m, 8H, CH_2), 2.29 (m, 4H, CH_2), 1.81 (b, 4H, CH_2), 1.60 (m, 8H, CH_2), 1.26 (m, 64H, CH_2), 0.87 (t, 12H, CH_3). T_m = 58 °C GPC: M_w: 6.3 kDa; PDI: 1.1.

3.5.3.2. 5nM

Pentaethylenehexamine (0.15 mL, 0.64 mmol) was dissolved in HPLC-grade CH_2Cl_2 (10 mL) and triethylamine (0.33 mL, 2.4 mmol). In a separate vessel, **0cM** (0.48 g, 0.079 mmol) was dissolved in HPLC-grade CH_2Cl_2 (10 mL) and subsequently added to the solution of ethylenediamine dropwise *via* syringe pump at a rate of 1.0 mL/hr. The reaction was stirred overnight (~ 17 hrs). The bright yellow reaction solution was diluted with CH_2Cl_2 and subsequently washed with 0.1 N HCl/brine (1x) and brine (2x). The combined aqueous portions were extracted with CH_2Cl_2 and the combined organics dried over $MgSO_4$, and concentrated to a cloudy yellow oil. The desired product was precipitated from the oil dissolved in CH_2Cl_2 (5 mL) by addition of 10-fold diethyl ether and cooling over dry ice for 1 hr. The solid was then collected by centrifugation at 3000 rpm for 5 min and the supernatant removed by decanting. The resulting white solid was dried under ambient atmosphere (12 hrs) and under high vacuum (12 hrs). Yield: 0.42 g, 86 %. ^{1}H-NMR (DMSO): δ 5.50 (m, 2H, CH), 5.11 (m, 2H, CH), 3.41 (m, ~0.45 kH,

CH_2O), 3.24 (s, 3H, OCH_3), 2.89 (m, 13 H, CH_2), 2.80 (bs, 2H, CH_2), 2.76 (bs, 7H, CH_2), 2.64 (bs, 6H, CH_2), 1.49 (m, 8H, CH_2), 1.24 (m, 64H, CH_2), 0.84 (t, 12H, CH_3). $T_m = 59$ °C. GPC: M_w: 6.4 kDa; PDI: 1.1.

3.5.3.3. Product 2 (2NHS-M12)

Product **1** (5.10 g, 5.43 mmol) and NHS (5.38 g, 46.8 mmol) were dissolved in anhydrous CH_2Cl_2 (100 mL) and anhydrous DMF (18 mL) under argon. Once a clear solution was obtained, N,N'-dicyclohexylcarbodiimide (17 mL, 17 mmol) was added and the reaction stirred at room temp under argon for 24 hours. The resulting solution with white suspension was stored at -4 °C overnight. The dicyclohexyl urea (DCU) byproduct was then removed by vacuum filtration and the filtrate washed with 0.1 N HCl and 50:50 brine/H_2O, dried over $MgSO_4$, and concentrated. The resulting white solid was then dissolved in a small amount of CH_2Cl_2 (5-10 mL) and stored at -4 °C for 2-3 hours. The resulting white suspension was filtered to remove residual DCU. The filtrate was then concentrated to dryness and the white solid dried under high vacuum overnight. Yield = 4.5 g, 73 %. ^{1}H-NMR ($CDCl_3$): δ = 5.96 (s, 2H, CH), 5.57 (s, 1H, CH), 2.81 (s, 8H, CH_2), 2.49 (m, 6H, CH_2), 2.37 (m, 2H, CH_2), 1.64 (m, 8H, CH_2), 1.27 (m, 64H, CH_2), 0.89 (t, 12H, CH_3).

3.5.3.4. 9nM

Pentaethylenehexamine (0.05 mL, 0.2 mmol) was dissolved in CH_2Cl_2 (3 mL) and triethylamine (0.15 mL, 1.1 mmol). In a separate vessel, **2** (0.10 g, 0.090 mmol) was dissolved in HPLC-grade CH_2Cl_2 (3 mL) and subsequently added to the solution of ethylenediamine dropwise *via* syringe pump at a rate of 1.0 mL/hr. The reaction was stirred at room temperature a total of 8 hrs. mPEG-SCM (0.45 g, 0.090 mmol) dissolved

in CH_2Cl_2 (7 mL) was then added to the yellow reaction solution dropwise *via* syringe pump at a rate of 1.0 mL/hr. The reaction was stirred at room temperature overnight (~ 17 hrs). The solvent was then removed from the reaction solution by rotary evaporation. The oil/solid was then redispersed in CH_2Cl_2 and filtered to remove the solid NHS-byproduct. The filtrate was concentrated to an oil and product precipitated from the oil dissolved in CH_2Cl_2 (5 mL) by addition of 10-fold diethyl ether. The solid was then collected by centrifugation at 3000 rpm for 5 min and the supernatant removed by decanting. The resulting white solid was washed with diethyl ether (1x) and dried under ambient atmosphere (12 hrs) and under high vacuum (12 hrs). Yield: 0.45 g, 87 %. ^{1}H-NMR $(CDCl_3)$: δ 7.26 (s, 4H, CH), 3.69 (m, ~0.44 kH, CH_2O), 3.38 (s, 3H, OCH_3), 3.05 (bm, 15H, CH_2), 2.55 (bm, 16H, CH_2), 2.07 (bm, 40H, CH_2), 1.65 (bs, 7H, CH_2), 1.48 (t, 5H, CH_2), 1.26 (m, 37H, CH_2), 0.88 (t, 12H, CH_3). T_m = 59 °C. GPC: M_w: 5.5 kDa; PDI = 1.1.

3.5.4. *In Vitro* Cytotoxicity

The in vitro cytotoxicity studies were performed by Alexander M. Harmon, a Ph.D. candidate in Chemistry and Chemical Biology (Rutgers University, Piscataway, NJ) supervised by Professor Kathryn E. Uhrich.

3.5.4.1. Cell Culture

All cell culture products were obtained from Invitrogen (Carlsbad, CA). U87 MG cells (ATCC HTB-14) were maintained in DMEM medium supplemented with 10% fetal bovine serum (FBS), L-glutamine, and penicillin-streptomycin.

3.5.4.2. Cell Viability Assay

U87 glioma cells were seeded into 96 well plates (Corning, Corning, NY) at 10,000 cells per well in Dulbecco's Modified Eagle Medium (DMEM) supplemented with 10 % FBS and 1 % penicillin-streptomycin and incubated overnight at 37 ºC, with 5 % CO_2. The media was removed by aspiration and replaced with 200 μL of the desired cationic AM or PEI dissolved in media at desired concentrations (n=4 per condition). Untreated control wells received media only. After 72 hours, cells were harvested by trypsinization (75 μL trypsin-EDTA followed with 75 μL complete media to neutralize trypsin) and 50 μL of staining solution (48:1:1 media:DMSO:Guava ViaCount Flex reagent (Guava Technologies, Hayward, CA) was added to each well. Cells were counted using a Guava EasyCyte Plus (Guava Technologies, Haywood CA) instrument with an original volume of 0.2 mL and a dilution factor of one.

3.5.5. Characterization of AM/siRNA Complexes

3.5.5.1. Gel Electrophoresis

Gel electrophoresis studies were performed by Carolyn Waite, a Ph.D. candidate in Chemical and Biochemical Engineering (Rutgers University, Piscataway, NJ) supervised by Professor Charles M. Roth.

Polymer/siRNA (Dharmacon, Lafayette, CO) complexes were first prepared at the desired nitrogen to phosphorous (N/P) ratios by mixing solutions of polymers (stocks maintained in DI water) and siRNA in PBS (final siRNA concentration of 12.5 μg/mL). Soutions were briefly vortexed, and incubated for 60 min at room temperature to allow for complex formation. Polymer/siRNA complexes were loaded into 1% agarose gels run in an electrophoresis chamber at 70 V for 40 minutes. Following electrophoresis, gels

were stained with SYBR Green II RNA gel stain (Invitrogen, Carlsbad, CA) for 30 minutes prior to imaging on a Bio-Rad Molecular Imager FX (Bio-Rad Laboratories, Hercules, CA) to visualize unbound siRNA. The fluorescence intensities (excitation: 254 nm, emission 520 nm) of bands were quantified using Quantity One Quantitation software (Bio-Rad Laboratories, Hercules, CA).

3.5.5.2. Hydrodynamic Diameter and Zeta Potentials

Dynamic light scattering (DLS) and zeta potential analyses were performed using a Malvern Instruments Zetasizer Nano ZS-90 instrument (Southboro, MA). DLS measurements were performed at a 90° scattering angle at 25°C. Size distributions by volume of measurements were collected in triplicate, averaged and reported. Zeta potential measurements were collected in triplicate, averaged and the Z-average charges reported. For all measurements, error bars represent peak widths of the average value. Complexes were prepared in picopure water at various nitrogen/phosphate (N/P) ratios. For size and zeta potential measurements, 2 mL of solutions containing AM/siRNA complexes were prepared at polymer concentrations sufficient for detection by the zetasizer instrument (1 mg/mL for **1** and **1nM**, and 2 mg/mL for **5nM** and **9nM**). Solutions were briefly vortexed and incubated for at least 60 min at room temperature to allow for complex formation prior to size and zeta potential analysis.

3.5.6. *In Vitro* Silencing and Uptake

In vitro silencing and uptake in U87 glioma cells were performed by Carolyn Waite, a Ph.D. candidate in Chemical and Biochemical Engineering (Rutgers University, Piscataway, NJ) supervised by Professor Charles M. Roth.

3.5.6.1. Cell Culture

All cell culture products were obtained from Invitrogen (Carlsbad, CA). A U87 cell line containing a stably integrated destabilized enhanced GFP (d1EGFP) transgene (U87-GFP) was generated as described previously, [27] and was maintained under constant selective pressure by G418 (500 µg/mL), and the growth medium was supplemented with sodium pyruvate and nonessential amino acids. U87-Luc, a human glioblastoma cell line with constitutive expression of firefly luciferase, was generously provided by Dr. Xu-Li Wang (Department of Pharmaceutics and Pharmaceutical Chemistry, University of Utah). U87-Luc cells were maintained in minimal essential medium supplemented with 10% FBS, penicillin-streptomycin, and maintained under selective pressure by G418.

3.5.6.2. siRNA Silencing Assay

U87-Luc cells were plated at a density of 5000 cells/well in 96-well plates approximately 20 hours prior to transfection. Immediately prior to transfection, polymer/siRNA complexes were prepared in 20 µL of PBS (N/P=50 for the AMs, and N/P=15 for linear PEI). Linear polyethyleneimine (Polysciences, Inc., Warrington, PA), a commonly used polymeric transfection reagent, was used as a positive control. A scrambled siRNA sequence not targeted against firefly luciferase was delivered as a negative control. The polyplexes were brought to a total volume of 100 µL in OptiMEM medium to obtain a final siRNA concentration of 100 nM. The serum-containing culture medium was aspirated from the cells, and each well treated with 100 µL of the polyplexes in OptiMEM medium. Each treatment was performed in triplicate. After a 4 hr incubation period, the transfection mixture was replaced with serum-containing growth medium and

maintained under normal growth conditions until the cells were assayed for firefly luciferase expression 24 hours after the initial treatment.

Cells were prepared for firefly luciferase detection using the Luciferase Assay System (Promega, Madison, WI) according to the manufacturer's protocol. Firefly luciferase was quantified using The Reporter microplate luminometer (Turner Biosystems, Sunnyvale, CA). Following luciferase quantification, cell lysates were assayed for total protein content using the BCA Protein Assay kit (Pierce, Rockford, IL) according to the manufacturer's protocol.

3.5.6.3. Uptake of Fluorescently-labeled siRNA

Uptake of Cy5-labeled siRNA (Dharmacon, Lafayette, CO) sequence into U87-GFP cells was evaluated using fluorescence microscopy. A similar transfection protocol as performed on U87-Luc cells above, was performed with U87-GFP cells seeded onto an 8-well LabTek coverglass chamber (Nalge Nunc, Naperville, IL) at a density of 5000 cells/well. U87-GFP cells were treated with a Cy5-labeled siRNA to facilitate imaging of cellular localization of siRNA. Imaging was performed 24 hours after siRNA transfection using an Olympus IX81 model fluorescent microscope (Olympus, Center Valley, PA). Imaging was performed at 20X magnification. The following excitation and emission wavelengths were used: GFP (excitation=482 nm, emission=536 nm) and Cy5 siRNA (excitation=628 nm, emission= 692 nm).

3.5.7. Statistical Analysis

Statistics were performed by Carolyn Waite, a Ph.D. candidate in Chemical and Biochemical Engineering (Rutgers University, Piscataway, NJ) supervised by Professor Charles M. Roth.

Statistical comparisons for zeta potential measurements, luciferase silencing and polymer cytotoxicity were performed using a one-way ANOVA test with a Fisher's all-pairs post hoc comparison test.

3.6. References

[1] C. Roth, S. Sundaram, *Annual Review of Biomedical Engineering* **2004**, *6*, 397.
[2] A. Gartel, E. Kandel, *Biomolecular Engineering* **2006**, *23*, 17.
[3] L. Aagaard, J. Rossi, *Advanced Drug Delivery Review* **2007**, *59*, 75.
[4] M. L. Edelstein, M. R. Abedi, J. Wixon, *The Journal of Gene Medicine* **2007**, *9*, 833.
[5] M. L. Edelstein, M. R. Abedi, J. Wixon, R. M. Edelstein, *The Journal of Gene Medicine* **2004**, *6*, 597.
[6] T. Tokatlian, T. Segura, *Nanomedicine and Nanobiotechnology* **2010**, *2*, 305.
[7] N. Nishiyama, K. Kataoka, *Pharmacology & Therapeutics* **2006**, *112*, 630.
[8] K. Osada, K. Kataoka, *Advances in Polymer Science* **2006**, *202*, 113.
[9] K. Kataoka, A. Harada, Y. Nagasaki, *Advanced Drug Delivery Review* **2001**, *47*, 113.
[10] M. Yokoyama, *Expert Opinion on Drug Delivery* **2010**, *7*, 145.
[11] K. Itaka, N. Kanayama, N. Nishiyama, W. Jang, Y. Yamasaki, K. Nakamura, H. Kawaguchi, K. Kataoka, *Journal of the American Chemical Society* **2005**, *126*, 13612.
[12] X. Xiong, H. Uludag, A. Lavasanifar, *Biomaterials* **2009**, *30*, 242.
[13] S. Matsumoto, R. Christie, N. Nishiyama, K. Miyata, A. Ishii, M. Oba, H. Koyama, Y. Yamasaki, K. Kataoka, *Biomacromolecules* **2009**, *10*, 119.
[14] T. Sun, J. Du, L. Yan, H. Mao, J. Wang, *Biomaterials* **2008**, *29*, 4348.
[15] C. Beh, W. Seow, Y. Wang, Y. Zhang, Z. Ong, P. Ee, Y. Yang, *Biomacromolecules* **2009**, *10*, 41.
[16] C. Zhu, S. Jung, S. Luo, F. Meng, X. Zhu, T. Park, Z. Zhong, *Biomaterials* **2010**, *31*, 2408.
[17] S. Kim, Y. Shi, J. Kim, K. Park, J. Cheng, *Expert Opinion on Drug Delivery* **2010**, *7*, 49.
[18] W. Kim, S. Kim, *Pharmaceutical Research* **2009**, *26*, 657.
[19] A. Zintchenko, A. Philipp, A. Dehshahri, E. Wagner, *Bioconjugate Chemistry* **2008**, *19*, 1448.
[20] J. Djordjevic, L. Del Rosario, J. Wang, K. Uhrich, *Journal of Bioactive and Compatible Polymers* **2008**, *23*, 532.
[21] Y. Wang, C.-T. Ke, C. W. Beh, S.-Q. Liu, S.-H. Goh, Y.-Y. Yang, *Biomaterials* **2007**, *28*, 5358.
[22] M. S. Shim, Y. J. Kwon, *Biomacromolecules* **2008**, *9*, 444.
[23] A. J. Geall, R. J. Taylor, M. E. Earll, M. A. W. Eaton, I. S. Blagbrough, *Bioconjugate Chemistry* **2000**, *11*, 314.

[24]   L. Brannon-Peppas, J. O. Blanchette, *Advance Drug Delivery Reviews* **2004**, *56*, 1649.

[25]   M. E. Davis, Z. Chen, D. M. Shin, *Nature Reviews Druge Discovery* **2008**, *7*, 771.

[26]   L. Tian, L. Yam, N. Zhou, H. Tat, K. Uhrich, *Macromolecules* **2004**, *37*, 538.

[27]   C. Waite, S. Sparks, K. Uhrich, C. Roth, *BMC Biotechnology* **2009**, *9*.

4. FUNCTIONALIZED AMs FOR WATER-SOLUBILIZING WHITE LIGHT-EMITTING NANOCRYSTALS

4.1. Introduction

Fluorescence is a common, versatile technique used to quantitatively detect the presence of fluorescent species. Fluorescence is particularly useful in the biomedical imaging applications described in detail in **Chapter 1** due to the non-destructive nature of the technique.[1] However, many biological substances of interest for imaging (e.g., DNA, RNA, and cells) and drug delivery vehicles of interest for imaging and tracking (e.g., polymers and liposomes) are non-fluorescent. Thus, these substances need to be fluorescently modified or "tagged" to image and/or track.

Organic fluorophores or dyes, such as fluorescein and Texas red, are commonly employed to tag biologically relevant systems. However, organic fluorophores generally have narrow and weak spectra, poor photostability, short fluorescence lifetime and pH sensitivity, such that they are only useful for short experiments under controlled conditions.[1, 2] In addition, organic fluorophores are not suited for multiplexed experimentation, in which multiple fluorophors are excited and emit fluorescence simultaneously, because often their excitation wavelengths are not the same or their emission bands overlap too much to obtain useful information.[1, 2]

Within the last decade, the use of fluorescent nanoparticles, such as semiconductor nanocrystals, for biomedical imaging applications has led to significant advances in fluorescence-based systems for imaging and tracking, as well as newer fluorescence-based techniques including biosensing, diagnostics and theragnostics.[2-4]

4.2. Background

4.2.1. Semiconductor Nanocrystals

Semiconductor nanocrystals, better known as fluorescent nanocrystals or quantum dots (QDs), are extremely small (1-20 nm) nanoparticles composed of semiconductor materials such as CdSe, CdS, or PbSe.[3-5] The extreme utility of QDs is realized due to the electronic structure of the materials, which lies between that of single molecules and bulk semiconductors, due to quantum confinement. This property yields unique optical properties – specifically, broadband absorption and narrow (often single wavelength) emission based upon crystal size, shape, and composition. Thus, multiple particles of the same composition with only modifications to the crystal size can be excited at the same wavelength, while emitting at different, very specific wavelengths (as shown in **Figure 4.1**).[2, 3, 6]

In addition to having optical properties useful for multiplexed imaging experiments, QDs have numerous other advantages over organic fluorophores including superior photostability and fluorescence lifetimes, high quantum yields, and a high resistance to chemical degradation.[2, 3] In combination, these properties make QDs extremely versatile with respect to their applications. Thus, they have been employed in lighting applications, photovoltaic devices and a host of biomedical applications as discussed in **Chapter 1**, including tracking, imaging, diagnostics, theragnostics and biosensing.[1-3, 5-18] They are particularly valuable in these biomedical applications as their size is comparable to that of many biomolecules, which is useful in biomoleculel imaging and detection.[3]
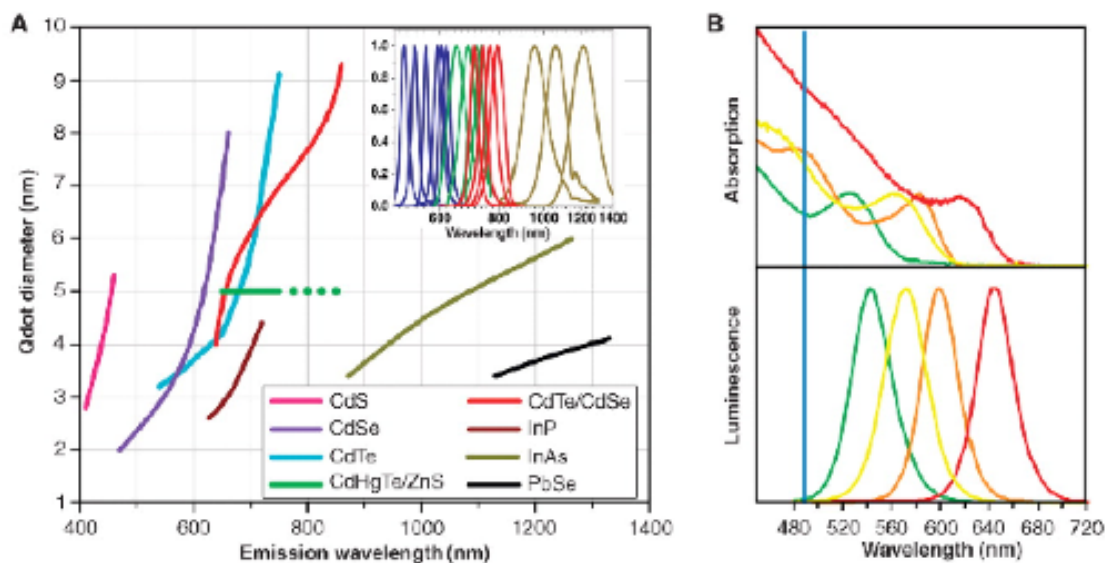
Figure 4.1. (A) Emission wavelengths with respect to diameter of varying compositions of QDs and (B) four CdSe/ZnS QDs of different sizes that exhibit broadband absorption (top curve) but narrow, single wavelength emission which results in different colored solutions (bottom curve).[3]

4.2.2. Water-solubilization of QDs

As mentioned in **Section 1.2.2**, as synthesized, the metal surface of QDs are coated with hydrophobic alkanes such as tri-octyl phosphine oxide (TOPO), hexadecylamine, or octadecylamine which solubilize the metal precursors during synthesis. The alkanes also protect the resulting nanocrystals from surface modifications, such as oxidation and/or acid etching, that decrease or deactivate fluorescence properties of QDs.[4, 19] The deactivation of the optical properties results from the high atom surface-to-volume ratio that renders their surfaces extremely reactive; surface modification provides pathways for excited electrons to become "captured" and thus the emission of their energy through radiative processes is quenched.[3] Overall, the presence of these

ligands on the surface renders the QDs hydrophobic, which is problematic for biological applications.

In addition to QDs being hydrophobic, due to their heavy metal composition, QDs are not biocompatible. Thus, for use in biological applications, QDs must be modified to render them both hydrophilic and biocompatible.[3]

Multiple methods to induce hydrophilicity and biocompatibility to QDs can be envisioned. Two commonly employed methods are encapsulation and ligand exchange (shown in **Figure 4.2**).[1, 2, 4]
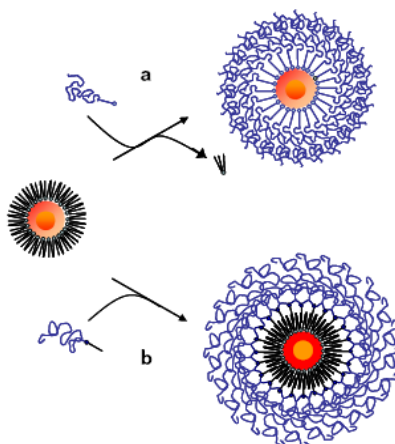
Figure 4.2. Schematic image of a) ligand exchange coating of semiconductor nanocrystals and b) ligand capping, or encapsulation, of semiconductor nanocrystals.[4]

Ideally, for biomedical applications, the method to induce water solubility, should yield systems that are: 1) protection of the nanocrystal from surface reactions, 2) maintainence small diameters, and 3) ameniable to further functionalization depending on the application, such as the ability to add targeting groups to enhance specificity.[3, 4]

4.2.2.1. Encapsulation of QDs

Encapsulation is a common method used to biostabilize QDs in which the QDs as synthesized, complete with their organic ligands, are directly entrapped within amphiphlic systems such as polymer micelles or liposomes.[1, 2, 4] The driving force for the encapsulation is purely based upon hydrophobic interactions between the hydrophobic QDs and the hydrophobic componont of the amphiphilic system (the lipid or the polymer). The advantage of encapsulation over other methods of solubilization is the ability to preserve the photophysical properties of the QDs because the surface of the crystals has not been altered. In contrast, encapsulation generally results in a significant increase in the size of the water-soluble QD systems.[1, 2, 4]

4.2.2.2. Ligand Exchange to Water-solubilize QDs

A second common method to biostabilize QDs is surface modification of the QDs with a water-soluble component *via* ligand exchange. This method of water-solubilization can be achieved using proteins or antibodies specific to the desired application or using organic acids, polymers or lipids that can directly interact with the metal surface of the QDs *via* coordination. The process of place-exchanging the hydrophobic ligands with water-soluble components on the surface of the quantum dots is called ligand exchange. This method of passivation results in a stronger interaction between the nonmetal of the coating and the nanocrystals (coordination of the nonmetal to the metal). This method of solubilization generally leads to sizes close to that of the original nanocrystal. A drawback to this method is the surface modification of the QDs that can decrease the quantum yield and significantly impact the physiochemical and photophysical stability of the QDs resulting in modified fluorescence properties.[1, 2, 4]

4.2.3. White Light-emitting Nanocrystals (WLNC)

In addition to the biological imaging applications discussed in **section 4.1.4**, QDs have also been studied as energy efficient alternatives to solid-state light lighting in the form of light-emitting diodes (LEDs).[20-23] To replace conventional white lighting systems, QDs have been studied for the development of pure white LEDs.[22, 23] To achieve white light with conventional QDs multiple colors, sizes, and/or compositions must be utilized. However, such alterations result in decreased fluorescence due to self-absorption and often result in impure white light.[23] Thus, for lighting applications, alternatives are necessary.

"Magic sized" QDs are 1.5 – 1.7 nm nanocrystals that have broadband absorption and broadband fluorescence emission properties, producing white light upon excitation with UV light.[20] As previously discussed, conventional QDs are broad-absorbing and narrow-emitting. This narrow emission is largely determined based upon band-edge emission, or the direct recombination of an electron and hole within the nanocrystal.[24-26] However, another type of emission, termed deep-trap emission, occurs in CdSe QDs when photogenerated holes created on the nanocrystal surface due to non-coordinated selenium atoms encounter an excited electron before it can relax non-radiatively.[26] In small nanocrystals (< 3.0 nm), deep-trap emission is quite common since the surface-to-volume ratio is higher than larger QDs, meaning that uncoordinated selenium sites are available to trap electron holes. However, the presence of a large band-edge emission feature allows the QDs to maintain their narrow emission features.[24, 25] In WLNCs, a so-called "magic-size" was achieved such that the band-edge emission features are largely diminished. The result is that the optical emission spectra of the WLNCs is dominated by

deep-trap emission, producing balanced white-light. Further, due to the short growth times necessary for the fabrication of WLNCs, their surfaces are likely to have more defects than conventional QDs and a larger ratio of uncoordinated surface selenium atoms.[20]

These WLNCs have been investigated for their utility as white-LEDs,[20, 21] because they do not suffer from self-absorption like other QD systems used to produce white-light[23]. Beyond solid-state lighting, the unique efficiency of their white-light emission has the potential for biomedical applications, particularly for biosensing applications where white light-emission could be used to simultaneously sense multiple analytes.[1, 2]

As discussed in **Section 4.1.3**, to utilize QDs in biological applications, the systems must first be water-solubilized. In this respect, WLNCs are no different than traditional QDs. However, due mostly to their small size, their surface-to-volume ratio is even larger than typical QDs. While they may have surface reactivity equivalent to that of other CdSe QDs, surface modifications have a greater effect on the overall photochemical properties, making WLNCs particularly sensitive to their environment. However, harnessed correctly, this environmental sensitivity could be the key to utilizing WLNCs as biosensors.

4.2.4. AMs to Water-solubilize WLNCs

AMs make an attractive candidate to biostabilize WLNC due to their ability to encapsulate hydrophobic materials and facile modification for ligand exchange. By achieving a balance between surface interaction and encapsulation, the WLNC can be

water-solubilized without affecting their emission properties while maintaining a nanoscale size.

In this work, AMs water-solubilize the WLNCs whilst maintaining the fluorescence emission properties and nanoscale sizes of the unmodified WLNCs. For water-solubilization, methods of encapsulation and ligand exchange were explored utilizing two AMs; a carboxy-terminated AM and a functionalized AM capable of coordinating to the nanocrystal surface. The properties of the water-solubilized WLNCs were evaluated *via* fluorescence spectroscopy and DLS with the goal of maintaining the white-light fluorescence emission and small, nanoscale size with the water-solubilized WLNCs. Utilizing a functionalized polymer capable of coordinating to the nanocrystal surface produced the optimal balance of fluorescence intensity and nanoscale size desired. In general, these preliminary studies highlight the ability to utilize AMs and functionalized AMs as a coating for insoluble, cytotoxic fluorescent nanocrystals without altering their emission properties. Additionally, with further study and optimization, AM-solubilized WLNCs may prove to be highly useful for future biological applications, specifically in biosensing applications.

4.3. Results and Discussion

4.3.1. Water-solubilization of WLNCs with AMs

Two polymers were employed to water-solubilize WLNC: a carboxylic acid-terminated AM, **1cM**, and a phosphonic acid-terminated AM, **1pM**. The **1cM** was utilized to encapsulate the WLNC while the **1pM** was modified from **0cM** to chemically incorporate a phosphonic acid moiety (as shown in **Scheme 4.1**). The **1pM** was designed

to ligand exchange with the organic ligands, TOPO and octadodecylphosphonic acid, on the WLNC surface, shown in **Figure 4.3**.[2, 4, 20]
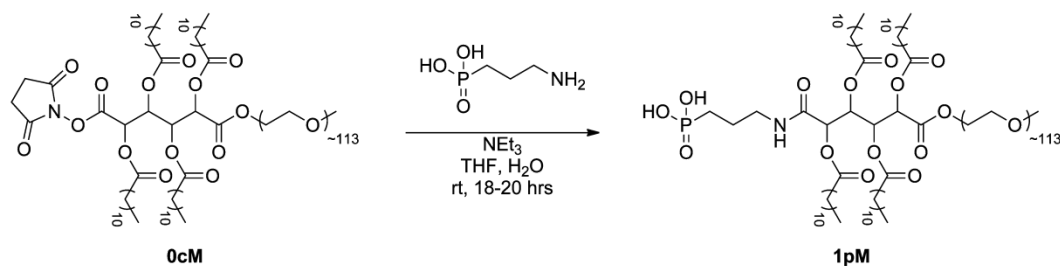
Scheme 4.1. Synthesis of **1pM** from **0cM** and 3-aminopropylphosphonic acid.
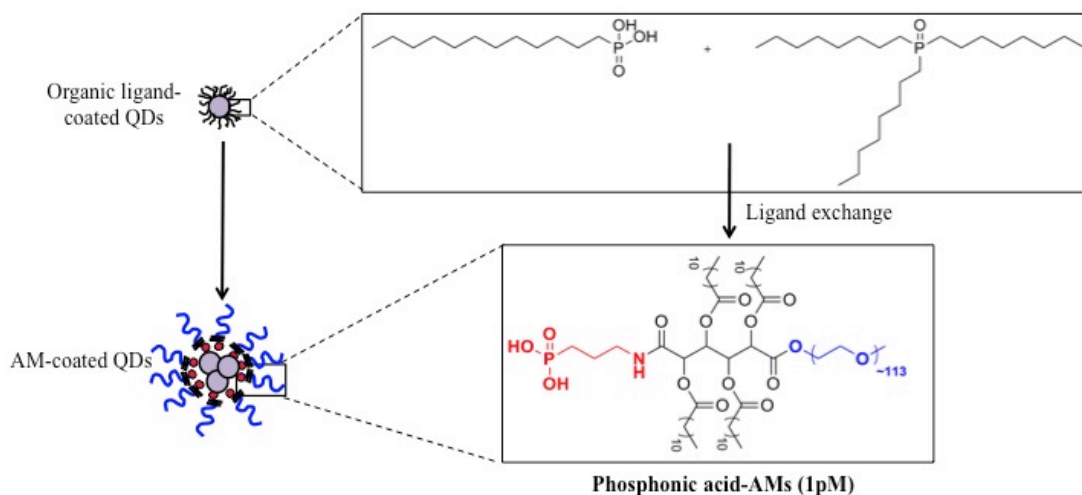
Figure 4.3. Schematic depicting the replacement of TOPO and octadecylphosphonic acid with the phosphonic acid-modified AM, **1pM**.

Synthesis of **1pM** was verified by proton nuclear magnetic resonance (^{1}H NMR) spectroscopy and molecular weight determined by gel permeation chromatography (GPC) relative to PEG standards. Due to the abundance of PEG in the polymer (~83 % of protons), the presence of new protons in the ^{1}H NMR spectra were difficult to detect, particularly from 0.8 to 2.4 ppm where the methylene protons of the hydrophobic chains

comprise the majority of that region. Thus, spectra were monitored for the disappearance of the protons of the activating group (N-hydroxysuccinimide) on **0cM**, which resonate at 2.8 ppm.

Following the successful synthesis of **1pM**, both **1cM** and **1pM** were employed to water-solubilize the WLNCs using a solvent evaporation method, as depicted in **Figure 4.4**. Variations on solvent evaporation methods are commonly used to water-solubilize fluorescent nanocrystals.[27-30] The method used in this work is carried out by dissolving the polymers and the WLNCs in a volatile, organic cosolvent (i.e., chloroform) and the solutions agitated in foil-covered vials for three hours. The chloroform was then removed by rotary evaporation and the resulting yellow films dried overnight (can be left as films longer) before re-dissolving in water by sonication.
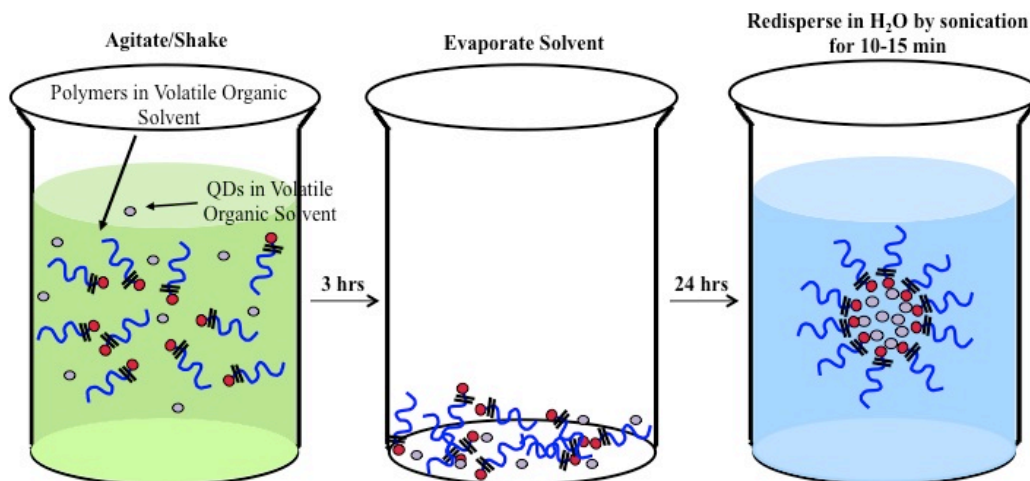
Figure 4.4. Schematic of the solvent evaporation method to water-solubilize the WLNC with AMs.

4.3.2. Characterization of Water-soluble WLNCs

Water-solubilization of the WLNCs was determined by visual inspection of the resulting solutions, as shown in **Figure 4.5**. Solubilized nanocrystals were uniformly

dispersed throughout the yellow solution, while unsolubilized nanocrystals deposited on the vial walls, as in the QD in water control. Both **1cM** and **1pM** were successful at solubilizing the WLNCs. The WLNCs in **1cM** solutions appeared cloudy and turbid, while WLNCs in **1pM** were more transparent.
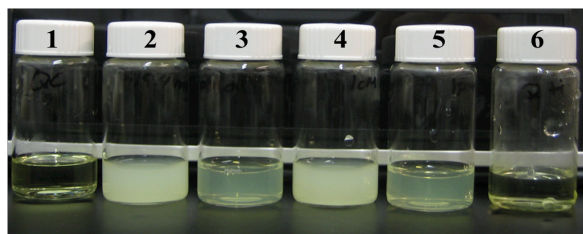
Figure 4.5. Digital photographs of WLNCs (1) dispersed in chloroform, (2) with **1cM** in H_2O, (3) with **1pM** in H_2O, (4) with **1cM** in H_2O, (5) with **1pM** in H_2O, and (6) dispersed in H_2O.

The solutions were then filtered with a 0.45 µm syringe filter to remove the larger particles. It was often necessary to use multiple filters when one became clogged, i.e. to filter 5 mL of sample 4-5 individual filters were necessary to filter the **1pM**-solubilized WLNCs where as 15-17 individual filters were necessary to filter the **1cM**-solubilized WLNCs. The use of more filters for the same sample volume indicates there are more assemblies larger than the filter size (i.e., 450 nm) in the **1cM**-solubilized WLNC solutions. Qualitatively, as shown in **Figure 4.6**, the filtered solutions of WLNC with **1cM** in H_2O contained far less nanocrystals judging by the decrease in yellow color and solution opacity. In contrast, the WLNC solutions with **1pM** in H_2O are visually similar to the unfiltered samples (Figure 4.5).
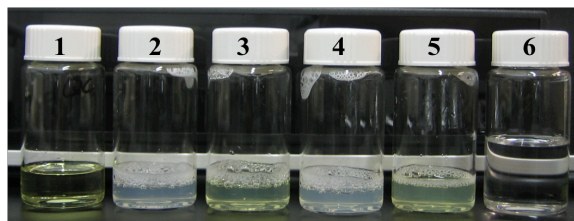
Figure 4.6. Digital photographs of WLNCs (1) dispersed in chloroform, (2) with **1cM** in H₂O, (3) with **1pM** in H₂O, (4) with **1cM** in H₂O, (5) with **1pM** in H₂O, and (6) dispersed in H₂O after filtration with a 0.45 μm syringe filter.

4.3.2.1. Turbidity

Turbidity was quantitatively determined using UV/Vis absorbance spectroscopy, shown in **Figure 4.7**. WLNCs dispersed in chloroform were tested as a standard for the amount of light that could be transmitted in solutions without turbidity, as the light transmitted is only that light which was not absorbed by the nanocrystals. Confirming the qualitative visual inspection, the WLNC samples with **1cM** dispersed in H₂O resulted in 0 – 6 % transmittance from 190-600 nm, while the WLNC solutions with **1pM** dispersed have a much higher % transmittance from 340 – 640 nm, with a curve similar to the WLNCs in chloroform. Following filtration, samples of WLNCs dispersed in water with both **1cM** and **1pM** have significantly higher light transmittance across the spectra complared to the samples without filtration. However, while both samples of **1pM**/WLNCs, filtered and unfiltered, have transmittance curves with features similar to the WLNCs in chloroform (i.e. peaks ~ 360, 390, and an approx. leveling off at ~ 490 nm), only the filtered sample of **1cM**/WLNCs has a curve that modestly resembles that of the WLNCs in chloroform.
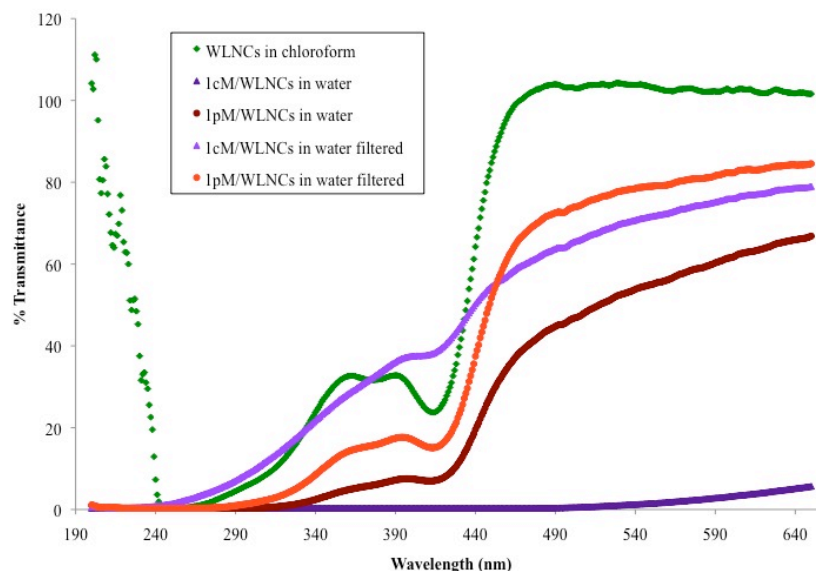
Figure 4.7. Percent transmittance for various WLNC samples from 200 – 650 nm.

Overall, the percent transmittance data correlates with the qualitative imaging results in that the samples of **1pM**-solubilized WLNCs are less turbid than the **1cM**-solubilized WLNCs. However, when the **1cM**-solubilized WLNC solution is filtered, the turbidity decreases significantly. Additionally, this data shows that the **1pM**-solubilized WLNCs maintain transmittance spectra more similar to the WLNCs in chloroform than do those nanocrystals water-solubilized using **1cM**.

4.3.2.2. Assembly Sizes

Hydrodynamic diameters of the aqueous WLNC solutions were determined using dynamic light scattering, the results are shown in **Figure 4.8**. For the unfiltered samples, the assemblies and/or aggregates of WLNC with each polymer existed as two distinct size distributions, with the smaller sized particles as the major solution component. In comparing the assemblies and/or aggregates of the **1cM**-solubilized WLNC (**1cM**/WLNCs) to the **1pM**-solubilized WLNC (**1pM**/WLNCs), ~60 % of the **1pM**-

solubilized WLNC assemblies are ~ 49 nm while the other ~40% are ~ 435 nm in diameter. In contrast, the larger sized particles of the **1cM**-solubilized WLNCs (~420 nm) account for 70 % of the volume, while the remaining 30 % is attributed to 5 μm size assemblies/aggregates.
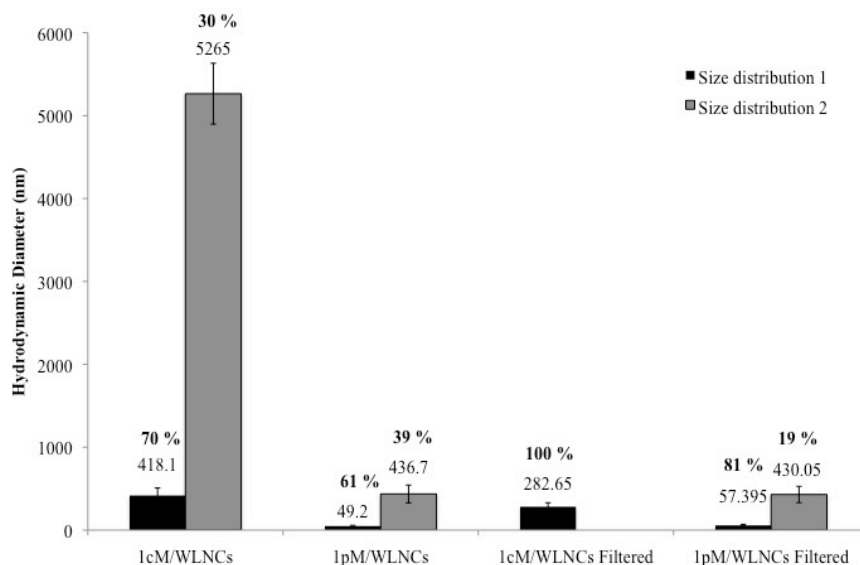
Figure 4.8. Hydrodynamic diameters of polymer/WLNC aggregates. In solutions where two distinct size distributions were present, the smaller size distribution is represented with a black bar while the larger distribution is represented in grey. The percentage of the observed size distributions are displayed directly above particle size (expressed in nm). Error bars represent peak widths.

Upon filtering the samples with a 0.45 μm syringe filter, the larger aggregates are greatly reduced as observed by DLS in **Figure 4.8** and in accordance with the visual results, **Figure 4.6 (bottom)**. For the **1cM**-solubilized WLNCs, the 5 μm assemblies/aggregates are completely removed and the remaining assemblies form sizes of ~ 280 nm, indicating that mechanical forces of the filter break up the larger aggregates.

Conversely, the **1pM**-solubilized WLNC still exist as two size distributions of 57 nm and 430 nm. However, the percentage of the smaller sized particles increased by about 20 %. This result again suggests that the mechanical force of filtration reduces the aggregate size. As a whole, these results are consistent with the turbidity data; the assemblies from **1cM**-solubilized WLNC are larger and transmit significantly less light than **1pM**-solubilized WLNC. Further, the qualitative results visualized before and after sample filtering (**Figure 4.5** and **Figure 4.6**) demonstrated that turbidity of the **1cM**-solubilized WLNC samples significantly decreased following filtration (ie, larger aggregates and assemblies were removed and/or disassociated) while minor changes were observed with **1pM**-solubilized WLNC.

4.3.2.3. Qualitative Fluorescence Emission

Fluorescence emission was qualitatively determined by excitation with a long wavelength UV lamp at 365 nm. As shown in **Figure 4.9 (top)**, All solutions except the WLNC dispersed in water only emit bright white light that is evenly dispersed throughout the solution, indicating successful solubilization. For WLNC samples in water, the WLNC adheres to the vial walls, indicating a lack of aqueous solubilization of the hydrophobic nanocrystals.

When the solutions were filtered with a 0.45 μm syringe filter, the white light fluorescence intensity for the aqueous WLNC solution with **1cM** significantly decreased compared with the unfiltered solutions, whereas the aqueous WLNC solution with **1pM** fluoresces as intensely as the unfiltered samples (shown in **Figure 2.9 (bottom)**). This observation indicates that the majority of the nanocrystals with **1cM** exist as assemblies or aggregates <u>larger</u> than 450 nm. However, the fluorescence intensity of the nanocrystals

with **1pM** have a qualitatively similar fluorescence intensity, suggesting the majority of

the assemblies and/or aggregates are <u>smaller</u> than 450 nm.

Unfiltered WLNCs

WLNC solutions filtered with a 0.45 μm syringe filter
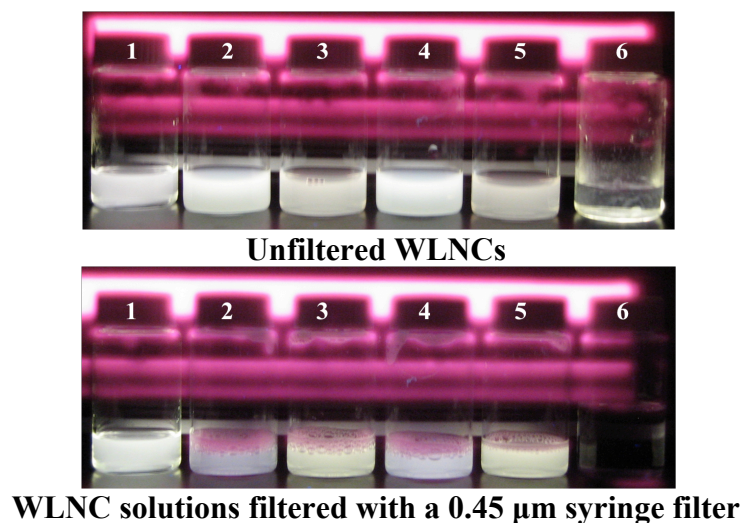
Figure 4.9. Digital photographs of WLNC solutions following excitation with a long

wavelength UV lamp at 365 nm. (top) WLNC (1) dispersed in chloroform, (2) with **1cM**

in H_2O, (3) with **1pM** in H_2O, (4) with **1cM** in H_2O, (5) with **1pM** in H_2O, and (6)

dispersed in H_2O, (bottom) WLNC (1) dispersed in chloroform, (2) with **1cM** in H_2O, (3)

with **1pM** in H_2O, (4) with **1cM** in H_2O, (5) with **1pM** in H_2O, and (6) dispersed in H_2O

after filtration with a 0.45 μm syringe filter.

4.3.2.4. Quantitative Fluorescence Emission

Quantitative fluorescence emission data for all samples was collected using

fluorescence spectroscopy from 380 – 800 nm following excitation at 365 nm (shown in

Figure 4.10).
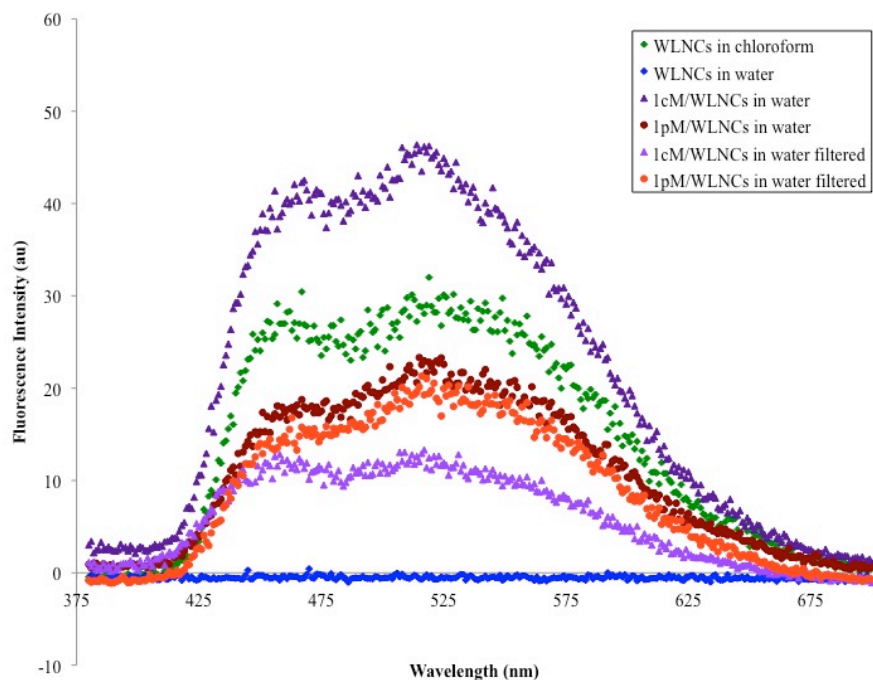
Figure 4.10. Fluorescence emission spectra of WLNC dispersed in the indicated solvent and, where applicable, solubilized by the indicated polymers.

All solutions of WLNC, with the exception of the nanocrystals in water only, shared a similar fluorescence profile (i.e., broadband white light-emission and similar λ_{max} peaks) as the nanocrystals dissolved in chloroform at the same concentration. The **1cM**-solubilized WLNCs (**1cM**/WLNCs in water) had fluorescence intensity significantly greater than the nanocrystals in chloroform (approximately 1.5 times greater) while the **1pM**-solubilized WLNCs (**1pM**/WLNCs in water) had a fluorescence emission approximately 70 % that of the nanocrystals in chloroform. When filtered, the **1pM**-solubilized WLNC (**1pM**/WLNC in water filtered) had approximately the same fluorescence intensity as the unfiltered sample across the spectrum. In contrast, the filtered sample of **1cM**-solubilized WLNCs (**1cM**/WLNC in water filtered) lost approximately 75 % of the fluorescence of the unfiltered sample, dropping to ~ 30 % of

the nanocrystal fluorescence in chloroform at the original concentration. This quantitiative fluorescence data is consistent with visual inspection (**Figure 4.9**).

Taken together with the sizing data, the **1cM**-solubilized WLNC data suggests that the majority of the solution fluorescence results from the assemblies/aggregates of 5 μm in size. This phenomonen is interesting, as these large particles only account for ~ 30 % of the overall size distribution for the sample. As the fluorescence intensity of this aqueous solution is greater than nanocrystals dissolved in chloroform at the same concentration, the data suggests that nanocrystal aggregations improve their fluorescence intensity compared to smaller sized assemblies. As the goal was to create systems that are small assemblies with fluorescence unaffected by water-solubilization, the **1pM**-solubilized WLNCs have the optimal balance of small size distrbutions and largely unaffected fluorescence emission profiles.

It should also be noted that a large emission peak was also observed for all AM-solubilized WLNC solutions at ~ 728 nm. This NIR emission peak can be attributed to the second diffraction peak from the excitation source passing through slits and a grating, which occurs when the sample is slightly scattering the excitation light.

4.3.2.5. Preliminary Cellular Uptake

The cellular uptake studies were performed by Nicole M. Plourde, a Ph.D. candidate in Chemical and Biochemical Engineering (Rutgers University, Piscataway, NJ) supervised by Professor Prabhas V. Moghe.

The ability of water-soluble WLNCs to be internalized was preliminarily evaluated in THP-1 macrophage cells. As shown in **Figure 4.11**, both **1cM**-solubilized WLNCs and **1pM**-solubilized WLNCs are internalized by cells and continue to emit

white light. In comparing the two polymer for solubilizing the WLNCs, it is clear in **Figure 4.11** that **1pM**-solubilized WLNCs (**Figure 4.11B**) are more effectively internalized due to the larger number of fluorescent cells and their higher intensity. In addition, as shown in **Figure 4.12**, cells incubated with **1pM**-solubilized WLNCs under the UV filter with increased magnification show the **1pM**-solubilized WLNCs appear to be localized within the nuclei of the cells. The cells appeared healthy, indicating the assemblies exhibited low cytotoxicity, as biocompatibility is often a barrier to using fluorescent QDs for biological applications.[3] This preliminary data shows that for cellular applications, **1pM**-solubilized WLNCs are more efficient, which is likely due to the smaller assembly size of these systems as compared to the **1cM**-solubilized WLNCs.
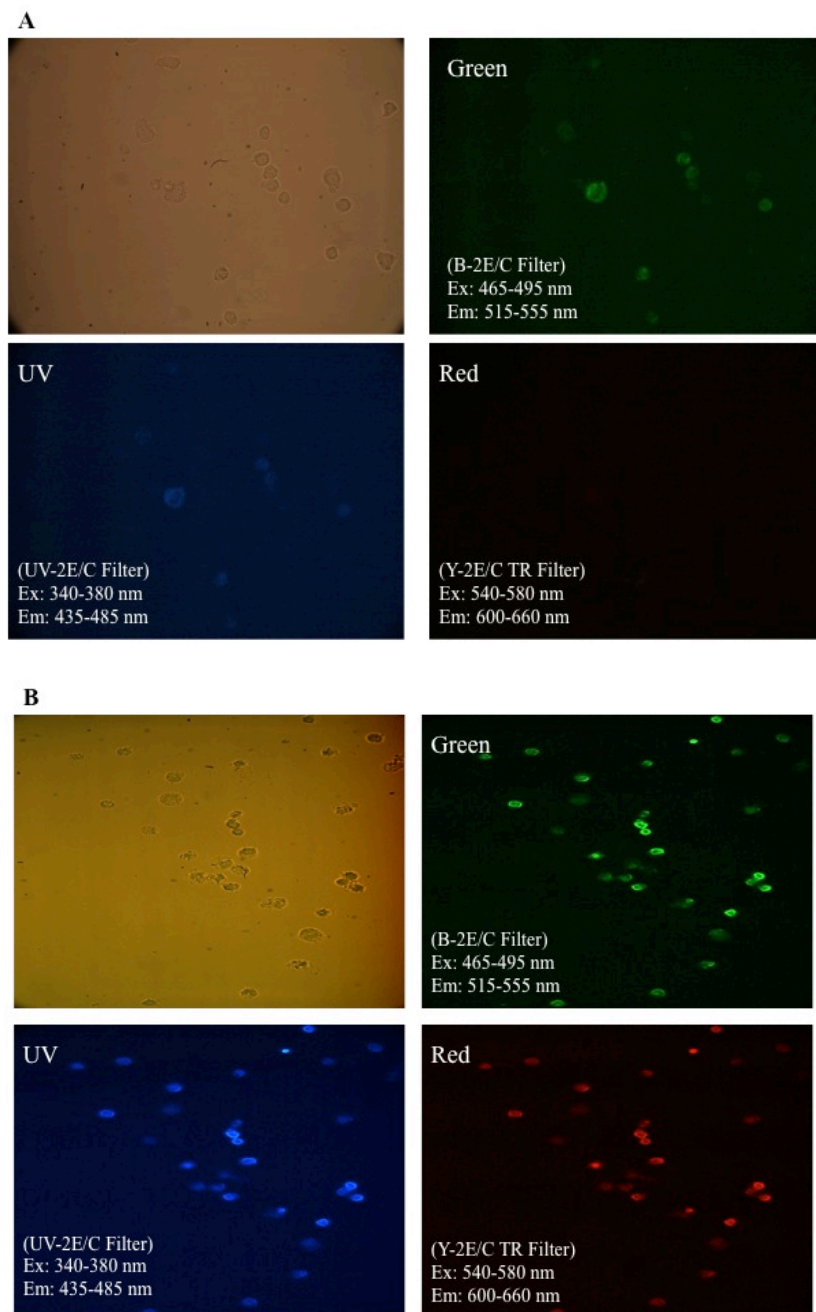
Figure 4.11. Uptake of A) **1cM**-solubilized WLNCs and B) **1pM**-solubilized WLNCs in THP-1 macrophage cells after 24 hours incubation. The cells were imaged at 20x magnification using multiple microscope filters to show retention of white-light emission.
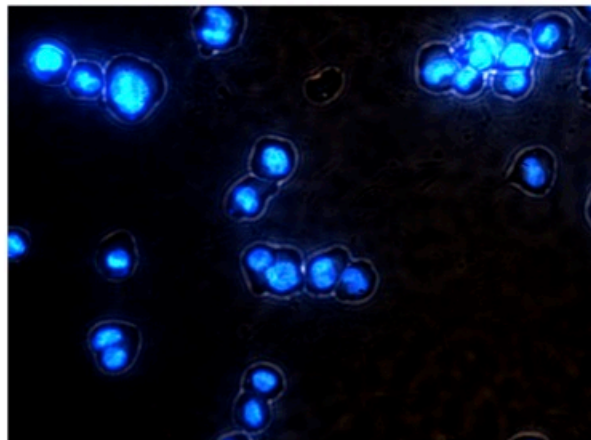
Figure 4.12. Uptake of **1pM**-solubilized WLNCs in THP-1 macrophage cells after 24 hours incubation under the UV filter (excitation: 340-380 nm, emission: 435-485 nm) at 40x magnification.

4.3.2.6. Evidence for Ligand Exchange Using 1pM

Hitherto, the **1pM** is referenced as a polymer capable of coordinating to the nanocrystal surface. While the previously discussed data shows a significant difference between **1pM** and **1cM**, direct evidence for solubilization by ligand exchange is scant. To investigate ligand exchange mechanisms, increasing polymer concentrations with respect to the nanocrystals was investigated; as more polymer becomes available to exchange the surface organic ligands, the WLNC fluorescence properties would be modified. As qualitatively shown in **Figure 4.13**, increasing the polymer:WLNC ratio from 10 to 80 gradually shifted the fluorescence emission from white to blue light. This data indicates increased interactions of the ligands with the QD surface resulting in altered fluorescence. Some potential causes are: 1) the ligands create additional surface defects causing excited electrons to be "captured" before emitting their energy radiatively, as discussed previously in **Section 4.1.3**, or 2) ligand interaction with the uncoordinated

surface selenium atoms decreasing the ability of the selenium to participate in deep-trap emission, as discussed in **Section 4.1.5**. Thus, in the case of the **1pM**-solubilized WLNCs, the shift from white-light emission to the emission of blue light suggests that those electrons relaxing through higher energy pathways continue to emit light while low energy electrons become trapped by ligands and/or relax through different, non-radiative pathways.
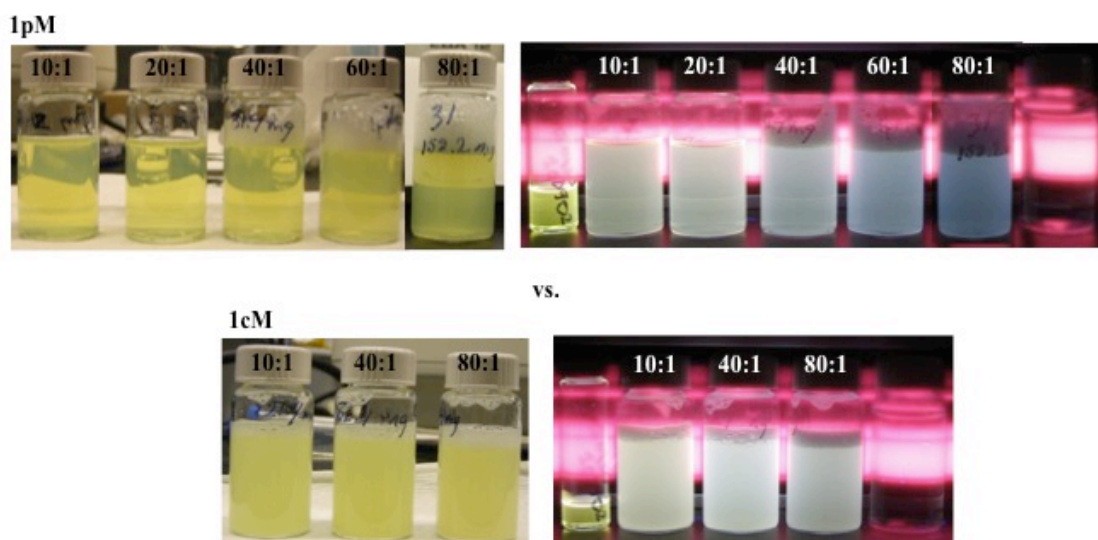
Figure 4.13. Qualitative images of increasing polymer concentration on the WLNC fluorescence emission, (top) increasing ratio of **1pM**:WLNC, (bottom) increasing ratio of **1cM**:WLNC.

This change is shown quantitatively in **Figure 4.14** for the **1pM**:WLNC ratio of 80:1 in which the peak at 524 nm substantially decreases relative to the unmodified nanocrystals in chloroform. When the ratio of **1cM**:WLNC is increased from 10 to 80, this shift from white to blue light emission by visual inspection in **Figure 4.13** is not observed. This result supports the hypothesis that increasing the concentration of **1pM** results in increased interactions between the polymer and nanocrystal surface. The

increased polymer-WLNC interactions result in significant changes in fluorescence emission, from white-light to blue light.
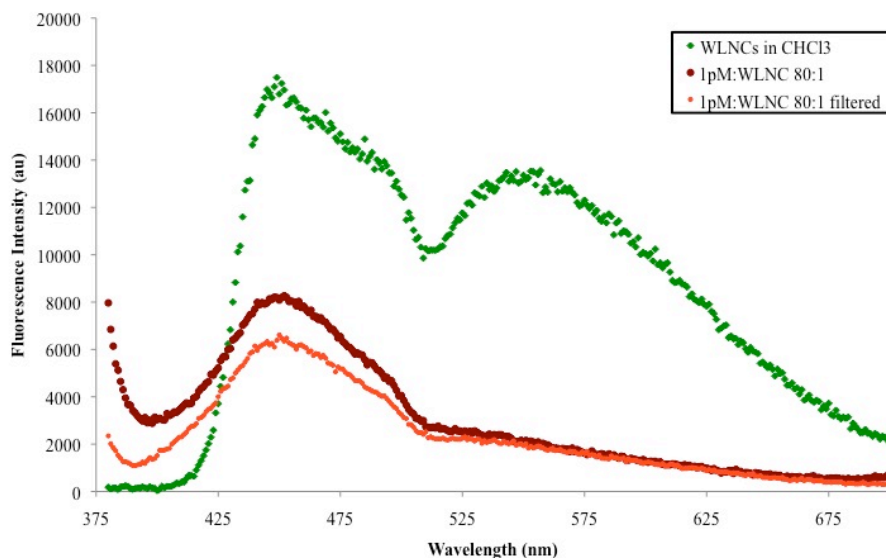
Figure 4.14. Fluorescence emission spectra of **1pM**-solubilized WLNCs at a ratio of 80:1 **1pM**:WLNC compared with the WLNCs in chloroform shows a decrease in the fluorescence emission intensity for **1pM**:WLNC 80:1 after 500 nm, yielding predominantly blue emission.

4.3.2.7. Storage Stability of 1pM-solubilized WLNC Assemblies

As discussed earlier, the goal of this work was to determine the best AM to water-solubilize the WLNCs. The optimal polymer was defined having the capability to water-solubilize the WLNCs into assemblies that maintain the nanocrystal size and fluorescence properties. Based upon the previously discussed results, the **1pM**-solubilized WLNCs were determined to be the best polymer – with small size distrbutions and largely unaffected fluorescence emission profiles. Therefore, the **1pM**-solubilized WLNCs were the only samples further evaluated for their storage stability.

To assess the appropriate storage conditions and stability of the **1pM**-solubilized WLNCs, samples at a polymer:nanocrystal ratio of 20:1 were tested for fluorescence emission over two weeks. The storage conditions included: a lyophilized condition (samples frozen and lyophilized on Day 0, then resolubilized and stored at -4 °C for the remainder of the two weeks); and solutions stored at -4 °C (freezer), 2-8 °C (refrigerator), and 25 °C (room temperature). Fluorescence emission data was collected from 380 – 800 nm following excitation at 365 nm. The data was then analyzed and the sample fluorescence intensity at 525 nm with respect to the original fluorescence (i.e., day 0) graphed in **Figure 4.15**.
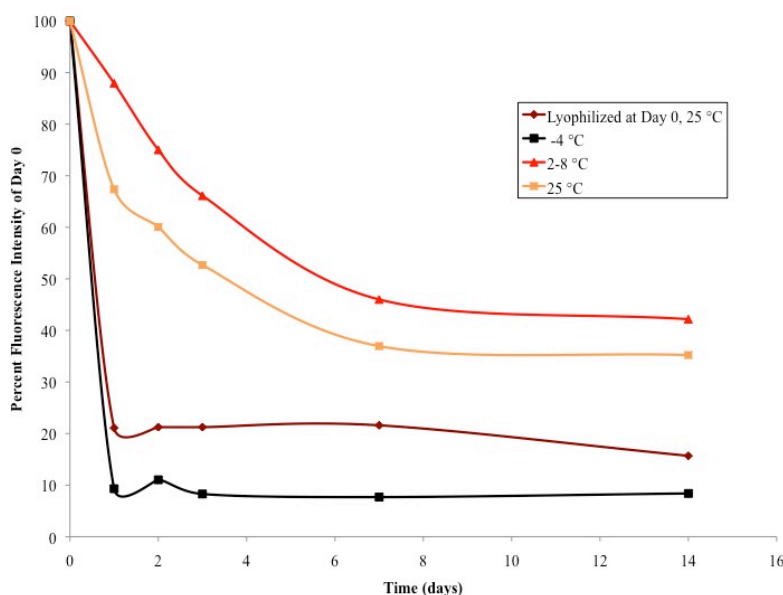
Figure 4.15. Storage stability of **1pM**-solubilized WLNCs at varying storage conditions quantified by precent fluorescence intensity at 525 nm (compared with day 0) over two weeks.

After 24 hours, the fluorescence intensity for all samples significantly decreased, but less so for solutions stored at 2-8 °C and 25 °C. After the first freeze-thaw cycle,

samples stored at -4˚C retained 10 % of their original intensity, while solutions stored at 2-8 °C or 25 °C continually decreased over fourteen days to ~40 % of their original fluoresecence intensity. While the data shown is only for the emission peak at 525 nm, the fluorescence intensity for all samples at the emission peak at ~450 nm similarly decreased, indicating an overall quenching of fluorescence properties. This data suggest that the first freeze-thaw cycle for nanocrystals water-solubilized using **1pM** has detrimental effects on the nanocrystal fluorescence, since after the first freeze-thaw cycle the fluorescence intensity remains constant regardless of subsequent freezer storage. Thus, solutions are best stored at refrigeration or room temperatures; however, intensity does significantly decrease with storage time.

4.4. Summary

Water-solubilization of WLNCs was achieved. Encapsulation using the carboxy-terminated AM (**1cM)** resulted in WLNCs with the most intense fluorescence, even greater than the original WLNCs dispersed in chloroform at the same concentration. However, smaller sizes were achieved by solubilzing the WLNCs with the functionalized AMs (**1pM**). Additionally, the sizes and fluorescence intensities were maintained for **1pM**-solubilized WLNCs following filtration through a 0.45 μm syringe filter, while the intensity of fluorescence emission for the **1cM**-solubilized WLNCs decreased to 75 % of its original intensity. In addition, evidence of ligand exchange was determined qualitatively; increased polymer concentrations resulted in a shift from white- to blue-light emission, indicating the surface of the WLNCs had been altered. Based on the disappearance of emission above 500 nm, the surface modification caused excited

electrons with low energy-emission to relax non-radiatively. Finally, the storage stability of the ligand exchange-solubilized systems was evaluated over fourteen days at a range of temperatures and it was determined that freshly solubilized samples displayed optimal fluorescence properties. However, if sample storage was necessary, refrigeration is best.

Future work to probe the polymer/WLNC interface would generate design criteria to optimize the water-solubilzes systems. Additionally, based upon our data, water-solubilized WLNCs should be explored for biosensing applications.

4.5. Experimental

4.5.1. Synthetic Materials

Unless otherwise stated, solvents and reagents were purchased from Fisher Scientific (Pittsburgh, PA) and Sigma-Aldrich (St. Louis, MO) and used as received. PEG 5 kDa was purchased from Polysciences, Inc. (Warrington, PA) and dried by azeotropic distillation from toluene before use. The **1cM** and **0cM** (starting material for **1pM**) were synthesized as previously described[31, 32] and the CdSe WLNCs were synthesized and provided as solutions in chloroform by Professor Sandra Rosenthal's group at Vanderbilt University, Department of Chemistry[20].

4.5.2. Characterization Methods

4.5.2.1. Proton Nuclear Magnetic Resonance (^{1}H NMR) Spectroscopy

Proton nuclear magnetic resonance (^{1}H-NMR) spectra of the products were obtained using a Varian 400 MHz or 500 MHz spectrophotometer. Samples were dissolved in chloroform-d, with a few drops of dimethyl sulfoxide-d_6 if necessary, with tetramethylsilane as an internal reference.

4.5.2.2. Gel Permeation Chromatography (GPC)

Molecular weights (M_w) and polydispersity indices (PDI) were determined using gel permeation chromatography (GPC) with respect to PEG standards (Sigma-Aldrich) on a Waters Stryagel® HR 3 THF column (7.8 x 300 mm). The Waters LC system (Milford, MA) was equipped with a 2414 refractive index detector, a 1515 isocratic HPLC pump, and 717plus autosampler. An IBM ThinkCentre computer with Waters Breeze Version 3.30 software installed was used for collection and processing of data. Samples were prepared at a concentration of 10 mg/mL in tetrahydrofuran, filtered using 0.45 μm pore size nylon or poly(tetrafluoroethylene) syringe filters (Fisher Scientific) and placed in sample vials to be injected into the system.

4.5.3. Polymer Synthesis

4.5.3.1. 1pM

In a 100 mL round bottom flask, 3-aminopropyl phosphonic acid (110 mg, 0.79 mmol) was dissolved in HPLC-grade H_2O (6 mL), HPLC-grade THF (12 mL), and triethylamine (0.38 mL, 2.7 mmol) and the solution stirred at room temperature. In a separate flask, **0cM** (1.10 g, 0.183 mmol) was dissolved in HPLC-grade THF (25 mL) and the solution added to the reaction flask. The yellow solution was stirred for 18-20 hrs at room temperature before the THF was removed by rotary evaporation. The resulting yellow oil was dissolved in CH_2Cl_2 and 0.1 N HCl and stirred for 20-30 min. The mixture was then transferred to a separatory funnel containing addition 0.1 N HCl and the organic layer separated and washed with brine (2x). The combined aqueous portions were extracted with CH_2Cl_2 and the combined organics dried over $MgSO_4$ and concentrated to a yellow oil. White product was precipitated from the yellow oil in CH_2Cl_2 by addition

of 10-fold diethyl ether in a 50 mL centrifuge tube. The suspension was place on a shaker for 10-15 min before the solid was collected by centrifugation and the supernatant removed by decanting. The solid was dissolved in CH_2Cl_2 (< 5 mL) and reprecipitated by adding 10-fold diethyl ether. The solid was collected by centrifugation, the supernatant removed, and the solid washed with ether (1x). The white solid was dried under ambient conditions (48 hrs) and under high vacuum (12 hrs). Yield: 0.896 g, 80 %. ^{1}H- NMR ($CDCl_3$): δ 5.70 (m, 2H, CH), 5.00 (m, 2H, CH), 4.20 (m, 4H, CH_2), 3.60 (m, ~0.45 kH, CH_2O), 3.38 (s, 3H, CH_3), 2.43 (m, 8H, CH_2), 1.61 (m, 10H, CH_2), 1.22 (m, 64H, CH_2), 0.87 (t, 12H, CH_3). GPC: M_w: 7.0 kDa; PDI: 1.06.

4.5.4. Water-solubilization of WLNCs by Solvent Evaporation

Two samples each of WLNCs solubilized by each polymer, exact amounts of all reagents and concentrations specified in **Table 4.1** below, were prepared by solvent evaporation. For a polymer:WLNC ratio of 20:1, 150 μL of a 1.0 mM solution of WLNCs in chloroform (concentration determined as previously described[33]) were added to a 1.25 mM solution of each polymer in chloroform (final volume − 2.900 mL chloroform). The solutions were agitated on a shaker for 3 hours are room temperature before the chloroform was removed by rotary evaporation. The resulting yellow films were dried under flowing argon gas for one minute and under ambient conditions for at least 12 hours. Water-solubilization was achieved by adding water (5.000 mL) to achieve a concentration of ~ 30.0 μM WLNCs and ~ 600 μM polymer. Filtered samples were prepared by passing the solutions through 0.45 μm Fisherbrand nylon syringe filters (Fisher Scientific).

	AM (mg)	AM (μmol)	WLNCs (μmol)	Stirring		Water-Soluble WLNCs		
Sample				[AM] (μM)	[WLNC] (μM)	[AM] (μM)	[WLNC] (μM)	AM:WLNC
1pM 1	20.9	3.43	0.150	1180	51.7	685.2	30.0	22.8
1pM 2	20.8	3.41	0.150	1180	51.7	682.0	30.0	22.7
1cM 1	19.4	3.29	0.150	1130	51.7	657.6	30.0	21.9
1cM 2	21.3	3.61	0.150	1240	51.7	722.0	30.0	24.1

Table 4.1. Specific amounts and concentrations of polymers and WLNCs used to formulate the water-solubilized nanocrystals.

Polymer-solubilized nanocrystal solutions evaluated in **Section 4.1.3.5.** were prepared using the general procedure described above. The specific amounts for each ratio are shown in **Table 4.2**, below. Generally, the appropriate amount of polymer necessary to obtain the desired polymer:WLNC ratio was dissolved in chloroform and 348 μL of a 0.935 mM solution of WLNCs in chloroform (concentration determined as previously described[33]) were added (final volume – 3.044 mL chloroform). The solutions were agitated on a shaker for 3 hours are room temperature before the chloroform was removed by rotary evaporation. The resulting yellow films were dried under flowing argon gas for one minute. Water-solubilization was achieved by adding water (15.000 mL) to achieve a concentration of 21.7 μM WLNCs.

				Stirring		Water-Soluble WLNCs		
Sample	AM (mg)	AM (µmol)	WLNCs (µmol)	[AM] (µM)	[WLNC] (µM)	[AM] (µM)	[WLNC] (µM)	AM:WLNC
1pM 10	21.0	3.44	0.325	1130	107	230	21.7	10.6
1pM 20	40.1	6.57	0.325	2160	107	438	21.7	20.2
1pM 40	81.9	13.4	0.325	4140	107	895	21.7	41.3
1pM 60	120.1	19.7	0.325	6470	107	1313	21.7	60.5
1pM 80	158.2	25.9	0.325	8520	107	1730	21.7	79.7
1cM 10	21.4	3.57	0.325	1170	107	238	21.7	11.0
1cM 40	82.4	13.7	0.325	4510	107	916	21.7	42.2
1cM 60	164.6	27.4	0.325	9010	107	1830	21.7	84.3

Table 4.2. Specific amounts and concentrations of polymers and WLNCs used to formulate the water-solubilized nanocrystals of varying polymer:WLNC ratios evaluated in **Section 4.1.3.5**.

4.5.5. Characterization of Water-soluble WLNCs

4.5.5.1. Qualitative Evaluation of Turbidity and Fluorescence

Turbidity of filtered and unfiltered solutions of water-solubilized WLNCs as compared with WLNCs in chloroform at the same concentration was qualitatively evaluated by visual inspection and images captured using a Canon PowerShot SD400 digital camera. Fluorescence of the solutions was qualitatively evaluated following excitation with a Spectroline ® Longlife[TM] Filter long wavelength UV lamp (365 nm) and images captured using a Canon PowerShot SD400 digital camera.

4.5.5.2. Quantitative Turbidity: Percent Transmittance

Turbidity of filtered and unfiltered solutions of water-solubilized WLNCs as compared with WLNCs in chloroform at the same concentration was evaluated quantitatively by UV/Visible absorbance on a Lambda Bio XLS instrument (Perkin Elmer, Waltham, MA) scanning from 190 – 650 nm.

4.5.5.3. Quantitative Fluorescence Emission

Fluorescence of water-solubilized WLNCs and WLNCs in chloroform at the same concentration from 380 – 800 nm was quantified using a Shimadzu RF-5301 PC spectrofluorophotometer, with an excitation wavelength of 365 nm. For simplicity, during data analysis duplicate samples were average and graphed.

4.5.5.4. Hydrodynamic Diameter

Hydrodynamic diameters were evaluated by dynamic light scattering (DLS) using a Malvern Instruments Zetasizer Nano ZS-90 instrument (Southboro, MA). DLS measurements were performed at a 90° scattering angle at 25°C. Size distributions by volume of measurements were collected in triplicate, averaged and reported.

4.5.5.5. Cellular Uptake in THP-1 Macrophages

[Cell studies were performed by Nicole Plourde, Department of Biomedical Engineering, Rutgers University, Piscataway, NJ, under the supervision of Professor Prabhas V. Moghe]

Internalization of AM-solubilized WLNCs by THP-1 macrophage cells was assayed by incubating the AM-solubilized WLNCs (prepared as described in **Section 2.4.4.** at a polymer concentration of 15 μM and a WLNC concentration of 3.75 μM) diluted to 1 μM with respect to the polymer, with cells for 24 hours at 37 °C and 5 %

CO_2, The cells were then washed once with PBS and imaged for cell-associated fluorescence using a Nikon Eclipse TE2000-S.

4.5.5.6. Storage Stability of 1pM-solubilzed WLNCs

Four 15 mL samples of **1pM**-solubilzed WLNCs as a polymer:WLNC ratio of 20 were prepared as described in **Section 2.5.4.** The four samples were distributed into three 5 mL aliquots then stored at four different storage conditions: 1) lyophilized on day 0 then stored at room temperature (~ 25 °C), 2) – 4 °C (freezer), 3) 2 – 8 °C (refrigeration), and 4) room temperature (~ 25 °C). At day 0, 1, 2, 3, 7 and 14, the fluorescence of each of the samples was quantified as described in **section 2.5.5.3**. For analysis, the three samples at each storage condition were averaged. For comparison, the fluorescence at 525 nm for each sample as a percentage of the orginal fluorescence (i.e., day 0) was graphed.

4.6. References

[1]   C. S. S. R. Kumar, *Nanomaterials for Biosensors, Vol. 8*, Wiley-VCH, Germany, **2007**.
[2]   A. Merkoci, *Biosensing Using Nanomaterials*, John Wiley & Sons, Inc, Hoboken, NJ, **2009**.
[3]   R. J. Martin-Palma, M. Manso, V. Torres-Costa, *Sensors* **2009**, *9*, 5149.
[4]   A. F. E. Hezinger, J. Tebmar, A. Gopferich, *European Journal of Pharmaceutics and Biopharmaceutics* **2008**, *68*, 138.
[5]   P. A. Alivisatos, W. Gu, C. Larabell, *Annual Review of Biomedical Engineering* **2005**, *7*, 55.
[6]   F. Pinaud, X. Michalet, L. A. Bentolila, J. M. Tsay, S. Doose, J. J. Li, G. Iyer, S. Weiss, *Biomaterials* **2006**, *27*, 1679.
[7]   V. K. Varadan, L. Chen, J. Xie, *Nanomedicine: Design and Applications of Magnetic Nanomaterials, Nanosensors, and Nanosystems*, John Wiley & Sons, Ltd, West Sussex, UK, **2008**.
[8]   K. T. Thurn, E. M. B. Brown, A. Wu, S. Vogt, B. Lai, J. Maser, T. Paunesku, G. E. Woloschak, *Nanoscale Research Letters* **2007**, *2*, 430.

[9]   K. L. Hultman, A. J. Raffo, A. L. Grzenda, P. E. Harris, T. R. Brown, S. O'Brien, *ACS Nano* **2008**, *2*, 477.

[10]   X. Michalet, F. F. Pinaud, L. A. Bentolila, J. M. Tsay, S. Doose, J. J. Li, G. Sundaresan, A. M. Wu, S. S. Gambhir, S. Weiss, *Science* **2005**, *307*, 538.

[11]   H. Duan, N. Shuming, *Journal of the American Chemical Society* **2007**, *129*, 3333.

[12]   C. Wu, B. Bull, C. Szymanski, K. Christensen, J. McNeill, *ACS Nano* **2008**, *2*, 2415.

[13]   K. Susumu, H. T. Uyeda, I. L. Medintz, T. Pons, J. B. Delehanty, H. Mattoussi, *Journal of the American Chemical Society* **2007**, *129*, 13987.

[14]   G. Ruan, A. Agrawal, A. I. Marcus, N. Shuming, *Journal of the American Chemical Society* **2007**, *129*, 14759.

[15]   J.-H. Park, G. von Maltzahn, E. Ruoslahti, S. N. Bhatia, M. J. Sailor, *Angewandte Chemie International Edition* **2008**, *47*, 7284.

[16]   B. Dubertret, P. Skourides, D. J. Norris, V. Noireaux, A. H. Brivanlou, A. Libchaber, *Science* **2002**, *298*, 1759.

[17]   S. D. Duhachek, J. R. Kenseth, G. P. Casale, G. J. Small, M. D. Porter, R. Jankowiak, *Analytical Chemistry* **2000**, *72*, 3709.

[18]   F. Pene, E. Courtine, A. Cariou, J.-P. Mira, *Critical Care Medicine* **2009**, *37*, S50.

[19]   N. I. Hammer, T. Emrick, M. D. Barnes, *2* **2007**.

[20]   M. J. Bowers II, J. R. McBride, S. J. Rosenthal, *Journal of the American Chemical Society* **2005**, *127*, 15378.

[21]   M. A. Schreuder, J. D. Gosnell, N. J. Smith, M. R. Warnement, S. M. Weiss, S. J. Rosenthal, *Journal of Materials Chemistry* **2008**, *18*, 970.

[22]   M. Achermann, M. A. Petruska, S. Kos, D. L. Smith, D. D. Koleske, V. I. Kllmov, *Nature* **2004**, *429*, 642.

[23]   A. H. Mueller, M. A. Petruska, M. Achermann, D. J. Werder, E. A. Akhadov, D. D. Koleske, M. A. Hoffbauer, V. I. Kllmov, *Nano Letters* **2005**, *5*, 1039.

[24]   C. F. Landes, M. Braun, M. A. El-Sayed, *Journal of Physical Chemistry B* **2001**, *105*, 10554.

[25]   C. B. Murray, D. J. Norris, M. G. Bawendi, *Journal of the American Chemical Society* **1993**, *115*, 8706.

[26]   D. F. Underwood, T. Kippeny, S. J. Rosenthal, *Journal of Physical Chemistry B* **2001**, *105*, 436.

[27]   A. M. Smith, H. Duan, M. N. Rhyner, G. Ruan, S. Nie, *Physical Chemistry Chemical Physics* **2006**, *8*, 3895.

[28]   D. L. Nida, N. Nitin, W. W. Yu, V. L. Colvin, R. Richards-Kortum, *Nanotechnology* **2008**, *19*, 1.

[29]   W. W. Yu, E. Chang, J. C. Falkner, J. Zhang, A. M. Al-Somali, C. M. Sayes, J. Johns, R. Drezek, V. L. Colvin, *Journal of the American Chemical Society* **2007**, *129*, 2871.

[30]   E. E. Lees, T.-L. Nguyen, A. H. A. Clayton, P. Mulvaney, *ACS Nano* **2009**, *3*, 1121.

[31]   L. Tian, L. Yam, N. Zhou, H. Tat, K. Uhrich, *Macromolecules* **2004**, *37*, 538.

[32]   J. Djordjevic, L. Del Rosario, J. Wang, K. Uhrich, *Journal of Bioactive and Compatible Polymers* **2008**, *23*, 532.

[33]   W. W. Yu, L. Qu, W. Guo, X. Peng, *Chemistry of Materials* **2003**, *15*, 2854.

A1. APPENDIX 1: CONTROLLED 1cM RELEASE FROM TITANIUM RODS AS A MODEL FOR STENT-MEDIATED DELIVERY

In this appendix, the ability to provide localized, stent-mediated release **1cM** to control cardiovascular disease was evaluated. This work is an extension of the research described in **Chapter 2**.

A1.1. Background & Introduction

As discussed in **Section 1.1**, limiting factors to therapeutic efficacy include 1) drug accumulation at the active site; and 2) maintainence of a therapeutic level.[1-3] While a localized delivery system, such as a drug-eluting stent, can address-site specificity, delivering therapeutics in a controlled manner remains critical to ensure therapeutic levels to eliminating frequent dosing.

One method for achieving controlled delivery of a water-soluble therapeutic, such as the amphiphilic polymers utilized in this work, is to utilize a water-insoluble coating over the water-soluble therapeutic. Styrenic block copolymers are one such type of water-insoluble polymer system utilized to control therapeutic delivery. These polymers can be synthesized to fine-tune the ratio of glassy, crystalline domains to elastomeric domains – the elastic domains allow the slow dissolution and release of the water-soluble therapeutic.[4] Poly (styrene-b-isobutylene-b-styrene) (SIBS) is the styrenic block copolymer utilized in Boston Scientific's TAXUS^{TM} drug-eluting stent.

In this work, a similar hydrophobic, elastomeric polymer, poly (styrene-b-ethylene butylene-b-styrene) (SEBS), structure shown in **Figure A1.1**, was evaluated to slow **1cM** release from titanium rods to simulate stent-mediated release.
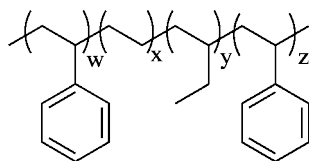
Figure A1.1. Chemical structure of the water-insoluble elastomer, SEBS.

A1.2. Results and Discussion

A1.2.1. Polymer Coating of the Titanium Rods

Due to the small size of cardiac stents, larger titanium rods were used to simulate stent-mediated **1cM** release. To coat the titanium rods with the polymers, an airbrush was used. The polymers were dissolved in a volatile organic solvent (200 mg/mL **1cM** in CH$_2$Cl$_2$ and 67 mg/mL SEBS in toluene) and were then spray-coated onto the rods. In a preliminary effort to evaluate the effects of SEBS, several combinations of **1cM** and SEBS were tested in singlet; **1cM** alone (control), SEBS alone (control), **1cM** under SEBS, **1cM** over SEBS, and **1cM** + SEBS, schematics of which are shown in **Figure A1.2**. For the **1cM** under SEBS sample, **1cM** was dispersed in chloroform, coated onto the stents using the spray-coater and allowed to dry overnight. The SEBS, dispersed in toluene, was then coated over top of the **1cM** and the resulting samples dried overnight. For the **1cM** over SEBS samples, the same process as that used for the **1cM** under SEBS was utilized except the **1cM** was coated over the SEBS layer. Finally, for the **1cM** + SEBS samples, the polymers were premixed and a 1:1 ratio, dispersed in toluene, and spray-coated onto the rods.
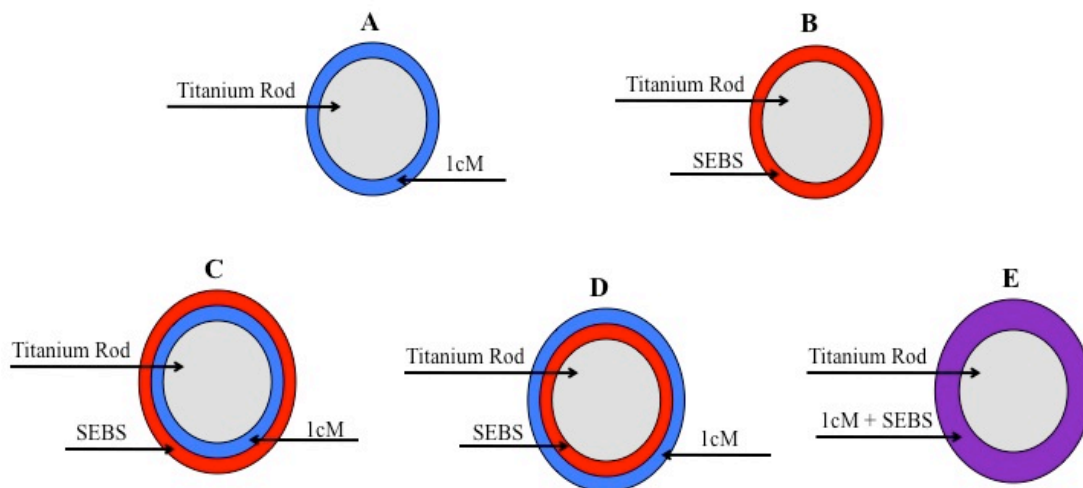
Figure A1.2. Schematic of titanium rods coated with a) **1cM** alone (control), b) SEBS (control), c) **1cM** under SEBS, d) **1cM** over SEBS, and e) **1cM** + SEBS.

A1.2.2. 1cM Release from the Coated Rods

To evaluate the release properties of the **1cM**, UV/Vis absorption spectroscopy was employed. A calibration curve for the absorption of the **1cM** with respect to concentration was prepared at 285 nm (the λ_{max} for **1cM**) in PBS. The rods prepared above were then incubated in PBS at 37 °C in an incubator shaker. The release of **1cM** was determined using the calibration curve at the indicated timepoints. The resulting data is shown in **Figure A1.3**.

As shown in **Figure A1.3A**, the addition of SEBS in any form does alter the release profile of **1cM**. However, the goal was to control **1cM** release for days-to-weeks to avoid the need for subsequent dosing. After five hours, all samples containing **1cM** achieved 100 % release of the polymer except for **1cM** under SEBS and **1cM** + SEBS. As shown in **Figure A1.3B**, the **1cM** + SEBS is fully released by 30 hours, or just over a

day. However, coating the SEBS over the **1cM** (**1cM** under SEBS) delays the **1cM**

release for over two weeks in a controlled fashion.
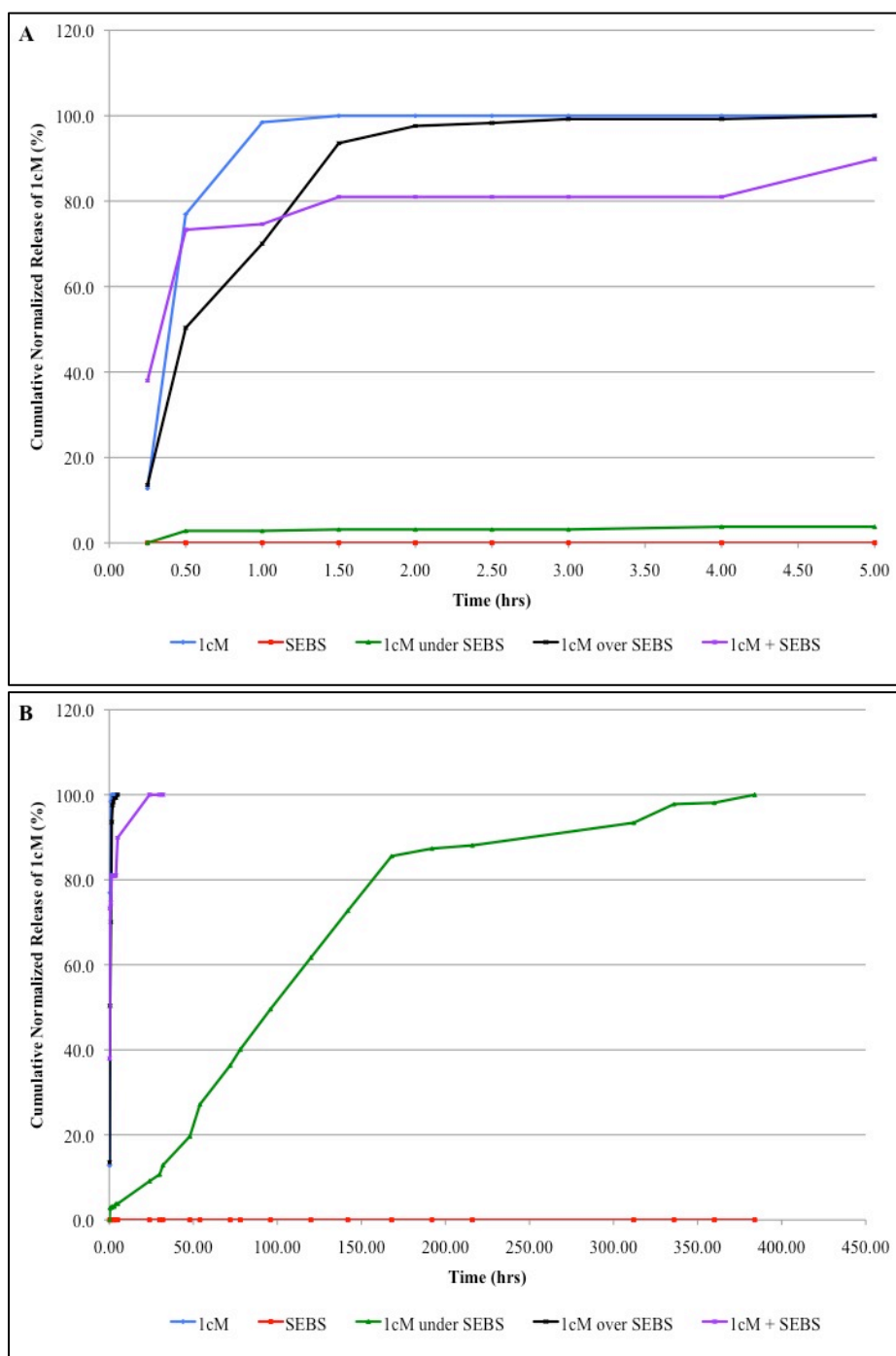
Figure A1.3. Release of **1cM** from the five samples of coated titanium rods for (A) the

first five hours and (B) over 16 days (368 hours).

The release of **1cM** from **1cM** under SEBS coatings was repeated in triplicate and the data shown in **Figure A1.4**. As shown, the controlled release was reproducible but extended to ~ 6 days (vs. 16 days). The difference in release time is likely due to the difficulty in the coating procedure; the SEBS needs exist as a thick, even layer over the **1cM**. Any irregularities in this SEBS coating (i.e., cracks) results in the **1cM** quickly leaching out the defect. Thus, perhaps a more efficient system for coating the rods should be developed.
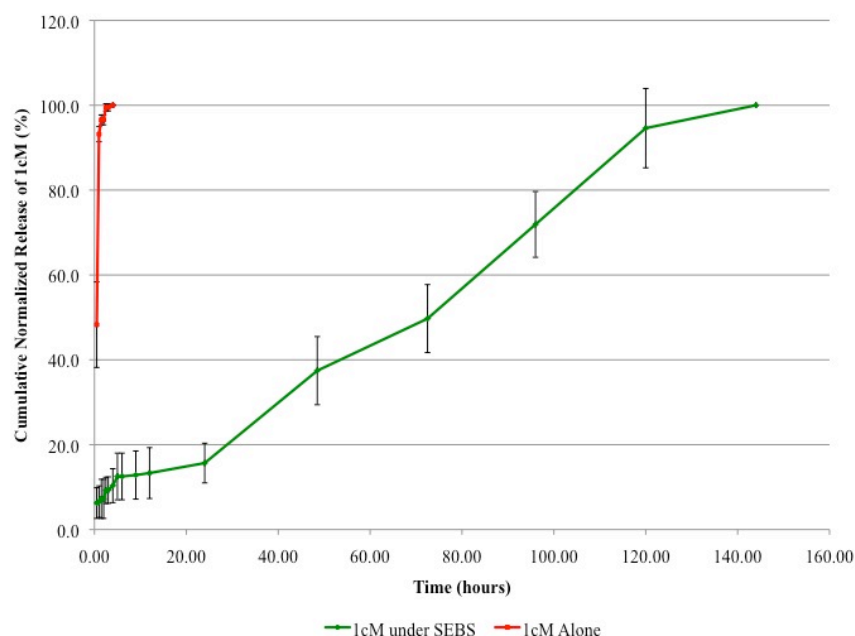
Figure A1.4. Release of **1cM** titanium rods over 144 hours.

A1.3. Summary & Future Work

To summarize the first part of this appendix, utilizing an elastomeric polymer such as SEBS has the capability to slow the release of **1cM** from titanium rods to achieve a controlled release drug delivery system. However, further work needs to be performed to find a more effective coating procedure to increase the reproducibility of the acquired

data. In addition, the efficacy of the polymer following release from this system *in vitro* must be evaluated.

A1.4. Experimental

A1.4.1. Synthetic Materials

Unless otherwise stated, solvents and reagents were purchased from Fisher Scientific (Pittsburgh, PA) and Sigma-Aldrich (St. Louis, MO) and used as received. PEG 5 kDa was purchased from Polysciences, Inc. (Warrington, PA) and dried by azeotropic distillation from toluene before use. The **1cM** used in this work was synthesized as previously described.[5] The Kraton® G SEBS was a gift from Kratin Polymers (Houston, TX).

A1.4.2. Methods

A1.4.2.1. Coating of Titanium Rods

Titanium rods, 49.2 mm x 4.2 mm, were spray-coated using a Badger model 350 single action, medium-tipped air brush. Solutions of **1cM** in CH_2Cl_2 at 200 mg/mL and poly (styrene-ethylene/butylene-styrene) SEBS in toluene at 67 mg/mL were prepared. The polymers were spray-coated onto the rods to achieve a smooth layer (10-20 mg per rod) and each coat allowed to dry overnight prior to additional coatings.

A1.4.2.1. 1cM Release

Polymer release from the titanium rods was performed in PBS at 37 °C. Aliquots were collected at the desired time points and analyzed *via* UV absorption on a Beckman DU 500 Series Spectrophotometer at 285 nm. Concentrations were determined using a calibration curve of **1cM** concentration vs. absorbance at 285 nm. For **Figure A1.5**, error

bars represent the standard deviation of the average of the indicated sample type, which

was evaluated in triplicate.

A1.5. References

[1]   V. K. Varadan, L. Chen, J. Xie, *Nanomedicine: Design and Applications of Magnetic Nanomaterials, Nanosensors, and Nanosystems*, John Wiley & Sons, Ltd, West Sussex, UK, **2008**.

[2]   V. T. Ranade, M. A. Hollinger, *Drug Delivery Systems*, Second ed., CRC Press, Boca Raton, London, New York, Washington, D.C., **2004**.

[3]   K. E. Uhrich, S. M. Cannizzaro, R. S. Langer, K. M. Shakesheff, *Chemical Reviews* **1999**, *99*, 3181.

[4]   S. Ranade, V., R. E. Richard, M. N. Helmus, *Acta Biomaterialia* **2005**, *1*, 137.

[5]   L. Tian, L. Yam, N. Zhou, H. Tat, K. Uhrich, *Macromolecules* **2004**, *37*, 538.

A2.   APPENDIX   2:   EVALUATION   OF   VARYING   POLYMER FUNCTIONALITIES TO WATER-SOLUBILIZE WLNCs

In this appendix, a series of polymers with varying functional groups were evaluated to biostabilize WLNCs with the same goals as **Chapter 4**; maintenance of WLNC size and white-light fluorescence emission.

A2.1. Background & Introduction

To optimize the AM-solubilized WLNCs, a variety of functional groups were chemically incorporated within the hydrophobic portion of the polymer backbone. Functional groups included acidic groups, such as sulphate and phosphate, basic moieties, such as amines and hydroxyls, and soft ligands, such as organophosphine and thiol. The soft ligands were chosen as they are known to coordinate well to soft metals (i.e., cadmium) based on hard-soft acid base chemistry[1, 2]. They are shown in **Figure A2.1**, and for clarity will be described as the hydrophobic functionality that is intended to interact with the nanocrystal surface. For two functionalities, phosphonic acid and hydroxyl, multiple lengths of the alkane spacer were utilized to elucidate steric effects imparted by the AM's alkylated arms which may limit the ability of the functional group to coordinate to the nanocrystal surface. For the four polymers, the number of carbons in the alkane spacer is indicated in parenthesis following the functionality to differentiate the two. As an example, phosphonic acid (propyl) indicates a three-carbon spacer between the phosphonic acid and the amide bond to the polymer where as phosphonic acid (butyl) indicates a four-carbon space between the phosphonic acid and the amide bond to the polymer. The N-hydroxysuccinimide (NHS)-terminal AM, the carboxylic

acid-terminal AM, the phosphonic acid (propyl)-terminal AM, and the sulfate-terminal AM are all polymers previously described in this thesis as **0cM**, **1cM**, **1pM**, and **1sM**, respectively. The **0cM** and **1cM** AMs were used as controls for polymers *not* anticipated to coordinate to the nanocrystals, while **1pM** was the standard, as it was shown in **Chapter 4** to be more efficient at solubilizing the WLNCs based upon polymer interaction with the nanocrystal surface.
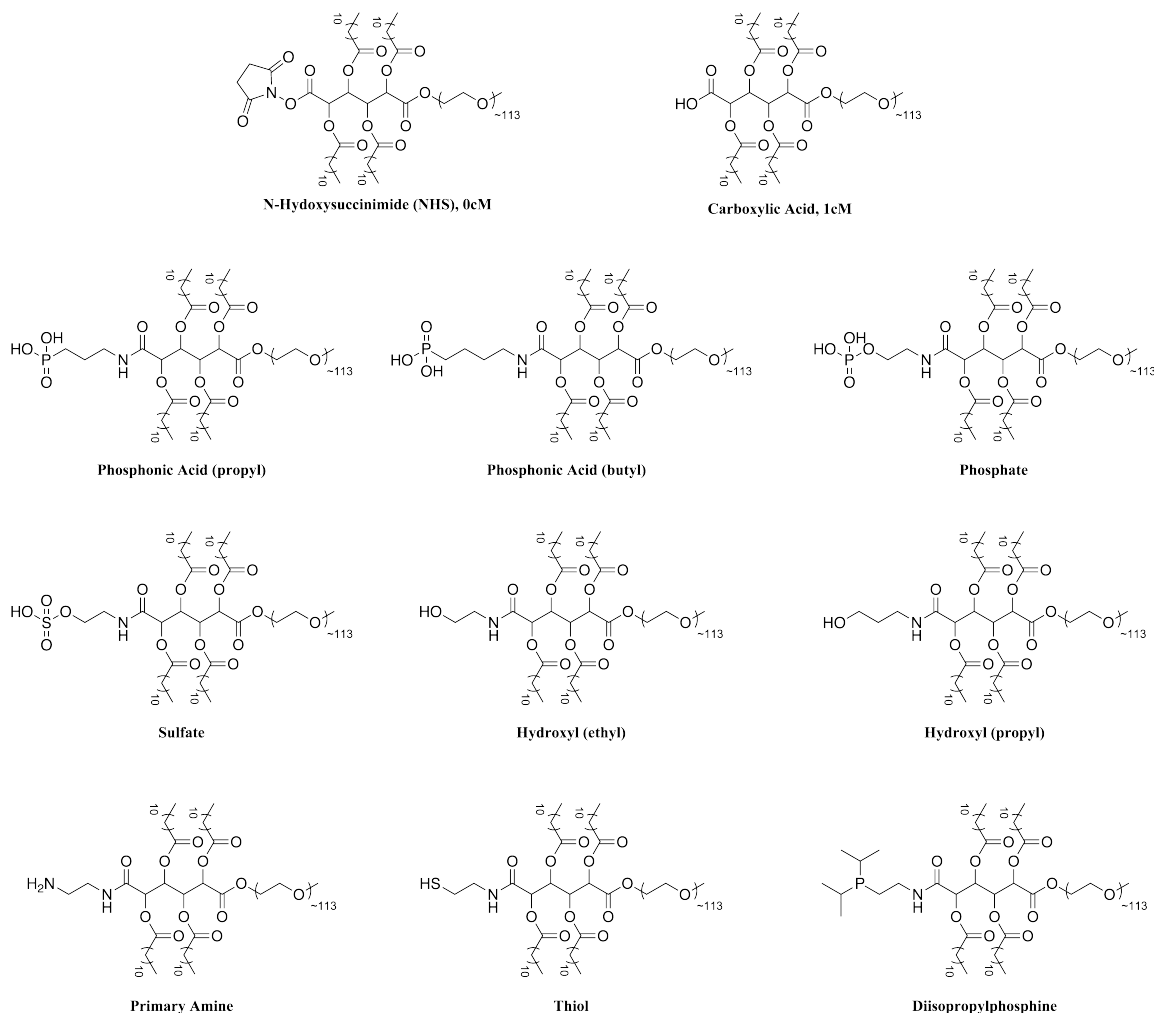
Figure A2.1. AMs with varying functional groups used to determine the optimal functionality to water-solubilize WLNCs.

The goal of this work was the same as that described in **Chapter 4**; namely, to efficiently solubilize the WLNCs into small, nanoscale assemblies that still emit white-light. The phosphonic acid moieties were anticipated to be effective, as shown in **Chapter 4**. Other moieties that were expected to be efficient towards coordination, and, therefore, water-solubilization were the soft ligands (i.e., thiol and diisopropylphosphine) due to the nature of their interaction with cadmium, a soft metal.[1, 2]

A2.2. Results and Discussion

A2.2.1. Polymer Synthesis & Water-solubilizaton

Synthesis of AMs with the varying hydrophobic functionalities shown in **Figure A2.1** were carried out using one of the two methods shown in **Scheme A2.1**, dependent upon the physical state of the amino starting material. For liquid staring materials (i.e., primary amine, diisopropylphosphine, and both hydroxyl-terminal AMs), the compounds were added to the **NHS**-terminal AM (**0cM**) using **Scheme A2.1B**, the same scheme used to synthesize the cationic polymers described in **Chapter 3**. For solid starting materials (i.e., phosphate, sulfate, thiol, and both phosphonic acid-terminal AMs), the compounds were added to the **NHS**-terminal AM (**0cM**) using **Scheme A2.1A**, as they were insoluble in methylene chloride and all polar organic solvents that are miscible with methylene chloride but were water-soluble. Tetrahydrofuran (86 % v/v) was added to the solutions to ensure no significant micelle formation resulting from the water-solubilization; our lab has previously shown that addition of 80 % v/v organic solvent to the polymers in water was sufficient to disrupt micelle formation (data not shown).
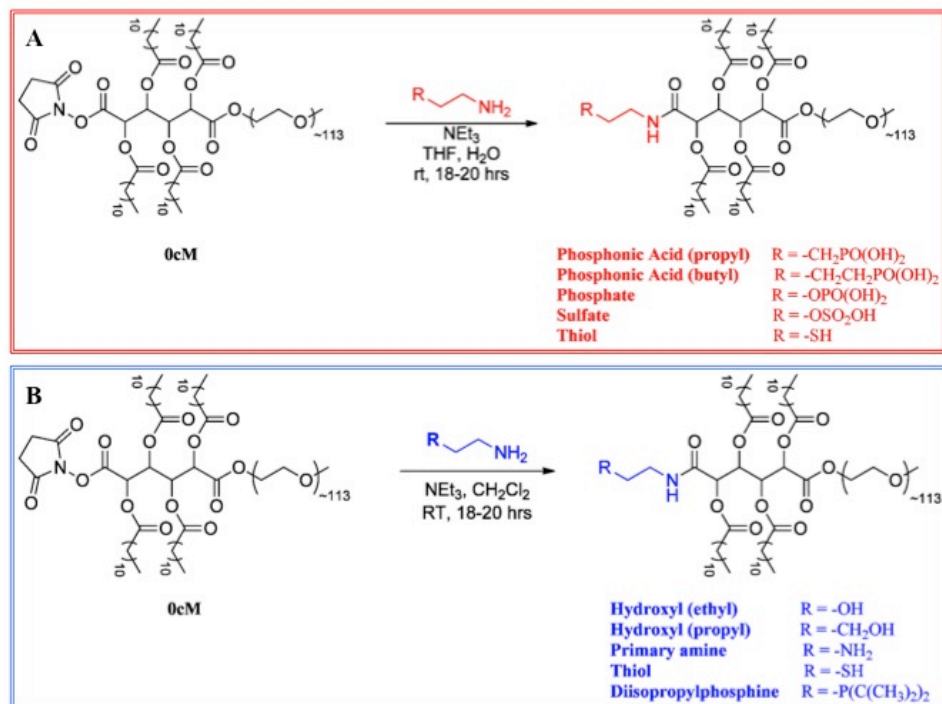
Scheme A2.1. Synthetic schemes used to prepare polymers of vary functionalities to water-solubilize the WLNCs. A) Synthetic scheme used to prepare functionalized AMs with solid amino starting materials, and B) synthetic scheme used to prepare functionalized AMs from amino starting materials in liquid form.

Successful synthesis of the polymers was verified by proton nuclear magnetic resonance (^{1}H NMR) spectroscopy and molecular weight determined by gel permeation chromatography (GPC) relative to PEG standards. Due to the abundance of PEG in the polymer (~83 % of protons), the presence of new protons in the ^{1}H NMR spectra were difficult to detect, particularly from 0.8 to 2.4 ppm where the methylene protons of the hydrophobic chains comprise the majority of that region. Thus, spectra were monitored for the disappearance of the protons of the activating group (N-hydroxysuccinimide) on **0cM**, which resonate at 2.8 ppm.

Following synthesis, the polymers were utilized to water-solubilize the WLNCs, employing the same solvent evaporation methods described in **Section 4.3.1.**

A2.2.2. Characterization of Water-soluble WLNCs

Water-solubilization of the WLNCs was determined by visual inspection of the resulting solutions, as shown in **Figure A2.2**. Solubilized nanocrystals were uniformly dispersed throughout the yellow solution, while unsolubilized nanocrystals deposited on the vial walls, as in the QD in water control. All functionalized AMs were capable of dispersing the WLNCs in the aqueous solutions. Solutions of the WLNCs dispersed in water using the **phosphonic acid**-terminal AMs (both propyl and butyl) and the **phosphate**-terminal AM, **Figure A2.2.** samples 3-5, appeared the most transparent of all dispersions. Solutions of the WLNCs in water using the **sulfate** and **thiol**-terminal AMs, **Figure A2.2.** samples 6 and 11, had some transparency while all others appeared cloudy and turbid, similar to the **carboxylic acid**-terminal AM.
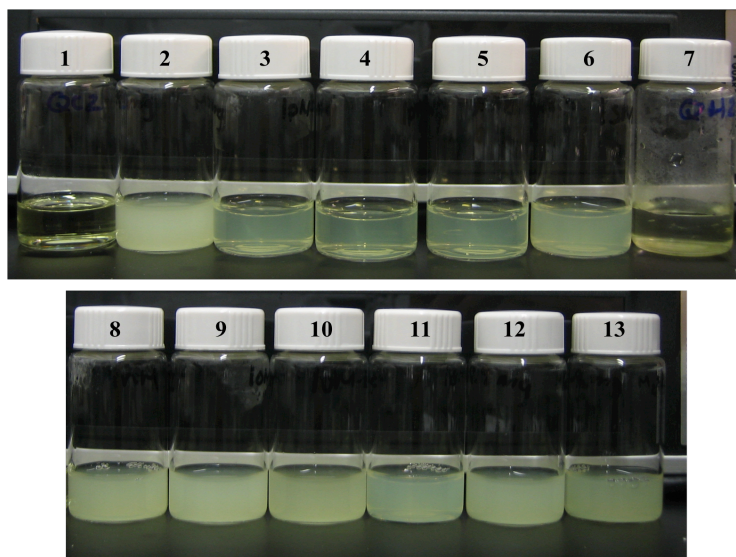
Figure A2.2. Digital photograph of WLNCs (1) dispersed in chloroform, (2) with the **carboxylic acid**-terminal AM in H_2O, (3) with the **phosphonic acid (propyl)**-terminal AM in H_2O, (4) with the **phosphonic acid (butyl)**-terminal AM in H_2O, (5) with the **phosphate**-terminal AM in H_2O, (6) with the **sulfate**-terminal AM in H_2O, (7) dispersed in H_2O, (8) with the **primary amine**-terminal AM in H_2O, (9) with the **hydroxyl (ethyl)**-terminal AM in H_2O, (10) with the **hydroxyl (propyl)**-terminal AM in H_2O, (11) with the **thiol**-terminal AM in H_2O, (12) with the **NHS**-terminal AM in H_2O, and (12) with the **diisopropylphosphine**-terminal AM in H_2O.

A2.2.2.1. Turbidity

Turbidity was quantitatively determined using UV/Vis absorbance spectroscopy, shown in **Figure A2.3**. WLNCs dispersed in water alone transmitted the most light across the tested wavelengths because all nanocrystals were adhered to the flask wall and, thus, the solution tested was only water. As a control, the turbidity of WLNCs dispersed in chloroform was tested. For these solutions, the only light transmitted was light not

absorbed by the nanocrystals themselves. Consistent with the qualitative images in **Figure A2.2**, solutions of the WLNCs dispersed in water using the **phosphonic acid**-terminal AMs (both propyl and butyl) and the **phosphate**-terminal AM transmitted the most light, with the solutions of **phosphonic acid (butyl)**-terminal AM-solubilized WLNCs transmitting the most light and, thus, being the least turbid. Solutions of the WLNCs dispersed in water using the **sulfate** and **thiol**-terminal AMs transmitted some light, as well, while all other functionalized AMs used to solubilize the WLNCs transmitted less than ~ 20% light even at their peak transmittance. All polymer synthesized using **Scheme A2.1A** are the polymers that subsequently solubilized the WLNCs yielding solutions with the least amount of turbidity. While the correlation between turbidity and synthetic methodology may be a coincidence, all functionalized polymers should be synthesized using the same methodology for future studies. Based upon these results, the synthetic method appears to influence turbidity of the functionalized-AMs and WLNC solutions.
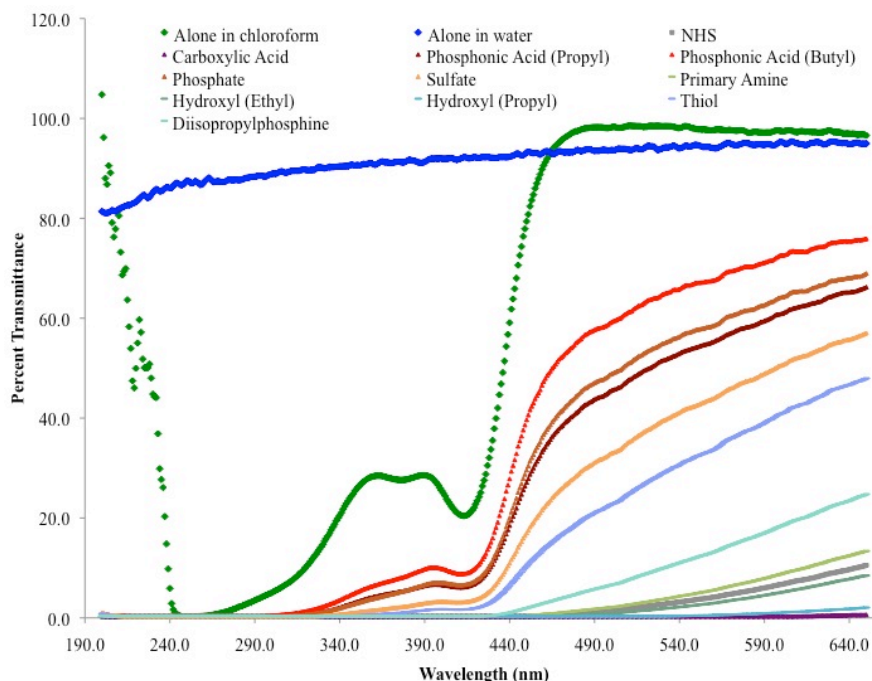
Figure A2.3. Percent transmittance data for solutions of WLNCs dispersed in water utilizing the indicated functionalized AMs.

The percent transmittance of all samples at 363 and 485 nm are shown in **Figure A2.4**. These wavelengths were chosen based upon the nanocrystals in dispersed chloroform; 363 nm is a peak for the percent transmittance and 485 nm is the wavelength at which maximum percent transmittance is obtained. The trends in **Figure A2.4** are the same as those discussed above, with nanocrystals dispersed in water using **phosphonic acid (butyl)**-terminal AM transmitting the most light, and the solutions of WLNCs with the **phosphonic acid (propyl)** and **phosphate**-terminal AMs transmitting 40-50 % light at 485 nm. Other polymers yielding solutions of water-soluble WLNCs that transmitted light were the **suflate**, **thiol**, and **diisopropylphosphine**-terminal AMs.
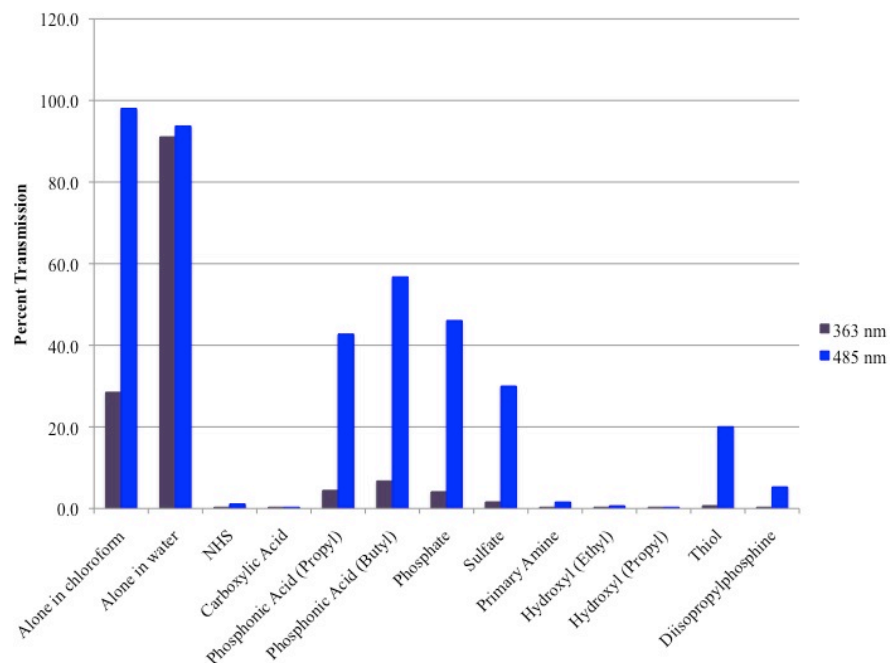
Figure A2.4. Percent transmittance data at 363 nm and 485 nm for solutions of WLNCs dispersed in water utilizing the indicated functionalized AMs.

A2.2.2.2. Assembly Sizes

Hydrodynamic diameters of the aqueous WLNC solutions were determined using dynamic light scattering. Graphical results are shown in **Figure A2.5** while the values are given in **Table A2.1**.
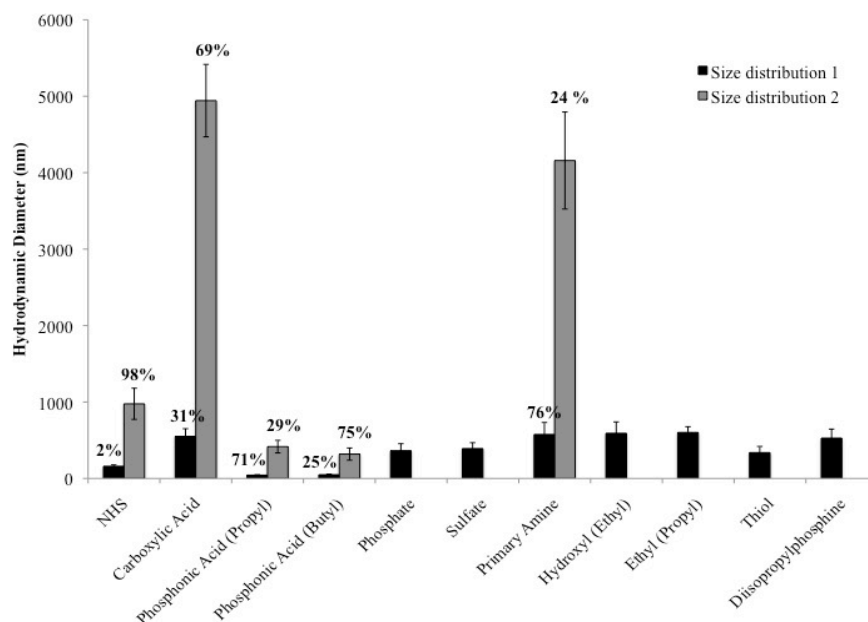
Figure A2.5. Graphical representation of the hydrodynamic diameters observed for water-soluble assemblies of WLNCs with the indicated functionalized AMs.

	Size Distribution 1 (nm)	Percentage of Volume (%)	Size Distribution 2 (nm)	Percentage of Volume (%)
NHS	159.3	2.4	976.6	97.6
Carboxylic Acid	550.4	31.3	4943	68.7
Phosphonic Acid (Propyl)	43.2	71.3	416.3	28.7
Phosphonic Acid (Butyl)	49.3	25.4	318.6	74.6
Phosphate	363.2	100		
Sulfate	390.9	100		
Primary Amine	575.7	75.6	4159	24.4
Hydroxyl (Ethyl)	591.2	100		
Ethyl (Propyl)	602.2	100		
Thiol	338.3	100		
Diisopropyl-phosphine	528.2	100		

Table A2.1. Hydrodynamic diameters observed for water-soluble assemblies of WLNCs with the indicated functionalized AMs.

The smallest assembly sizes were obtained using both **phosphonic acid**-terminal AMs, with one size distribution of 40-50 nm. However, the **phosphonic acid (propyl)**-terminal AM produced water-soluble WLNC solutions with the greatest percent by volume of the small size distribution (71 % compared with only 25 % for the **phosphonic acid (butyl)**-terminal AM-WLNC solutions). The other size distribution for each solution is consistent with the smallest size distributions (300-400 nm) observed for other AM-solubilized WLNC solutions using AMs synthesized by **Scheme A2.1A** (i.e. **phosphate**, **sulfate**, and **thiol**). For all other polymers, no assembly sizes smaller than 500 nm were observed.

As expected, this data is consistent with the turbidity data – the least turbid solutions contained assemblies of smaller sizes. Together, these data suggest a difference between the two synthetic methodologies and, thus, further experiments need to be performed utilizing the same synthetic methodology.

A2.2.2.3. Qualitative Fluorescence Emission

Fluorescence emission was qualitatively determined by excitation with a long wavelength UV lamp at 365 nm. As shown in **Figure A2.6, a**ll solutions except the WLNC dispersed in water only (sample **7**) emit bright white light that is evenly dispersed throughout the solution, indicating successful solubilization.
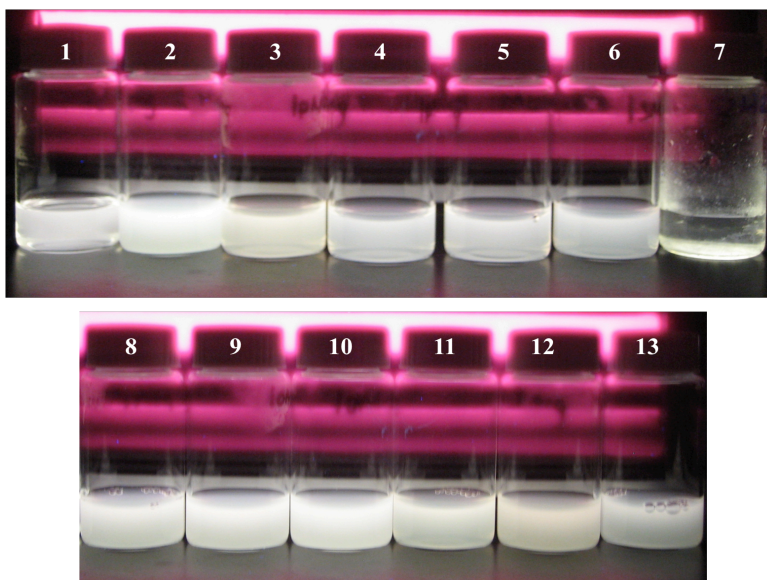
Figure A2.6. Digital photographs following excitation with a long wavelength UV lamp (excitation = 365 nm) of WLNCs (1) dispersed in chloroform, (2) with the **carboxylic acid**-terminal AM in H_2O, (3) with the **phosphonic acid (propyl)**-terminal AM in H_2O, (4) with the **phosphonic acid (butyl)**-terminal AM in H_2O, (5) with the **phosphate**-terminal AM in H_2O, (6) with the **sulfate**-terminal AM in H_2O, (7) dispersed in H_2O, (8) with the **primary amine**-terminal AM in H_2O, (9) with the **hydroxyl (ethyl)**-terminal AM in H_2O, (10) with the **hydroxyl (propyl)**-terminal AM in H_2O, (11) with the **thiol**-terminal AM in H_2O, (12) with the **NHS**-terminal AM in H_2O, and (12) with the **diisopropylphosphine**-terminal AM in H_2O.

For WLNC samples in water only, the WLNCs adhere to the vial walls, indicating a lack of aqueous solubilization of the hydrophobic nanocrystals. The nanocrystal adherence to the walls is observed by tipping the solutions on their sides, as shown in **Figure A2.7**. In comparison to the WLNCs dispersed in water using the **sulfate**-terminal AM (left flask) in which the solution, even when tipped, emits evenly dispersed white-

light, the WLNCs dispersed in water only (right flask) have few nanocrystals dispersed in solution. Rather, the nanocrystals adhere to the flask.
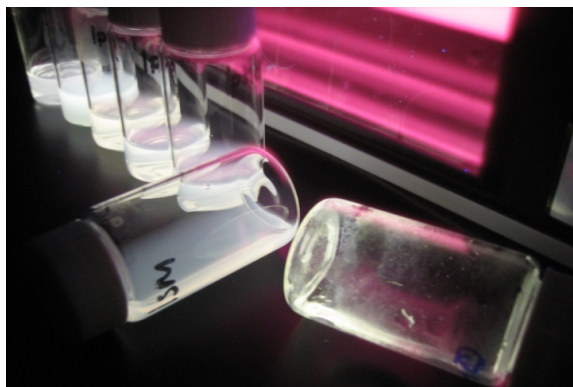
Figure A2.7. Digital photographs following excitation with a long wavelength UV lamp (excitation = 365 nm) of WLNC solutions highlighting the even dispersion of WLNCs in water when utilizing AMs. The tipped flasks are (left) the **sulfate**-terminal AM-solubilized WLNCs in water and (right) WLNCs in water only, showing that the WLNCs are evenly dispersed in the left flask where as in the right flask, they are adhered to the flask.

A2.2.2.4. Quantitative Fluorescence Emission

Quantitative fluorescence emission data for all samples imaged qualitatively was collected using fluorescence spectroscopy from 380 – 800 nm following excitation at 365 nm (shown in **Figure A2.8**).
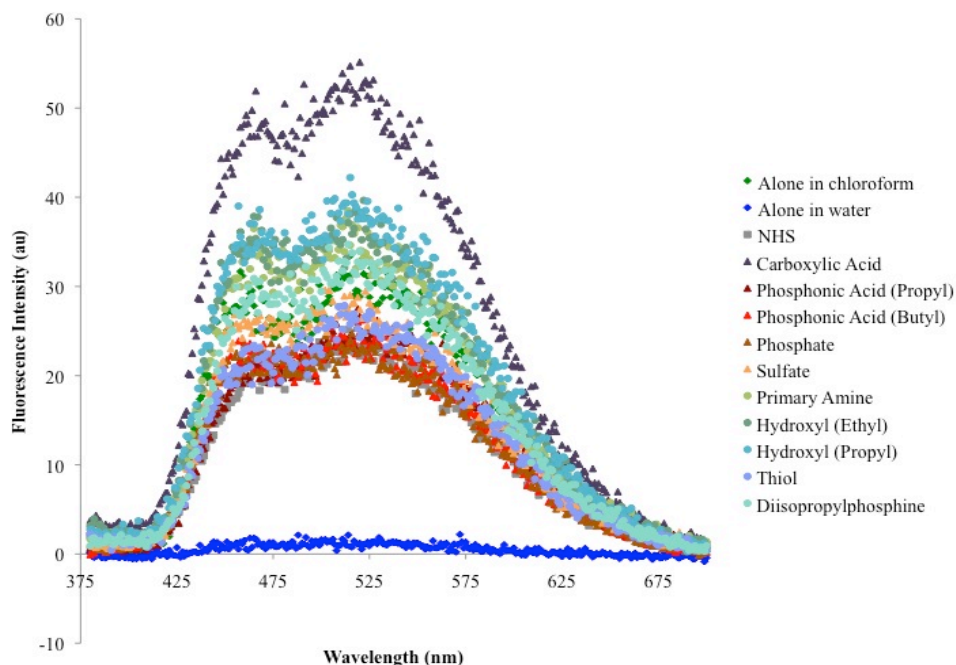
Figure A2.8. Fluorescence emission spectra of WLNCs dispersed in the indicated solvent and, where applicable, solubilized by the indicated functionalized AMs.

All solutions of WLNC, with the exception of the nanocrystals in water only, shared a similar fluorescence profile (i.e., broadband white light-emission and similar λ_{max} peaks) as the nanocrystals dissolved in chloroform at the same concentration. Overall, the WLNC water-solubilized utilizing the **carboxylic acid**-terminal AM had fluorescence intensity significantly greater than the nanocrystals in chloroform, consistent with the observations made in **Section 4.3.1.4**. To more easily compare the fluorescence intensities of the other samples, the fluorescence intensity at two wavelengths, 464 and 525 nm (the two λ_{max} peaks observed for the WLNCs in chloroform) are graphed for each sample in **Figure A2.9**.
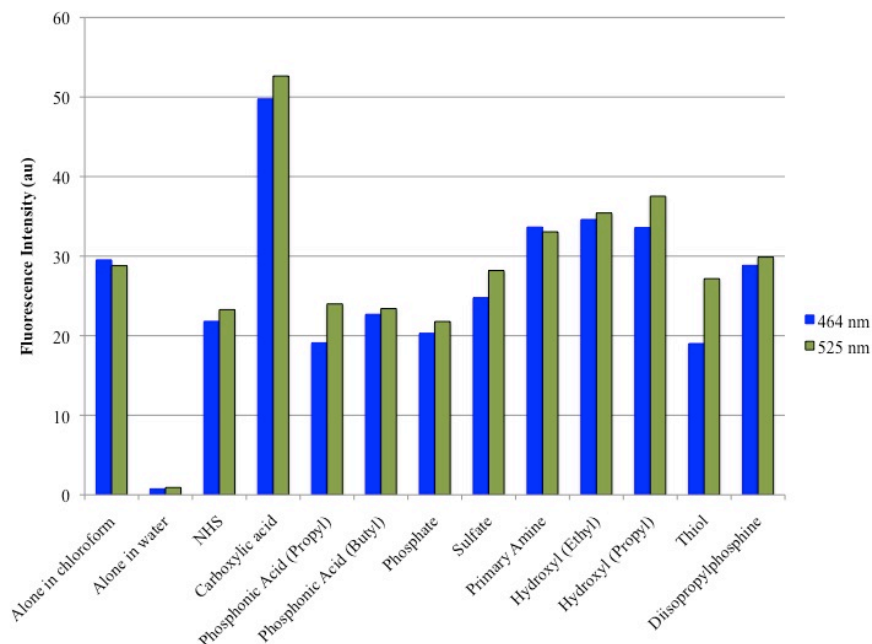
Figure A2.9. Fluorescence emission spectra of WLNCs dispersed in the indicated solvent and, where applicable, solubilized by the indicated functionalized AMs at 464 and 525 nm.

As shown in **Figure A2.9**, only the data for the WLNCs water-solubilized by the **primary amine**-terminal AM follows the same trend for the WLNCs in chloroform in that the peak at 464 nm is slightly more intense than the emission peak at 525 nm. With respect to overall intensity, three of four of the functionalized AMs synthesized using **Scheme A2.1B** (the **primary amine** and both **hydroxyl**-terminal polymers), all water-solubilized the WLNCs in a manner that enhances their fluorescence intensity as compared with the WLNCs in chloroform at the same nanocrystal concentration. As discussed in **Section 4.3.1.4**, taken together with the size distributions, this data implies that solubilization of the nanocrystals into larger aggregates results in an overall enhancement of their fluorescence intensity. However, it should be considered that when

1cM was filtered with a 0.45 μm syringe in **Section 4.3.1.4**, the fluorescence intensity of the solutions significantly decreased. Given the similarities in this data, when the samples are similarly filtered, it is likely the same effect on fluorescence intensity would be observed.

The water-solubilization of the WLNCs using the **diisopropylphosphine** and **sulfate**-terminal AMs resulted in fluorescence similar to that of the nanocrystals in chloroform while the all other AMs resulted in fluorescence approximately 70 % that of the nanocrystals in chloroform.

Again, due to the apparent difference in properties that appear to correlate with the synthetic methodology used, it is difficult to make any conclusions based upon ligand type without further work – namely, evaluation of the polymers to water-solubilize the nanocrystals using the same synthetic methods.

A2.3. Summary & Future Work

In summary, eleven polymers of varying functionalities were evaluated for their ability to water-solubilize WLNCs, retain nanoscale size and emit white light. Due to the differing physical states and solubilities of the amino-terminated starting materials, two synthetic methodologies were employed to synthesize polymers with the desired functionalities. In general, both turbidity and fluorescence data shows significant differences in polymer samples that, at first glance, correlate to the synthetic methods used. While clear differences were observed, further work is required (i.e., polymers generated with the same same synthetic methodology) to clarify and correlate these effects. Based upon current data, it appears that both **phosphonic acid**-terminal AMs

results in water-soluble WLNCs with the smallest sizes whilst maintaining white-light emission. In addition, based upon the results obtained in **Chapter 4**, the fluorescence emission of solutions of WLNCs in water with these polymers would be largely unaffected by filtration with 0.45 μm syringe filters due to the small-size assemblies.

For future work, the polymers should be synthesized using the same methodology to better isolate differences between all polymer functionalities. In addition, measurements following filtration of the water-soluble WLNCs needs to be performed to decrease assembly size for increased biological utility. Finally, *in vitro* cellular uptake of the optimal water-solubilized WLNCs needs to be performed to determine its biocompatibility en route to further evaluation for biological imaging.

A2.4. Experimental

A2.4.1. Synthetic Materials

Unless otherwise stated, solvents and reagents were purchased from Fisher Scientific (Pittsburgh, PA) and Sigma-Aldrich (St. Louis, MO) and used as received. PEG 5 kDa was purchased from Polysciences, Inc. (Warrington, PA) and dried by azeotropic distillation from toluene before use. The **carboxylic acid**-terminal AM (**1cM**) and **0cM** (starting material for all functionalized AMs) were synthesized as previously described.[3, 4] The synthesis of the **sulfate**-terminal AM was previously described in **Chapter 2**, the **primary amine**-terminal AM was previously described in **Chapter 3**, and the **phosphonic acid (propyl)**-terminal AM was previously described in **Chapter 4.** The CdSe WLNCs were synthesized and provided as solutions in chloroform by Professor Sandra Rosenthal's group at Vanderbilt University.[5]

A2.4.2. Characterization Methods

A2.4.2.1. Proton Nuclear Magnetic Resonance (^{1}H NMR) Spectroscopy

Proton nuclear magnetic resonance (^{1}H-NMR) spectra of the products were obtained using a Varian 400 MHz or 500 MHz spectrophotometer. Samples were dissolved in chloroform-d, with a few drops of dimethyl sulfoxide-d_6 if necessary, with tetramethylsilane as an internal reference.

A2.4.2.2. Gel Permeation Chromatography (GPC)

Molecular weights (M_w) and polydispersity indices (PDI) were determined using gel permeation chromatography (GPC) with respect to PEG standards (Sigma-Aldrich) on a Waters Stryagel® HR 3 THF column (7.8 x 300 mm). The Waters LC system (Milford, MA) was equipped with a 2414 refractive index detector, a 1515 isocratic HPLC pump, and 717plus autosampler. An IBM ThinkCentre computer with Waters Breeze Version 3.30 software installed was used for collection and processing of data. Samples were prepared at a concentration of 10 mg/mL in tetrahydrofuran, filtered using 0.45 μm pore size nylon or poly(tetrafluoroethylene) syringe filters (Fisher Scientific) and placed in sample vials to be injected into the system.

A2.4.3. Polymer Synthesis

A2.4.3.1. Phosphonic Acid (Butyl)-terminal AM

In a 50 mL round bottom flask, 4-aminobutyl phosphonic acid (58.7 mg, 0.383 mmol) was dissolved in HPLC-grade H_2O (4 mL), HPLC-grade THF (6.5 mL), and triethylamine (0.20 mL, 1.4 mmol) and the solution stirred. In a separate flask, **0cM** (531 mg, 0.0885 mmol) was dissolved in HPLC-grade THF (6 mL) and the solution added to the reaction flask. The yellow solution was stirred for 18-20 hrs at room temperature

before the THF was removed by rotary evaporation. The resulting yellow oil was dissolved in CH_2Cl_2 and 0.1 N HCl and stirred for 20-30 min. The mixture was then transferred to a separatory funnel containing addition 0.1 N HCl and the organic layer separated and washed with brine (2x). The combined aqueous portions were extracted with CH_2Cl_2 and the combined organics dried over $MgSO_4$ and concentrated to a yellow oil. White product was precipitated from the yellow oil in CH_2Cl_2 by addition of 10-fold diethyl ether in a 50 mL centrifuge tube. The suspension was place on a shaker for 10-15 min before the solid was collected by centrifugation and the supernatant removed by decanting. The solid was dissolved in CH_2Cl_2 (< 5 mL) and reprecipitated by adding 10-fold diethyl ether. The solid was collected by centrifugation, the supernatant removed, and the solid washed with ether (1x) and cold hexanes (1x). The white solid was dried under ambient conditions (24 hrs) and under high vacuum (24 hrs). Yield: 0.38 mg, 71 %.

^{1}H- NMR ($CDCl_3$): δ 5.67 (m, 2H, CH), 5.20 (m, 2H, CH), 4.20 (m, 2H, CH_2), 3.66 (m, ~0.45 kH, CH_2O), 3.39 (s, 3H, CH_3), 2.39 (m, 8H, CH_2), 1.58 (m, 10H, CH_2), 1.27 (m, 64H, CH_2), 0.89 (t, 12H, CH_3). GPC: M_w: 7.2 kDa; PDI: 1.1.

A2.4.3.2. Phosphate-terminal AM

In a 50 mL round bottom flask, 4-aminopropyl dihydrogen phosphate (47 mg, 0.33 mmol) was dissolved in HPLC-grade H_2O (2.5 mL), HPLC-grade THF (5 mL), and triethylamine (0.16 mL, 1.2 mmol) and the solution stirred. In a separate flask, **0cM** (451 mg, 0.0752 mmol) was dissolved in HPLC-grade THF (6.2 mL) and the solution added to the reaction flask. The yellow solution was stirred for 18-20 hrs at room temperature before the THF was removed by rotary evaporation. The resulting yellow oil was dissolved in CH_2Cl_2 and 0.1 N HCl and stirred for 20-30 min. The mixture was then

transferred to a separatory funnel containing addition 0.1 N HCl and the organic layer separated and washed with brine (2x). The combined aqueous portions were extracted with CH_2Cl_2 and the combined organic portions dried over $MgSO_4$ and concentrated to a yellow oil. White product was precipitated from the yellow oil in CH_2Cl_2 by addition of 10-fold diethyl ether in a 50 mL centrifuge tube. The suspension was place on a shaker for 10-15 min before the solid was collected by centrifugation and the supernatant removed by decanting. The solid was dissolved in CH_2Cl_2 (< 5 mL) and reprecipitated by adding 10-fold diethyl ether. The solid was collected by centrifugation, the supernatant removed, and the solid washed with ether (1x) and cold hexanes (1x). The white solid was dried under ambient conditions (24 hrs) and under high vacuum (24 hrs). Yield: 0. 30 g, 66 %. ^{1}H- NMR ($CDCl_3$): δ 5.70 (m, 2H, CH), 5.19 (m, 2H, CH), 4.23 (m, 3H, CH_2), 3.67 (m, ~0.45 kH, CH_2O), 3.39 (s, 3H, CH_3), 2.37 (m, 8H, CH_2), 1.65 (m, 13H, CH_2), 1.27 (m, 68H, CH_2), 0.89 (t, 12H, CH_3). GPC: M_w: 7.3 kDa; PDI: 1.1.

A2.4.3.3. Hydroxyl (Ethyl)-terminal AM

In a 50 mL round bottom flask, ethanolamine (36.8 μL, 0.612 mmol) was dissolved in HPLC-grade CH_2Cl_2 (2.5 mL) and triethylamine (0.17 mL, 1.2 mmol) and the solution stirred. In a separate flask, **0cM** (459 mg, 0.0765 mmol) was dissolved in HPLC-grade CH_2Cl_2 (7.7 mL) and the solution added to the reaction flask dropwise *via* syringe pump at a rate of 1.0 mL/hr. The reaction was stirred for 18-20 hrs at room temperature before the bright yellow solution was filtered to remove the white solid (NHS by-product) and the filtrate washed with 0.1 N HCl/brine (1x) and brine (2x). The combined aqueous portions were extracted with CH_2Cl_2 and the combined organic portions dried over $MgSO_4$ and concentrated to a yellow oil. White product was

precipitated from the yellow oil in CH_2Cl_2 by addition of 10-fold diethyl ether in a 50 mL centrifuge tube. The suspension was place on a shaker for 10-15 min before the solid was collected by centrifugation and the supernatant removed by decanting. The solid was dissolved in CH_2Cl_2 (< 5 mL) and reprecipitated by adding 10-fold diethyl ether. The solid was collected by centrifugation, the supernatant removed, and the solid washed with ether (1x) and cold hexanes (1x). The white solid was dried under ambient conditions (24 hrs) and under high vacuum (24 hrs). Yield: 0.31 g, 68 %. ^{1}H- NMR ($CDCl_3$): δ 5.68 (m, 2H, CH), 5.15 (m, 2H, CH), 4.19 (m, 4H, CH_2), 3.60 (m, ~0.45 kH, CH_2O), 3.39 (s, 3H, CH_3), 2.38 (m, 8H, CH_2), 1.62 (m, 14H, CH_2), 1.27 (m, 64H, CH_2), 0.89 (t, 12H, CH_3). GPC: M_w: 7.4 kDa; PDI: 1.1.

A2.4.3.4. Hydroxyl (Propyl)-terminal AM

In a 50 mL round bottom flask, 3-amino-1-propanol (46.8 μL, 0.612 mmol) was dissolved in HPLC-grade CH_2Cl_2 (2.5 mL) and triethylamine (0.17 mL, 1.2 mmol) and the solution stirred. In a separate flask, **0cM** (0.46 g, 0.077 mmol) was dissolved in HPLC-grade CH_2Cl_2 (7.8 mL) and the solution added to the reaction flask dropwise *via* syringe pump at a rate of 1.0 mL/hr. The reaction was stirred for 18-20 hrs at room temperature before the bright yellow solution was filtered to remove the white solid (NHS by-product) and the filtrate washed with 0.1 N HCl (1x) and brine (2x). The combined aqueous portions were extracted with CH_2Cl_2 and the combined organic portions dried over $MgSO_4$ and concentrated to a yellow oil. White product was precipitated from the yellow oil in CH_2Cl_2 by addition of 10-fold diethyl ether in a 50 mL centrifuge tube. The suspension was place on a shaker for 10-15 min before the solid was collected by centrifugation and the supernatant removed by decanting. The solid was

dissolved in CH_2Cl_2 (< 5 mL) and reprecipitated by adding 10-fold diethyl ether. The solid was collected by centrifugation, the supernatant removed, and the solid washed with diethyl ether (1x) and cold hexanes (1x). The white solid was dried under ambient conditions (24 hrs) and under high vacuum (24 hrs). Yield: 0.34 g, 74 %. ^{1}H- NMR ($CDCl_3$): δ 5.68 (m, 2H, CH), 5.21 (m, 2H, CH), 4.26 (m, 4H, CH_2), 3.67 (m, ~0.45 kH, CH_2O), 3.39 (s, 3H, CH_3), 2.35 (m, 8H, CH_2), 1.65 (m, 25H, CH_2), 1.27 (m, 57H, CH_2), 0.89 (t, 12H, CH_3). GPC: M_w: 7.4 kDa; PDI: 1.1.

A2.4.3.5. Thiol-terminal AM

In a 50 mL round bottom flask, cysteamine (30.5 mg, 0.395 mmol) was dissolved in HPLC-grade H_2O (1 mL), HPLC-grade THF (6.9 mL), and triethylamine (0.17 mL, 1.2 mmol) and the solution stirred. In a separate flask, **0cM** (0.475 g, 0.0791 mmol) was dissolved in HPLC-grade THF (7.5 mL) by warming to 37 °C. The clear, yellow solution was then added to the reaction flask. The clear, yellow solution was stirred for 19 hrs before the THF was removed by rotary evaporation. The resulting yellow solid was dissolved in CH_2Cl_2 and 0.1 N HCl and stirred for 20-30 min. The mixture was then transferred to a separatory funnel containing addition 0.1 N HCl and the organic layer separated and washed with brine (2x). The combined aqueous portions were extracted with CH_2Cl_2 and the combined organic portions dried over $MgSO_4$ and concentrated to a yellow oil. White product was precipitated from the yellow oil in CH_2Cl_2 by addition of 10-fold diethyl ether in a 50 mL centrifuge tube. The suspension was place on a shaker for 10-15 min before the solid was collected by centrifugation and the supernatant removed by decanting. The solid was dissolved in CH_2Cl_2 (< 5 mL) and reprecipitated by adding 10-fold diethyl ether. The solid was collected by centrifugation, the supernatant

removed, and the solid washed with ether (1x) and cold hexanes (1x). The white solid was dried under ambient conditions (24 hrs) and under high vacuum (48 hrs). Yield: 0.39 g, 82 %. ^{1}H- NMR (CDCl$_3$): δ 5.63 (m, 2H, CH), 5.15 (m, 2H, CH), 4.27 (m, 2H, CH$_2$), 3.65 (m, ~0.45 kH, CH$_2$O), 3.39 (s, 3H, CH$_3$), 2.38 (m, 8H, CH$_2$), 1.75 (m, 4H, CH$_2$), 1.58 (m, 8H, CH$_2$), 1.27 (m, 64H, CH$_2$), 0.89 (t, 12H, CH$_3$). GPC: M$_w$: 7.2 kDa; PDI: 1.1.

A2.4.3.6. Diisopropylphosphine-terminal AM

In a 50 mL round bottom flask, 2-(diisopropylphosphino)ethyl amine (0.114 g, 0.709 mmol) was dissolved in anhydrous CH$_2$Cl$_2$ (2.8 mL) and triethylamine (0.19 mL, 1.4 mmol) and the solution stirred. In a separate flask, **0cM** (0.431 g, 0.0861 mmol) was dissolved in anhydrous CH$_2$Cl$_2$ (8.7 mL) and the solution added to the reaction flask dropwise *via* syringe pump at a rate of 1.0 mL/hr. The reaction was stirred for 24 hrs at room temperature before the yellow solution was washed with 0.1 N HCl (1x) and brine (2x). The combined aqueous portions were extracted with CH$_2$Cl$_2$ and the combined organic portions dried over MgSO$_4$ and concentrated to a yellow oil. A beige product was precipitated from the yellow oil in CH$_2$Cl$_2$ by addition of 10-fold diethyl ether in a 50 mL centrifuge tube. The suspension was place on a shaker for 10-15 min before the solid was collected by centrifugation and the supernatant removed by decanting. The solid was dissolved in CH$_2$Cl$_2$ (< 5 mL) and reprecipitated by adding 10-fold diethyl ether. The solid was collected by centrifugation, the supernatant removed, and the solid washed with ether (1x) and cold hexanes (1x). The white solid was dried under ambient conditions (24 hrs) and under high vacuum (24 hrs). Yield: 0.36 g, 69 %. ^{1}H- NMR (CDCl$_3$): δ 5.66 (m, 2H, CH), 5.15 (m, 2H, CH), 4.22 (m, 2H, CH$_2$), 3.60 (m, ~0.45 kH, CH$_2$O), 3.38 (s, 3H, CH$_3$), 2.38 (m, 8H, CH$_2$), 1.99 (m, 3H, CH$_3$), 1.80 (m, 3H, CH$_3$), 1.50 (m, 8H, CH$_2$), 1.23

(m, 64H, CH$_2$), 0.89 (t, 12H, CH$_3$). GPC: M$_w$: 7.4 kDa; PDI: 1.1.

A2.4.4. Water-solubilization of WLNCs by Solvent Evaporation

Water-solubilization was performed using the solvent evaporation method detailed in **Section 4.5.4**, using a WLNC stock solution in chlorofom with a concentration of 0.660 μM (determined as previously described [6]), a final volume during stirring of 3.2 mL, and the specific amounts described in **Table A2.2** below.

				Stirring		Water-Soluble WLNCs		
Functionalized AM	AM (mg)	AM (μmol)	WLNCs (μmol)	[AM] (μM)	[WLNC] (μM)	[AM] (μM)	[WLNC] (μM)	AM:WLNC
NHS	19.9	3.32	0.165	1040	51.6	663	33.0	20.1
Carboxylic Acid	19.9	3.32	0.165	1040	51.6	663	33.0	20.1
Phosphonic Acid (Propyl)	20.4	3.34	0.165	1050	51.6	669	33.0	20.3
Phosphonic Acid (Butyl)	19.9	3.26	0.165	1020	51.6	653	33.0	19.8
Phosphate	19.9	3.26	0.165	1020	51.6	653	33.0	19.8
Sulfate	20.8	3.41	0.165	1070	51.6	682	33.0	20.7
Primary Amine	20.8	3.47	0.165	1080	51.6	693	33.0	21.0
Hydroxyl (Ethyl)	20.5	3.42	0.165	1070	51.6	683	33.0	20.7
Hydroxyl (Propyl)	20.2	3.37	0.165	1050	51.6	673	33.0	20.4
Thiol	19.6	3.27	0.165	1020	51.6	653	33.0	19.8
Diisopropyl-phosphine	19.9	3.32	0.165	1040	51.6	663	33.0	20.1

Table A2.2. Specific amounts and concentrations of functionalized AMs and WLNCs used to formulate the water-solubilized nanocrystals.

A2.4.5. Characterization of Water-soluble WLNCs

A2.4.5.1. Qualitative Evaluation of Turbidity and Fluorescence

Turbidity of water-solubilized WLNCs as compared with WLNCs in chloroform at the same concentration was qualitatively evaluated by visual inspection and images captured using a Canon PowerShot SD400 digital camera. Fluorescence of the solutions was qualitatively evaluated following excitation with a Spectroline ® Longlife[TM] Filter long wavelength UV lamp (365 nm) and images captured using a Canon PowerShot SD400 digital camera.

A2.4.5.2. Quantitative Turbidity: Percent Transmittance

Turbidity of water-solubilized WLNCs as compared with WLNCs in chloroform at the same concentration was evaluated quantitatively by UV/Visible absorbance on a Lambda Bio XLS instrument (Perkin Elmer, Waltham, MA) scanning from 190 – 650 nm.

A2.4.5.3. Quantitative Fluorescence Emission

Fluorescence of water-solubilized WLNCs and WLNCs in chloroform at the same concentration from 380 – 800 nm was quantified using a Shimadzu RF-5301 PC spectrofluorophotometer, with an excitation wavelength of 365 nm.

A2.4.5.4. Hydrodynamic Diameter

Hydrodynamic diameters were evaluated by dynamic light scattering (DLS) using a Malvern Instruments Zetasizer Nano ZS-90 instrument (Southboro, MA). DLS measurements were performed at a 90° scattering angle at 25°C. Size distributions by volume of measurements were collected in triplicate, averaged and reported.

A2.5. References

[1]   R. G. Pearson, *Journal of the America Chemical Society* **1963**, *85*, 3533.
[2]   R. G. Pearson, J. Songstad, *Journal of the America Chemical Society* **1967**, *89,* 1827.
[3]   J. Djordjevic, L. Del Rosario, J. Wang, K. Uhrich, *Journal of Bioactive and Compatible Polymers* **2008**, *23*, 532.
[4]   L. Tian, L. Yam, N. Zhou, H. Tat, K. Uhrich, *Macromolecules* **2004**, *37*, 538.
[5]   M. J. Bowers II, J. R. McBride, S. J. Rosenthal, *Journal of the American Chemical Society* **2005**, *127*, 15378.
[6]   W. W. Yu, L. Qu, W. Guo, X. Peng, *Chemistry of Materials* **2003**, *15*, 2854.

A3. APPENDIX 3: ADDITIONAL POLYMERS

In this appendix, additional polymers were synthesized as an extension of the research described previously. The materials and methods are compiled in **Section A3.3.**

A3.1. An Additional Cationic Polymer for Nucleic Acid Delivery: 7nM

A3.1.1. Background

In **Chapter 2**, three cationic AMs were synthesized and evaluated for their ability to complex with and deliver siRNA. However, only one polymer, namely **9nM**, was efficient at complexing with a delivering siRNA. To create a second polymer for evaluation as a cationic AM for siRNA delivery, **7nM** was synthesized. The polymer was initially evaluated as a potential nucleic acid delivery vehicle by measuring its hydrodynamic diameter and, more importantly, the polymer zeta potential.

A3.1.2. Synthesis 1

In this first synthesis, **7nM** was synthesized *via* the same methodology used to synthesize **9nM** in **Chapter 2**, as shown in **Scheme A3.1**. In this synthetic method, the formation of oligomers is controlled by stoichiometry and the slow addition of the starting materials *via* the syringe pump.
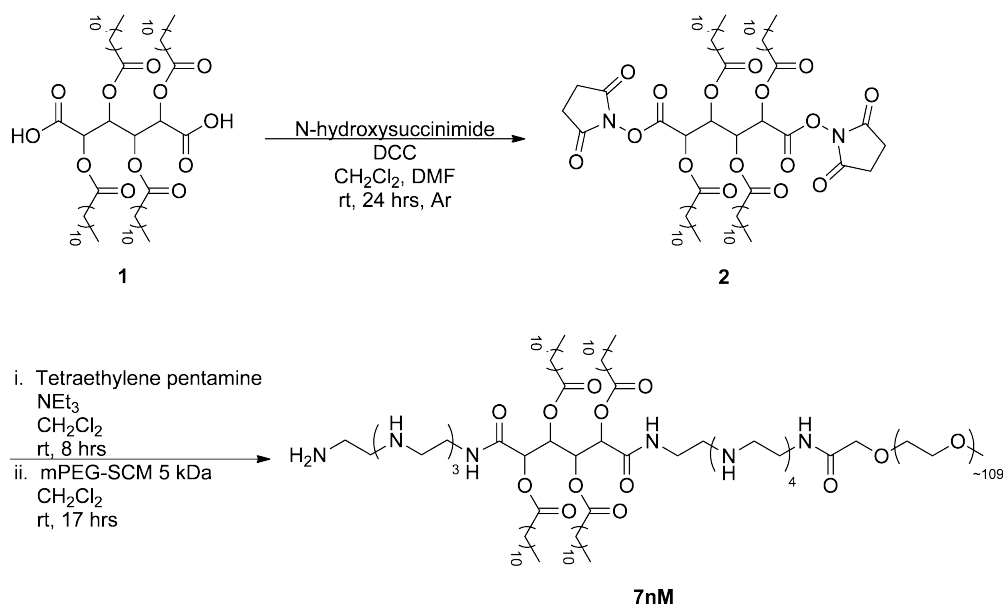
Scheme A3.1. Synthesis of **7nM**.

A3.1.2.1. Characterization of 7nM

Successful synthesis of the polymer was verified by proton nuclear magnetic resonance (^{1}H NMR) spectroscopy and molecular weight determined by gel permeation chromatography (GPC) relative to PEG standards. Due to the abundance of PEG in the polymer (~83 % of protons), the presence of new protons in the ^{1}H NMR spectra were difficult to detect, particularly from 0.8 to 2.4 ppm where the methylene protons of the hydrophobic chains comprise the majority of that region. Thus, spectra were monitored for the disappearance of the protons of the activating group (N-hydroxysuccinimide) on **2**, which resonate at 2.8 ppm. In addition, a new, broad peak resonating at ~ 2.30 ppm for the ethylene spacer indicates successful conjugation of the tetraethylene pentamine to the polymer. However, integrations indicate there is a mixture of di-PEGylated polymer and mono-PEGylated polymer (i.e. 2 PEGs to 4 alkylated arms).

The polymer was further characterized by dynamic light scattering for its ability to form micelles and by zeta potential to confirm a cationic polymer was indeed obtained. This data is summarized with respect to the previously evaluated AMs for nucleic acid delivery, **1nM**, **5nM**, and **9nM**, in **Figure A3.1** below. The hydrodynamic diameter was determined to be 92.2 ± 39.4 nm while the zeta potential was 30.7 ± 2.9 mV.

Thus, a second cationic AM with a zeta potential similar to that of **9nM** was synthesized. Due to the large, positive magnitude of the zeta potential, this polymer is a good candidate for further evaluation towards its ability to deliver siRNA.

A3.1.3. Additional Synthetic Routes to 7nM

In the previously describe synthetic procedure for **7nM** and **9nM**, the only control over the formation of oligomers is the stoichiometry and the slow addition of the starting materials using the syringe pump. To better control the synthesis of these polymers and isolate a more pure product, two protection schemes were designed and evaluated below.

A3.1.3.1. One Protection Step (7nM_2)

To control the final structure of **7nM** and **9nM**, a protection step was added to the synthetic procedure. As a model synthesis, only **7nM** was evaluated. The protections step, the addition of benzyl chloroformate (CBZ-Cl) was added following the addition of tetraethylene pentamine to **2**, as shown in **Scheme A3.2**. It should be noted that an effort was made to isolate and purify **3**, but once it was isolated as a white solid it was insoluble in further solvents for chemical characterization. Thus, in the final synthesis, it was not isolated. The CBZ protecting group was removed by hydrogenation in the final step of the synthesis.
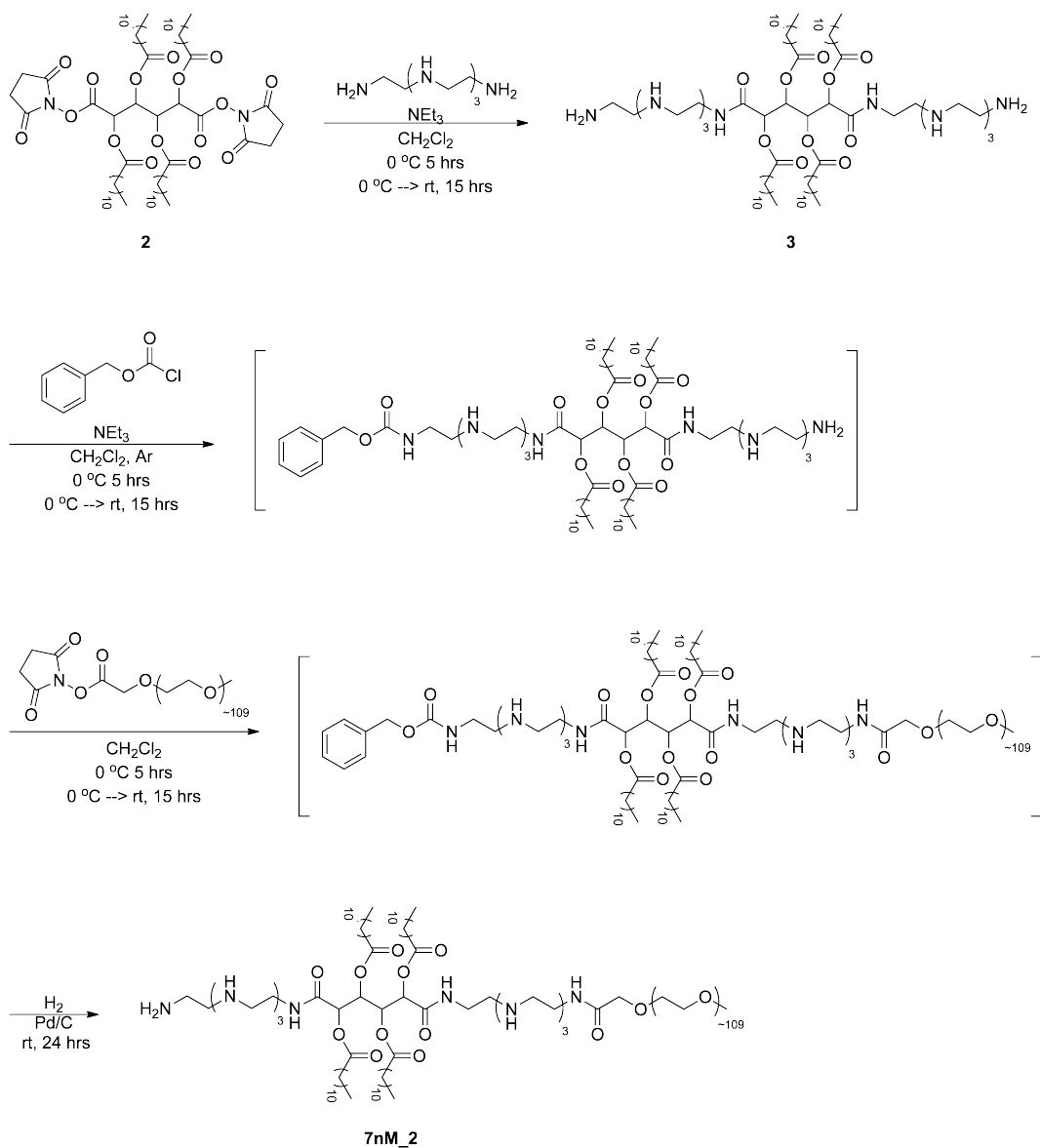
Scheme A3.2. Synthesis of **7nM_2** utilizing one CBZ-Cl protection step.

A3.1.3.1.1. Characterization of 7nM_2

In comparison to the **7nM** synthesized in **Section A3.1.2**, the ^{1}H NMR of **7nM_2** had several differences. Specifically, in the spectra for **7nM**, the broad peak at 2.30 ppm was assigned to the ethylenes of the tetraethylene pentamine groups. However, in the spectra for **7nM_2**, two new, distinct peaks were observed and assigned to the ethylenes

of the tetraethylene pentamine groups and the hydrogens of the alkylated arms on the mucic acid derivative, which are shifted downfield due to the amino groups. The first was a quartet at 3.12 ppm integrating for ~ 22 protons and the second a quartet at ~ 1.42 ppm integrating for ~32 protons. The number of protons is due to overlap of the ethylenes of the tetraethylene pentamine groups with some methylenes of the alkylated arms, which shift downfield due to interactions with the electronegative amino groups (the peak that normally exists at ~ 2.4 ppm integrating for 8 protons is no longer there). In addition, a broad peak at 12.2 ppm integrating for 7 protons was assigned the amino hydrogens.

The polymer was further characterized by dynamic light scattering for its ability to form micelles and by zeta potential to confirm a cationic polymer was indeed obtained. This data is summarized with respect to the previously evaluated AMs for nucleic acid delivery, **1nM**, **5nM**, and **9nM**, in **Figure A3.1** below. The hydrodynamic diameter was determined to be 174.4 ± 42.5 nm while the zeta potential was 24.9 ± 3.1 mV.

Thus, this synthetic procedure appears to be a viable candidate for further evaluation as a method to better control the resulting cationic polymer synthesized.

A3.1.3.2. Two Protection Steps (7nM_3)

To control the final structure of **7nM** and **9nM**, two protection steps were added to the synthetic procedure. Again, as a model synthesis, only **7nM** was evaluated. In this synthetic procedure, shown in **Scheme A3.3**, prior to addition to **2**, the tetraethylene pentamine was first mono-protected with CBZ-Cl, which was controlled stoichiometrically. The mono-protected tetraethylene pentamine was then added to **2** *in situ*. The CBZ protecting group was then removed *via* hydrogenation overnight and then CBZ-Cl was again utilized to mono-protect **3**. Again, it should be noted that an effort was

made to isolate and purify **3**, but once it was isolated as a white solid it was insoluble in further solvents for chemical characterization. Thus, in the final synthesis, it was not isolated. Following the addition of the NHS-activated PEG, the CBZ protecting group was removed by hydrogenation in the final step of the synthesis.
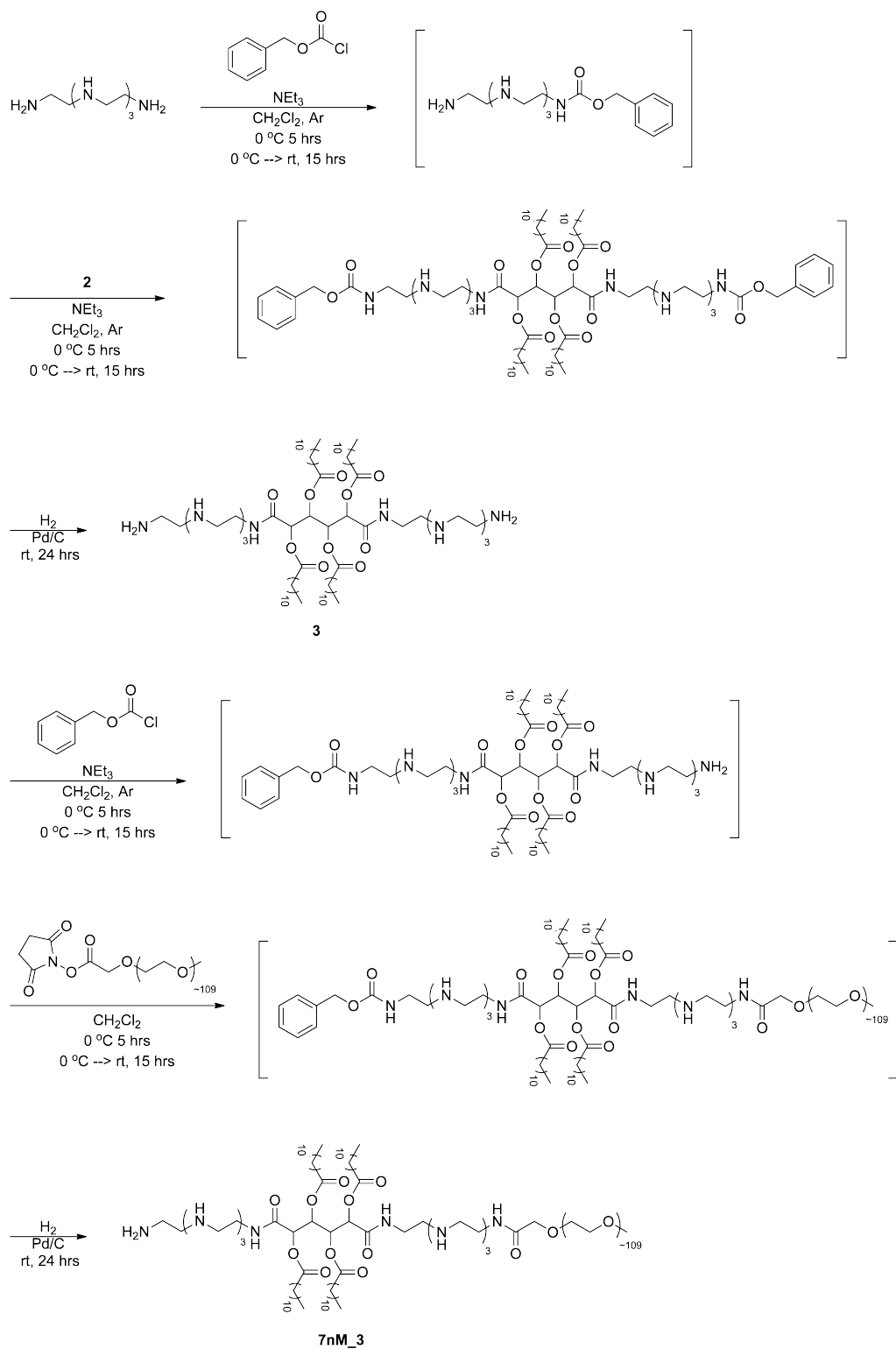
Scheme A3.3. Synthesis of **7nM_3** utilizing two CBZ-Cl protection steps.

A3.1.3.2.1. Characterization of 7nM_3

In comparison to the other **7nM** polymers synthesized, this synthetic procedure was largely ineffective due to in efficient coupling of the PEG. Similar to the **7nM_2** the same two new, distinct peaks at 1.42 ppm and 3.12 ppm were observed and assigned to the ethylenes of the tetraethylene pentamine groups and the hydrogens of the alkylated arms on the mucic acid derivative, which were shifted downfield due to the addition of the amino groups. In addition, a broad peak at 12.2 ppm was assigned the amino protons. However, these peaks integrated for far too many protons as compared with the PEG, indicating that the PEG coupling step was ineffective. The lack of PEG coupling is likely due to incomplete deprotection of the CBZ protection group from product **3** which resulted in most primary amines being protecting during the PEG coupling step.

Even though the synthesis was ineffective, the resulting polymer was still characterized by dynamic light scattering for its ability to form micelles and by zeta potential to confirm a cationic polymer was indeed obtained. This data is summarized with respect to the previously evaluated AMs for nucleic acid delivery, **1nM**, **5nM**, and **9nM**, in **Figure A3.1** below. The hydrodynamic diameter was determined to be 88.22 ± 15.1 nm while the zeta potential was -3.85 ± 3.6 mV.

Thus, while this synthetic procedure may be a viable candidate to better control the resulting cationic polymers, further development is necessary to ensure the first deprotection step is carried of sufficiently prior to adding the PEG.

A3.1.4. Summary & Future Work

In summary, a second, highly cationic polymer, **7nM**, has been synthesized for further evaluation as to its potential to complex with a deliver nucleic acids. Both the

hydrodynamic size and zeta potential are comparable to **9nM** (shown in **Figure A3.1**), which was shown to have some efficacy to deliver siRNA in **Chapter 2**.

In addition, a synthetic method that appears to yield more well-defined cationic polymers, **7nM_2** as a model, has been described and carried out in **Section A3.1.3.1**. Again, the hydrodynamic size and zeta potential are comparable to **9nM** and **7nM**, as shown in **Figure A3.1**. However, further validation as to its efficacy and reproducibility is necessary.

Finally, a longer methodology that has the protential to control the polymer structure has been outlined in **Section A3.1.3.3**. However, this synthethic scheme needs further exploration to determine its utility.
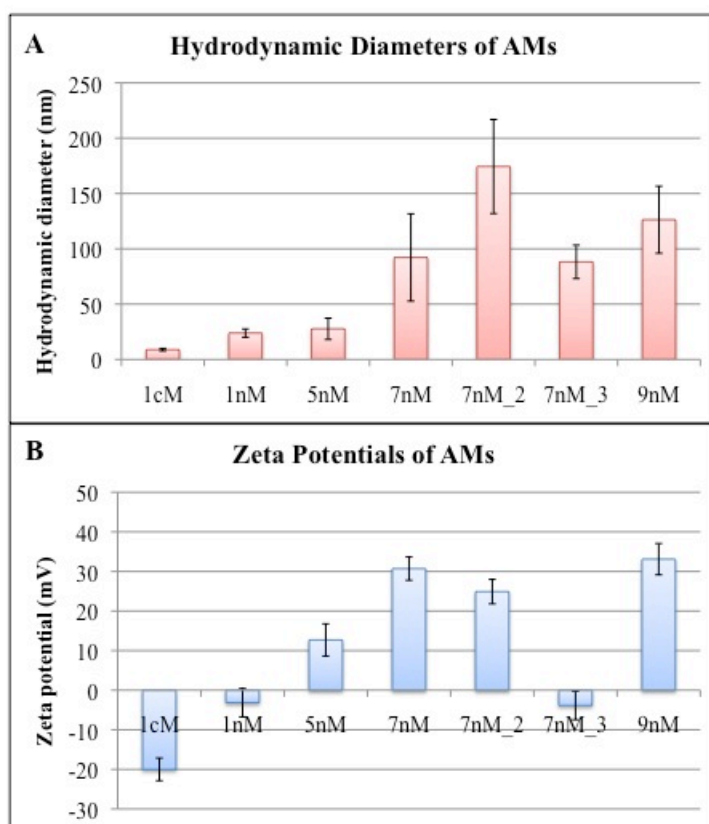
Figure A3.1. Summary of the a) hydrodynamic diameters and b) zeta potentials of the **7nM** polymers synthesized in this section as compared with **1cM, 1nM, 5nM,** and **9nM**.

A3.2. A Fluorescent Polymer: 1cM-FITC

As discussed in **Section 1.2.3.1**, one way to follow the short-term fate of nanomaterials is through the use of a fluorescent tag. To follow the short-term fate of **1cM**, a fluorescein (FITC) tag was added to the PEG end as outlined in **Scheme A3.4**.
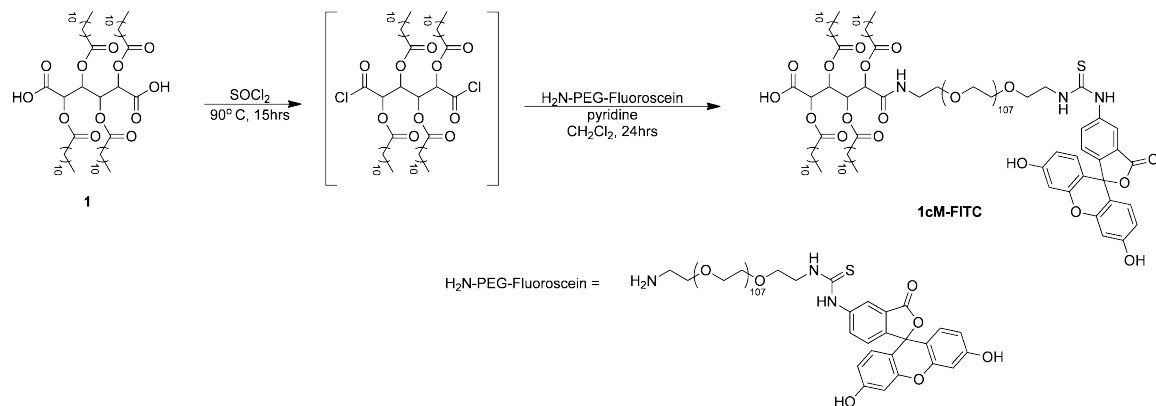
Scheme A3.4. Synthesis of **1cM-FITC** *via* thionyl chloride activation of **1**.

Successful synthesis of the polymer was verified by proton nuclear magnetic resonance (^{1}H NMR) spectroscopy and molecular weight determined by gel permeation chromatography (GPC) relative to PEG standards. This polymer was subsequently used in numerous applications to follow both **1cM** and **1cM**-stabilized liposomes as outlined by Harmon, et al..[1, 2]

A3.3. Experimental

A3.3.1. Synthetic Materials

Unless otherwise stated, solvents and reagents were purchased from Fisher Scientific (Pittsburgh, PA) and Sigma-Aldrich (St. Louis, MO) and used as received. PEG 5 kDa was purchased from Polysciences, Inc. (Warrington, PA) and dried by

azeotropic distillation from toluene before use. Functionalized PEGs, namely methoxy-PEG-succinimidyl carboxymethyl (MW 5 kDa) (mPEG-SCM) and amino-PEG-fluorescein (H_2N-PEG-FITC), was purchased from Laysan Bio, Inc (Arab, AL) and used as received. Product **1** was synthesized as previously described[3] and product **2** was synthesized as described in **Chapter 3**.

A3.3.2. Characterization Methods

A3.3.2.1. Proton Nuclear Magnetic Resonance (^{1}H NMR) Spectroscopy

Proton nuclear magnetic resonance (^{1}H-NMR) spectra of the products were obtained using a Varian 400 MHz or 500 MHz spectrophotometer. Samples were dissolved in chloroform-d, with a few drops of dimethyl sulfoxide-d_6 if necessary, with tetramethylsilane as an internal reference.

A3.3.2.2. Gel Permeation Chromatography (GPC)

Molecular weights (M_w) and polydispersity indices (PDI) were determined using gel permeation chromatography (GPC) with respect to PEG standards (Sigma-Aldrich) on a Waters Stryagel® HR 3 THF column (7.8 x 300 mm). The Waters LC system (Milford, MA) was equipped with a 2414 refractive index detector, a 1515 isocratic HPLC pump, and 717plus autosampler. An IBM ThinkCentre computer with Waters Breeze Version 3.30 software installed was used for collection and processing of data. Samples were prepared at a concentration of 10 mg/mL in tetrahydrofuran, filtered using 0.45 μm pore size nylon or poly(tetrafluoroethylene) syringe filters (Fisher Scientific) and placed in sample vials to be injected into the system.

A3.3.3. Polymer Synthesis

A3.3.3.1. 7nM

In a 50 mL round bottom flask, tetraethylenepentamine (36.5 μL, 0.191 mmol) was dissolved in CH_2Cl_2 (3.1 mL) and triethylamine (0.14 mL, 1.0 mmol). In a separate vessel, **2** (0.108 g, 0.0955 mmol) was dissolved in HPLC-grade CH_2Cl_2 (3.2 mL) and subsequently added to the solution of tetraethylenepentamine dropwise *via* syringe pump at a rate of 1.00 mL/hr. The reaction was stirred at room temperature a total of 8 hrs before mPEG-SCM (0.477 g, 0.0955 mmol) dissolved in HPLC-grade CH_2Cl_2 (7.4 mL) was added to the yellow reaction solution dropwise *via* syringe pump at a rate of 1.0 mL/hr. The reaction was stirred at room temperature overnight (18-20 hrs). The solvent was then removed from the reaction solution by rotary evaporation. The oil/solid was then re-dispersed in CH_2Cl_2 and filtered to remove the solid NHS-byproduct. The filtrate was concentrated to an oil and a white product precipitated from the oil dissolved in CH_2Cl_2 (5 mL) by addition of 10-fold diethyl ether. The tube was then placed on the shaker for 15-20 min to allow all solid to precipitate out and the solid then collected by centrifugation at 3000 rpm for 5 min. The supernatant was then removed by decanting and the solid reprecipitated out of CH_2Cl_2 (< 5 mL) with ether and collected by centrifugation. The white solid was then washed with ether (1x) and then dried in the hood overnight. Residual solvent was removed under high vacuum overnight. Yield: 0.51 g, 85 %. ^{1}H-NMR (CDCl$_3$): δ 5.62 (s, 2H, CH), 3.99 (m, 4H, CH), 3.74 (m, ~0.44 kH, CH_2O), 3.39 (s, 3H, OCH_3), 3.05 (bm, 11H, CH_2), 2.31 (bm, 47H, CH_2), 1.60, (bm, 3H, CH_2), 1.48 (t, 4H, CH_2), 1.26 (m, 27H, CH_2), 0.89 (t, 6H, CH_3). GPC: M_w: 6.2 kDa; PDI = 1.1.

A3.3.3.2. 7nM_2

In an oven-dried 50 mL round bottom flask, tetraethylenepentamine (47.7 mg, 0.252 mmol) was dissolved in anhydrous CH_2Cl_2 (12.5 mL) and triethylamine (0.42 mL, 3.0 mmol) under argon gas. The reaction vessel was then submerged in an ice/H_2O bath. In a separate vessel, **2** (0.143 g, 0.126 mmol) was dissolved in anhydrous CH_2Cl_2 (12.5 mL) and subsequently added to the solution of tetraethylenepentamine on ice dropwise *via* syringe pump at a rate of 1.00 mL/hr. The reaction solution was kept at 0°C in an ice bath for 3-4 hrs and was subsequently warmed to room temperature slowly overnight. The reaction was stirred a total of 20 hrs. The reaction solution was then submerged in an ice/H_2O bath and 2.0 mL of a 0.064 M solution of benzyl chloroformate (0.13 mmol) in anhydrous CH_2Cl_2 was subsequently added dropwise *via* syringe pump at a rate of 1.00 mL/hr. The reaction was stirred at 0 °C for 3-4 hrs and before the solution was warmed to room temperature slowly overnight. After stirring for 20 hrs, the reaction solution was again submerged in an ice/H_2O bath. A solution of mPEG-SCM (0.630 g, 0.126 mmol) in anhydrous CH_2Cl_2 (4.0 mL) was then added to the reaction flask dropwise *via* syringe pump at a rate of 1.00 mL/hr. The reaction was stirred at 0 °C in an ice bath for ~ 5 hrs and was then slowly warmed to room temperature overnight. After 20 hrs total stir time, 10 % Pd/C (58.4 mg) was added to the solution. Ambient air was removed from the system using high vacuum and replaced with H_2 using a balloon. The reaction was stirred at room temperature a total of 24 hrs before the H_2 balloon was removed, the H_2 atmosphere removed by high vacuum, and the flask opened to ambient air. The Pd/C was removed by vacuum filtration through celite. The filtrate was then concentrated and residual Pd/C removed by filtering the resulting oil through a 0.2 μm PTFE syringe filter

(Fisher). A white solid was precipitated from the yellow oil dissolved in CH_2Cl_2 (5 mL) by addition of 10-fold diethyl ether in a 50 mL centrifuge tube. The tube was then placed on the shaker for 15-20 min to allow all solid to precipitate out and the solid then collected by centrifugation at 3000 rpm for 5 min. The supernatant was then removed by decanting and the solid reprecipitated out of CH_2Cl_2 (< 5 mL) by adding 10-fold diethyl ether. The solid was collected by centrifugation, the supernatant removed, and the solid washed with ether (1x) and cold hexanes (1x). The white solid was dried under ambient conditions (48 hrs) and under high vacuum (24 hrs). Yield: 0.61 g, 77 %. ^{1}H-NMR ($CDCl_3$): δ 7.20 (bs, 7H, NH), 5.15 (s, 2H, CH), 4.17 (m, 2H, CH_2), 3.65 (m, ~0.44 kH, CH_2O), 3.39 (s, 3H, OCH_3), 3.12 (q, 22H, CH_2), 2.72 (s, 2H, CH_2), 1.72 (bs, 20H, CH_2), 1.41 (q, 33H, CH_2), 1.26 (m, 25H, CH_2), 0.88 (t, 9H, CH_3). GPC: M_w: 6.8 kDa; PDI = 1.0.

A3.3.3.3. 7nM_3

In an oven-dried 50 mL round bottom flask, tetraethylenepentamine (51.9 mg, 0.274 mmol) was dissolved in anhydrous CH_2Cl_2 (24 mL) and triethylamine (0.46 mL, 3.3 mmol) under flowing argon gas. The reaction vessel was then submerged in an ice/H_2O bath. In a vial under argon gas, benzyl chloroformate (0.03 mL, 0.2 mmol) was added to anhydrous CH_2Cl_2 (3 mL) and the solution added to the reaction flask dropwise *via* syringe pump at a rate of 1.00 mL/hr. The reaction was stirred under Ar gas at 0 °C in an ice bath for ~ 5 hrs and was subsequently warmed to room temperature slowly overnight. The reaction was stirred a total of 20 hrs before the solution was returned to 0 °C in an ice bath. A solution of **2** (0.155 mg, 0.137 mmol) in anhydrous CH_2Cl_2 (5.6 mL) was then added dropwise *via* syringe pump at a rate of 1.00 mL/hr. The reaction was

stirred under Ar gas at 0 °C in an ice bath for 4-5 hrs and was subsequently warmed to room temperature slowly overnight. The reaction was stirred a total of 20 hrs before 10 % Pd/C (58.4 mg) was added. Ambient air was removed from the system using high vacuum and replaced with H_2 using a balloon. The reaction was stirred at room temperature a total of 24 hrs before the H_2 balloon was removed, the H_2 atmosphere removed by high vacuum, and the flask opened to ambient air. The Pd/C was removed by vacuum filtration through celite. The filtrate was the concentrated to a crystalline solid and dried under high vacuum for 12 hrs. The solid was then redissolved in andhydrous CH_2Cl_2 (12.5 mL) and triethylamine (0.19 mL, 1.4 mmol) under flowing argon gas. The reaction vessel was then submerged in an ice/H_2O bath before 1.6 mL of a 0.089 M solution of benzyl chloroformate (0.14 mmol) in anhydrous CH_2Cl_2 was subsequently added dropwise *via* syringe pump at a rate of 1.00 mL/hr. The reaction was stirred at 0 °C for 3-4 hrs before the solution was warmed to room temperature slowly overnight. After stirring for 20 hrs, the reaction solution was again submerged in an ice/H_2O bath. A solution of mPEG-SCM (0.628 g, 0.126 mmol) in anhydrous CH_2Cl_2 (4.0 mL) was then added to the reaction flask dropwise *via* syringe pump at a rate of 1.00 mL/hr. The reaction was stirred at 0 °C in an ice bath for ~ 5 hrs and was then slowly warmed to room temperature overnight. After 20 hrs total stir time, 10 % Pd/C (58.4 mg) was added to the solution. Ambient air was removed from the system using high vacuum and replaced with H_2 using a balloon. The reaction was stirred at room temperature a total of 24 hrs before the H_2 balloon was removed, the H_2 atmosphere removed by high vacuum, and the flask opened to ambient air. The Pd/C was removed by vacuum filtration through celite. The filtrate was then concentrated and a white solid was precipitated from the

yellow oil dissolved in CH_2Cl_2 (5 mL) by addition of 10-fold diethyl ether in a 50 mL centrifuge tube. The tube was then placed on the shaker for 15-20 min to allow all solid to precipitate out and the solid then collected by centrifugation at 3000 rpm for 5 min. The supernatant was then removed by decanting and the solid reprecipitated out of CH_2Cl_2 (< 5 mL) by adding 10-fold diethyl ether. The solid was collected by centrifugation, the supernatant removed, and the solid washed with ether (1x) and cold hexanes (1x). The white solid was dried under ambient conditions (48 hrs) and under high vacuum (24 hrs). Yield: 0.99 g, Mixture of products. ^{1}H-NMR ($CDCl_3$): δ 7.20 (bs, 27H, NH), 4.17 (s, 2H, CH_2), 3.67 (m, ~0.44 kH, CH_2O), 3.39 (s, 4H, OCH_3), 3.12 (q, 119H, CH_2), 2.71 (s, 2H, CH_2), 1.69 (bs, 24H, CH_2), 1.40 (q, 175H, CH_2), 1.28 (m, 28H, CH_2), 0.89 (t, 11H, CH_3). GPC: M_w: 6.6 kDa; PDI = 1.0.

A3.3.3.4. 1cM-FITC

In an oven-dried 50 mL round bottom flask, the carboxylic acids of **1** (0.319 g, 0.339 mmol) were activated with excess thionyl chloride (20-30 mL) at 90 °C overnight. Residual thionyl chloride was removed by rotary evaporation and the resulting yellow oil used immediately without further purification. The activated compound was dissolved in anhydrous CH_2Cl_2 (8 mL) under argon. Anhydrous pyridine (0.14 mL, 1.7 mmol) was then added resulting in the emission of a small amount of gas. Subsequently, H_2N-PEG-FITC (0.27 g, 0.050 mmol) dissolved in anhydrous CH_2Cl_2 (8 mL) and added to the reaction flask dropwise *via* syringe pump at a rate of 1.0 mL/hr. The reaction was stirred under argon gas and light restrictive conditions for 24 hrs at room temperature. The solution was then acidified with 0.05 N HCl and the organic phase washed with 50:50 brine:H_2O (2x), dried over $MgSO_4$, and concentrated to a yellow oil. Minimal CH_2Cl_2

was then added and product precipitated by the addition of 10-fold diethyl ether. The solid was then collected by centrifugation and supernatant removed by decanting. Solid was dried under ambient atmosphere and light restrictive conditions (24 hrs) and under high vacuum (34 hrs). Yield: 0.23 g, 77 %. ^{1}H-NMR (CDCl$_3$): δ 7.08 (m, 3H, ArH), 6.88 (d, 1H, ArH), 6.75 (m, 3H, ArH), 6.60 (m, 4H, ArH), 3.62 (m, ~0.50 kH, CH$_2$O), 2.66 (m, 4H, CH$_2$), 2.33 (m, 4H, CH$_2$), 1.62 (m, 8H, CH$_2$), 1.26 (m, 58H, CH$_2$), 0.88 (t, 12H, CH$_3$). T$_m$ = 48 °C. GPC: M$_w$: 4.8 kDa; PDI: 1.1.

A3.3.4. Hydrodynamic Diameter and Zeta Potentials

Dynamic light scattering (DLS) and zeta potential analyses were performed using a Malvern Instruments Zetasizer Nano ZS-90 instrument (Southboro, MA). Solutions were prepared by dissolving the polymers at a concentration of 1.0 mg/mL in HPLC-grade H$_2$O and the solutions were subsequently filtered with a 0.45 μm Fisherbrand nylon syringe filter prior to collecting data. DLS measurements were performed at a 90° scattering angle at 25°C. Size distributions by volume of measurements were collected in triplicate, averaged and reported. Zeta potential measurements were collected in triplicate, averaged and the Z-average charges reported. For all measurements, error bars represent peak widths of the average value.

A3.4. References

[1]   A. Harmon, *Thesis (Ph.D.) -- Rutgers University* **2011**.
[2]   A. M. Harmon, M. H. Lash, S. M. Sparks, K. E. Uhrich, *under review*.
[3]   L. Tian, L. Yam, N. Zhou, H. Tat, K. Uhrich, *Macromolecules* **2004**, *37*, 538.

A4: APPENDIX 4: GLOSSARY

A4.1. Terms

Amphiphilic – term used to describe substances that contain both a polar, or hydrophilic, part and a nonpolar, or hydrophobic, part[1]

Atherosclerosis – a type of arteriosclerosis; the term for the process of fatty substances, cholesterol, cellular waste products, calcium ad fibrin (a clotting material in the blood) building up in the inner lining of an artery[2]

Biocompatible – the condition of being non-toxic or non-injurious to living tissue or a living system[3]

Biodegradable – capable of being broken down by the action of living things (such as microorganisms)[3]

Critical micelle concentration (CMC) – the lowest concentration of a monomeric amphiphile at which micelles form[4,5]

Cytotoxic – toxic to cells, preventing their reproduction or growth[3]

Diagnostic – an agent or substance used in diagnosis[3]

Fluorescence – the optical phenomenon for which a molecule or a material, after being energetically excited, returns to its minimum energy state (ground state) by emitting light[6]

Functionlization – the addition of functional groups[7]

Gel Electrophoresis – technique by which molecules migrate through a gel from a negatively charged electrode to a positively charged electrode and separate into bands according to size[3]

Gene Therapy – the insertion of usually genes into cells especially to replace defective genes in the treatment of genetic disorders or to provide a specialized disease-fighting function[3]

Glioblastoma – a malignant rapidly growing nerve-tissue tumor composed of astrocytes of the central nervous system[3]

Hydrodynamic Diameter – the diameter of a particle in aqueous media[8]

Hydrophilic – having a strong affinity for water[3]

Hydrophobic – having a lack of affinity for water; resistant to or avoiding wetting[3]

Low-density lipoprotein (LDL) – a lipoprotein of blood plasma that is composed of a moderate proportion of protein with little triglyceride and a high proportion of cholesterol and that is associated with increased probability of developing atherosclerosis[3]

Macromolecule – a large molecule (such as a protein, nucleic acid, or rubber) built up from smaller chemical structures[3]

Macrophage – a phagocytic tissue of the immune system that may be fixed or freely motile, is derived from a monocyte, functions in the destruction of foreign antigens (such as bacteria and viruses), and serves as an antigen-presenting cell[3]

Micelle – Colloidal dispersions of amphiphiles that self-assemble in aqueous media to form a hydrophobic core and a hydrophilic shell[4,5]

Nuclease – enzymes that cleave (degrade) nucleic acids[3]

Nucleic Acid – any of various acids (as an RNA or a DNA) composed of nucleotide chains[3]

Polyplex – Complex of a cationic polymer with an anionic nucleic acid[9]

Quantum Dots (QDs) – single crystals a few nanometers in diameter with composition- and size-dependent absorption and emission properties[6]

Scavenger Receptor – A large family of structurally unrelated distinct gene products, expressed by myeloid and selected endothelial cells that have roles in normal homeostasis and are also able to recognize modified low-density lipoproteins[10]

Small interfering RNA (siRNA) – an antisense method of gene therapy used to inhibit the expression of a target gene[11]

Stent – a short narrow metal or plastic tube often in the form of a mesh that is inserted into the lumen of an anatomic vessel (such as an artery or bile duct) especially to keep a previously blocked passageway open[3]

Vector – an agent (such as a plasmid, virus, or polymer) that contains or carries modified genetic material (such as recombinant DNA) and can be used to introduce exogenous genes into the genome of an organism[3]

Therapeutic – of or relating to the treatment of disease or disorders by remedial agents or methods[3]

Turbid – thick or opaque with matter in suspension: cloudy or muddy in appearance[3]

Zeta Potential – The potential surrounding a particle at the surface of hydrodynamic shear[12]

A4.2. References

[1]   M. Yoshikiyo, *Micelles: Theoretical and Applied Aspects*, Plenum Press, New York, **1992**.
[2]   American Heart Association: **2010**, http://www.americanheart.org
[3]   U.S. National Library of Medicine Medline Plus: National Institutes of Health; Bethesda, MD; 2010.

[4]   G. Bonacucina, M. Cespi, M. Misici-Falzi, G. F. Palmieri, *Journal of Pharmaceutical Sciences* **2009**, *98(1),* 1.

[5]   V. P. Torchilin, *Pharmaceutical Research* **2006**, *24(1)*, 1.

[6]   C. S. S. R. Kumar, *Nanomaterials for Biosensors, Vol. 8*, Wiley-VCH, Germany, **2007**.

[7]   In Wikipedia: The Free Encyclopedia; Wikimedia Foundation, Inc.: 2006 http://www.wikipedia.org/wiki

[8]   Dynamic Light Scattering (DLS), Malvern Instruments Ltd: http://www.malvern.com/LabEng/technology/dynamic_light_scattering/dynamic_light_scattering.htm.

[9]   C. M. Roth, S. Sundaram, *Annual Review of Biomedical Engineering* **2004**, *6*, 397.

[10]   S. Mukhopadhyay, S. Gordon, *Immunobiology* **2004**, *209*, 39.

[11]   L. K. Lee, C. M. Roth, *Current Opinion in Biotechnology* **2003**, *14*, 505.

[12]   Zeta Potential: An Introduction in 30 Minutes, Malvern Instruments Ltd; Technical Note available from www.malvern.co.uk.

CURRICULUM VITAE

SARAH MARIE SPARKS

EDUCATION

8/2006 – 1/2011   Rutgers University, Piscataway, NJ
Ph.D. Organic, Polymer Chemistry, 4.0/4.0

8/2001 – 6/2006   Union College, Schenectady, NY
B.S. Chemistry, Honors, ACS Certified, Cum Laude, 3.5/4.0

POSITIONS HELD

8/2010 – present   Postdoctoral Faculty Fellow, Department of Chemistry
Supervisors: Joseph Favaza, Ph.D.; Louis Liotta, Ph.D.
Dean of Faculty; Professor of Chemistry and Department Chair
Stonehill College; Easton, MA

8/2009 – 8/2010   Schering-Plough Graduate Fellow, Department of Chemistry
Supervisor: Kathryn E. Uhrich, Ph.D.
Professor and Dean of Mathematical and Physical Sciences
Rutgers University; Piscataway, NJ

6/2007 – 7/2009   Graduate Fellow, Department of Chemistry
Supervisor: Kathryn E. Uhrich, Ph.D.
Professor and Dean of Mathematical and Physical Sciences
Rutgers University; Piscataway, NJ

8/2006 – 5/2007   Teaching Assistant, Department of Chemistry
Supervisor: Donald Seigel, Ph.D.
Professor and Dean of Mathematical and Physical Sciences
Rutgers University; Piscataway, NJ

6/2006 – 8/2006   Medicinal Chemistry Intern
Supervisor: Scott B. Hoyt, Ph.D.
Merck & Co., Inc; Rahway, NJ

PUBLICATIONS

Sparks, SM*; Waite, CL*; Harmon, AM; Roth, CM; Uhrich, KE. Efficient Intracellular siRNA Delivery by Ethyleneimine-Modified Amphiphilic Macromolecules. *Under review.*

Sparks, SM; Schreuder, MA; Plourde, NM; Moghe, PV; Rosenthal, SJ; Uhrich, KE. Water-solubilization of White-light Emitting Nanocrystals by Phosphonic Acid-functionalized Amphiphilic Macromolecules. *In preparation.*

Harmon, AM; Lash, MH; **Sparks, SM**; Uhrich, KE. Preferential Cellular Uptake of Amphiphilic Macromolecule-Lipid Complexes with Enhanced Stability and Biocompatibility. *Under review.*

Iverson, N; Plourde NM; **Sparks, SM**; Wang, J; Patel, E; Nackman, GB; Uhrich, KE; Moghe, PV. Bioactive Polymers for Multimodal Inhibition of Inflammation and Atherogenesis in Activated Macrophages. *Under review.*

Iverson, N*; **Sparks, SM***; Demirdirek, B; Uhrich, KE; Moghe, PV. Controllable Inhibition of Cellular Uptake of Oxidized Low Density Lipoprotein: Structure-Property Relationships for Nanoscale Amphiphilic Macromolecules. *Acta Biomaterialia*, **2010**, 6 (8), 3081-3091.

Waite, CL; **Sparks, SM**; Uhrich, KE; Roth, CM; Acetylation of PAMAM Dendrimers for Cellular Delivery of siRNA. *BMC Biotechnology*. **2009**, 9 (38).

Kehlbeck, JD; Dimise, EJ; **Sparks, SM**; Ferrara, S; Tanski, JM; Anderson, CM. A practical and efficient synthesis of 5'-substituted *m*-terphenyls. *Synthesis*, **2007**, 13, 1979-1983.

Sparks, SM; Waite, CL; Harmon, AM; Roth, CM; Uhrich, KE. Oligoethyleneimine-Functionalized Nanoscale Amphiphilic Macromolecules for Intracellular Delivery of Nucleic Acids. *Polymer Preprints*. **2010**, 51(2), 596-597.

Bodnar, Stan; Griffin, J; Gu, L; Halperin, F; Harmon, AM; Harper, I; Langowski, BA; Lavelle, L; Rosario-Melendez, R; **Sparks, SM**; Uhrich, KE. Impact of radiation on the physiochemical properties of novel polymer therapeutics. *Polymer Preprints*. **2010**, 51(2), 628-629.

Sparks, SM: Schreuder, MA; Plourde, NM; Tilyou, TE; Moghe, PV; Rosenthal, SV; Uhrich, KE. Nanoscale Amphiphilic Macromolecules to Biostabilize White Light-Emitting CdSe Nanocrystals. *Abstracts of Papers, 240th ACS National Meeting*, Boston, MA, United States, August 22-26, **2010**.

Laviska, DA; **Sparks, SM**; Goldman, AS. Introducing the LEEDAR program, learning enhanced through experimental design and analysis with Rutgers: Giving high school

students some insight into what it means to be a scientist. *Abstracts of Papers, 240th ACS National Meeting*, Boston, MA, United States, August 22-26, **2010**.

Sparks, SM; Iverson, N; Plourde, N; Moghe, PV; Uhrich, KE. Nanoscale amphiphilic macromolecules: Multifunctional polymers for management of cardiovascular disease. *PMSE Preprints*. **2009**, 101, 1324-1325.

Laviska, DA; **Sparks, SM**; Stephen, K; Goldman, AS. Evolution of an innovative university-to-high school outreach program: The importance of mentoring in encouraging students to think about careers in chemistry. *Abstracts of Papers, 238th ACS National Meeting*, Washington, DC, United States, August 16-20, **2009**.

Harmon, AM; Lash, MH; **Sparks, SM**; Uhrich, KE. Complexation of amphiphilic macromolecules (AM) with cationic and neutral lipids for improved cellular interactions and therapeutic delivery. *Abstracts of Papers, 238th ACS National Meeting*, Washington, DC, United States, August 16-20, **2009**.

Laviska, DA; Stephen, K; **Sparks, SM**; Pelczar, EM; Spink, R; Goldman, AS. Designing an outreach curricula to focus on mentoring hich school students: The relationship between greenhouse gases and global warming. *Abstracts of Papers, 237th ACS National Meeting*, Salt Lake City, UT, United States, March 22-26, **2009**.

Laviska, DA; Stephen, K; **Sparks, SM**; Pelczar, EM; Spink, R; Goldman, AS. Building a bridge between high school education and CENTC research: An interactive program for integrated outreach, mentoring, and education on greenhouse gases and global warming. *Abstracts of Papers, 237th ACS National Meeting*, Salt Lake City, UT, United States, March 22-26, **2009**.

Sparks, SM; Waite, CL; Harmon, AM; Roth, CM; Uhrich, KE. Aminated AmphiphilicScorpion-like Macromolecules as Delivery Vehicles for Nucleic Acids. *Polymer Preprints*. **2008**, 49(2), 1034-1035.

Del Rosario, LS; **Sparks, SM**; Harmon, A; Wang, J; Uhrich, KE. Amphiphilic scorpion-like macromolecules (AScM)-based micelles as carriers for camptothecin. *PMSE Preprints*, **2008**, 98, 699-701.

Sparks, SM; Wang, J; del Rosario, L; Uhrich, KE. Synthesis of functionalized amphiphilic scorpion-like macromolecules for biomedical applications. *PMSE Preprints*, **2007**, 97, 695-696.

Sparks, SM; Kehlbeck, JD; Anderson, C. Synthesis and characterization of novel meta-terphenyl compounds. *Abstracts of Papers, 231st ACS National Meeting*, Atlanta, GA, United States, March 26-30, **2006**.

*Equal Contribution